Mauricio Roche Tabata

Modeling and analysis of blast furnace drainage

Åbo Akademi University

Modeling and analysis of blast furnace drainage

Mauricio Roche Tabata

Thermal and Flow Engineering
Faculty of Science and Engineering
Åbo Akademi University
Åbo, Finland, 2020

Supervisor

Prof. Henrik Saxén.
Laboratory of Process and Systems Engineering,
Åbo Akademi University, Finland.

Reviewer and Opponent

Emer. Prof. Rob Boom.
TU Delft, the Netherlands.

Reviewer

Prof. Zongshu Zou.
Northeastern University, China.

ISBN 978-952-12-3982-3 (printed)
ISBN 978-952-12-3983-0 (digital)
Painosalama Oy, Turku, Finland 2020

Preface

The work reported in this this thesis was conducted at the Process and Systems Engineering Laboratory of Åbo Akademi University during the years 2016-2020. The research was mainly supported by the European Union's Research Fund for Coal and Steel (RFCS) as well as the Åbo Akademi University Foundation and Walter Ahlström Foundation. I gratefully acknowledge the financial support, which enabled me to put full-time efforts into the thesis work.

I would very much like to thank my supervisor Professor Henrik Saxén for sharing his knowledge and for his positive energy throughout these years; his guidance and motivation has made this thesis possible. I would like also to thank Dr. Mikko Helle for his very valuable help and clever inputs to my research, to reviewers Prof. Zongshu Zou and Prof. Rob Boom for their insightful comments and feedback.

Thank you to Docent Frank Pettersson and Professor Ron Zevenhoven for your instructive and valuable courses and discussions, to Alf Hermanson and Vivéca Sundberg for their help and support, and to my past and present colleagues. I would also thank to Gerard Louwerse, Jan van der Stel and Joost Storm from the Research and Development department of Tata Steel (IJmuiden) for their support and hospitality during my visits to Tata Steel.

I would like to thank my friends near and far away with whom I have shared great moments throughout these years and a special thanks to my friend Claudio Carletti for his recommendation and encouragement to do my doctoral degree. Finally, I want to express how grateful I am to my mother María Esperanza and my brother Argenis for their unconditional support all my life.

Åbo, September 2020,

Mauricio Roche

Abstract

The blast furnace is the prevailing unit process for iron-making in the steelmaking process and the present growing global demand for steel leads to higher requirements set on the efficiency and productivity of the process. The lower part of the blast furnace, where iron and slag accumulate, the hearth, is key to the furnace performance both from short-term and long-term perspectives, so a monitoring of the hearth state is a critical task for a successful operation. However, it is difficult to provide a detailed description of the processes due to the complex dynamic phenomena that take place in the hearth, beside the extreme chemical and thermal conditions that prevent or at least strongly limit the access to direct measurements. As consequence, the hearth state is for the most part unknown.

The models presented in this thesis aim to shed some light on the hearth conditions and the drainage of iron and slag based on estimates of the production rates of iron and slag, measurements of the outflow rates of iron and slag, and other process measurements interpreted by mathematical models. Drainage data available at a large furnace with three tapholes was used in the analysis. The observed draining rates were filtered and systematically organized by a method based on principal component analysis, which revealed interesting outflow patterns and evolutions of these in time. On the basis of the results, some assumptions regarding the hearth state, primarily about the dead man and the taphole, were evaluated in two off-line models that were developed to estimate the iron and slag levels in the hearth. The approaches of these off-line models were a two-pool hearth with liquid outflows expressed by a parameterized expression inspired by measurements in the plant, and a single-pool hearth with a physical description of the conditions at and in the taphole.

To be able to provide a real-time view of the conditions, an on-line model of a multi-pool hearth system was developed based on inflow and outflow estimates continuously obtained from the plant to reconstruct the liquid levels.

The sensitivity of the models to changes in their parameters was studied and the results were appropriately compared with observations from the reference furnace. Fairly good correlations between the calculated and observed variables were found, gaining confidence in some of the assumptions made in the modeling. Particular focus was put on analyzing the role of coke permeability at the taphole and the taphole conditions. The fluctuations and drifting seen in the process data indicates a high level of complexity of the system at hand. Despite these challenges, the models developed are deemed to have a potential of being applied as tools to assess different hearth states and the system's response to certain conditions. Furthermore, the on-line model can be applied to perform the crucial task of estimating and tracking the liquid levels in the hearth. Future work will be

focused on extending and integrating some of the features of the models to yield a better description of the hearth state. Furthermore, an adaptation of the off-line models should be studied to track changing states of the blast furnace hearth.

Referat

Masugnen är den dominerande enhetsprocessen för produktion av råjärn som används vid ståltillverkning. Ett ökande behov av stål i världen ställer idag allt högre krav på produktionsprocessernas effektivitet. Tillståndet hos masugnens under del, eller ställ, där järn och slagg samlas upp före de tappas ur ugnen, är av stor betydelse för ugnens prestanda samt livslängd och kräver därför en noggrann uppföljning under driften. Det är emellertid svårt att få en detaljerad bild av ställets förhållanden p.g.a. komplexa fördelningar och dynamiska fenomen som karakteriserar denna del av masugnen. Extremt höga temperaturer och fientliga omständigheter (slitage, kemisk attack, etc.) gör det nästan omöjligt att direkt uppmäta variabler i masugnsstället. Av denna orsak har ställets interna tillstånd länge varit obekant.

De matematiska modeller som presenteras i föreliggande avhandling har som mål att belysa vissa fenomen och tillstånd i masugnsstället, med speciell focus på ställets dränering av råjärn och slagg. För detta ändamål utnyttjades mätningar av utflödena i en referensmasugn, estimat av produktions-hastigheten av råjärn och slagg erhållna via materialbalanser samt några andra centrala mätningar. Tappningsdata från masugnens tre tapphål analyserades i avhandlingen och fungerade även som referens vid en jämförelse mellan beräknade och uppmätta förlopp då modellerna validerades.

I en data-baserad modell filtrerades först tappdata, varefter datamängden komprimerades genom huvudkomponentanalys (eng. principal component analysis, PCA). Metoden avslöjade intressanta mönster som utflödena uppvisade och hur dessa förändrades tidsmässigt. På basis av resultaten kunde man dra slutsatser om ställets funktion, primärt berörande tillståndet hos koksbädden (den ”döda mannen”) samt tapphålet.

Två off-line-modeller utvecklades även för att teoretiskt studera masugnens dränering och för att få en bättre förståelse för hur smältornas nivåer varierar i stället. Den ena modellen tillämpar en uppdelning av stället i två kommunicerande kärl och beskriver tappningarna med ett förenklat uttryck som anpassats till utflöden som observerats i driften. Den andra modellen, som inte beaktar nivåskillnader mellan olika delar av stället (förutom den lokala lutningen av fluidernas gränsytor vid tapphålet) baserar sig på strömningsmekaniska ekvationer för att beskriva förhållandena framför och i tapphålet. Modellerna utnyttjades för att få grundläggande förståelse för förloppen under och mellan ugnens tappningar.

Med avsikt att förse operatörerna med en realtidsbild av masugnsställets tillstånd utvecklades ytterligare en modell som automatiskt skattar järn- och slaggnivåerna i masugnsstället på basis av tillgängliga mätningar. Modellen, som beaktar möjliga nivåskillnader i olika delar av stället, korrigerar massbalanserna för järn och slagg genom att matcha fluidnivåerna vid givna punkter under tappcykeln.

Modellernas känslighet i avseende på värden hos modellparametrar undersöktes och deras resultat jämfördes med observationer som gjorts vid referensmasugnen. Man fann en relativt god överensstämmelse av resultaten vilket indikerar att modellerna i framtiden kunde användas för att få bättre insikt i masugnsställets komplexa funktion. Speciellt studerades hur koksbäddens permeabilitet vid tapphålen påverkade tappningarna. De stokastiska fluktuationer och den drift man observerade i processdata ger en indikation om det fysikaliska systemets komplexitet och utgör en utmaning vid tolkning av mätdata. On-line-modellen som framtogs kan dock ge en systematisk bild av hur smältornas nivåer i ugnen varierar, vilket möjliggör en bättre reglering av processen. Kommande arbete borde fokuseras på att integrera och tillämpa lovande delar av de olika modellerna för att förse personalen vid stålverket med en bättre bild av masugnsställets ögonblickliga tillstånd. För detta skulle även krävas att off-line-modellerna kunde anpassas till centrala observationer från driften.

Objectives and structure of the thesis

The blast furnace hearth is a complex system with a large number of variables and parameters. A detailed modelling of the hearth requires the consideration of many poorly known phenomena. The main objective of this thesis is to describe the hearth state with models of a reasonable complexity in order to reconstruct and predict the drainage of iron and slag and the evolution of the liquid levels in the hearth. The research work is presented in four articles, which focus on analyzing process data available to develop mathematical models that describe the blast furnace hearth drainage.

The thesis can be summarized as follows. In Chapter 1, an introduction to the topic is presented with some general overview of the iron-making business. In Chapter 2, a brief description of the blast furnace and the production process is provided with emphasis on the hearth and the variables of key interest for the drainage. Furthermore, this chapter also includes a description of the tapping procedure and the tap cycle, as well as the treatment and application of process data. Chapter 3 presents experimental work and mathematical models in the literature that have addressed the hearth state and liquid drainage in terms of the residual slag ratio, liquid levels and drainage pattern as well as pertinent studies about the hearth state. Some conclusions of the literature review are also provided. Chapter 4 includes a brief description of the models presented in the papers of the thesis and the corresponding key findings. Section 4.1 presents an analysis of the outflow patterns of iron and slag based on principal component analysis (Paper I). Section 4.2 introduces the two off-line models developed, for a two-pool hearth with changing pool size (Paper II) and a single-pool hearth with a physical description of the outflows (Paper III). A brief sensitivity analysis of the two models is included in the section. Section 4.3 presents the on-line model of a multi-pool hearth. Finally, Chapter 5 presents conclusions of the work and Chapter 6 suggests possible directions of future work.

List of publications and contribution of the authors

The thesis is based on formulations and results presented in the following four publications, which are referred in the text of the thesis as Papers I-IV. The publications are found in the Appendix of the thesis.

The author of the thesis is the main contributor to these publications. The main author with the expert counselling of supervisors Saxén and Helle developed the mathematical models presented. The author performed the case studies described in the papers and was responsible for writing most of Papers I-IV. Drafts of the papers were revised by the author based on comments from the supervisors. The models were based on process data from BF7 of Tata Steel Europe in IJmuiden (the Netherlands) provided by co-authors Stel, Louwerse and Storm. Particular advising was provided by co-author Shao for Paper II.

I. Roche, M.; Helle, M.; Saxén H. Principal Component Analysis of Blast Furnace Drainage Patterns. *Processes,* 2019, vol. 7, 519.

II. Roche, M.; Helle, M.; v. d. Stel, J.; Louwerse, G.; Shao, L.; Saxén, H. Off-line Model of Blast Furnace Liquid Levels. *ISIJ Int.,* 2018, vol. *58*, 2236-2245.

III. Roche, M.; Helle, M.; v. d. Stel, J.; Louwerse, G.; Storm, J.; Saxén, H. Drainage Model of Multi-taphole Blast Furnace. *Met. & Mater. Trans. B,* 2020, vol. 51, 1731–1749.

IV. Roche, M.; Helle, M.; v. d. Stel, J.; Louwerse, G.; Shao, L.; Saxén, H. On-Line Estimation of Liquid Levels in the Blast Furnace Hearth. *Steel research int.,* 2019, vol. *90*, 1800420.

Table of contents

1. Introduction

Steel is one of the most essential materials in engineering and its broad use in many areas from infrastructure and transportation to domestic appliances and diverse metal products proves its versatility and relevance in the modern world. As new processes, technologies and construction projects have emerged across industries so has the steel demand increased. In 2018, Finland had about 390 kg of apparent crude steel use per capita in contrast with 240 kg of the global use, which represents one example of the high levels of demand among industrialized countries. To keep up with the demand the global production of crude steel has steadily increased for the past decades and particularly at a higher rate during the 21st century even considering the production setback as consequence of the financial crisis of 2009. The world's largest producer, China, reported higher production during that year.

When it comes to the production, the two main types of steelmaking processes are the basic oxygen furnace (BOF) and electric arc furnaces (EAF). Molten iron, the main virgin raw material for steelmaking, is produced primarily via two processes: blast furnace (BF) and direct reduction (DR), where 91.7% was produced in BFs in 2018. About 70% of the total global production of steel comes from the BF-BOF route taking into account the scrap metal recycled. Figure 1 shows the global production of crude steel. The production via EAF has stayed virtually constant over the years, where the rest of production came via BOF. The iron produced via BF has doubled during this period.

The ironmaking process has diversified in recent years and novel techniques have emerged mainly involving direct reduction or flexibility in using different feed materials. However, many of the new techniques are in the early stages of development or represent a modest part of the commercial production. In view of this, the BF process is expected to be the predominant ironmaking practice for the next decades. Even though the blast furnace process is well established, the growing demand and capacity have pushed for higher productivity and efficiency. To achieve these goals it is crucial to develop models and strategies that can guide the operation and suppress disturbances.

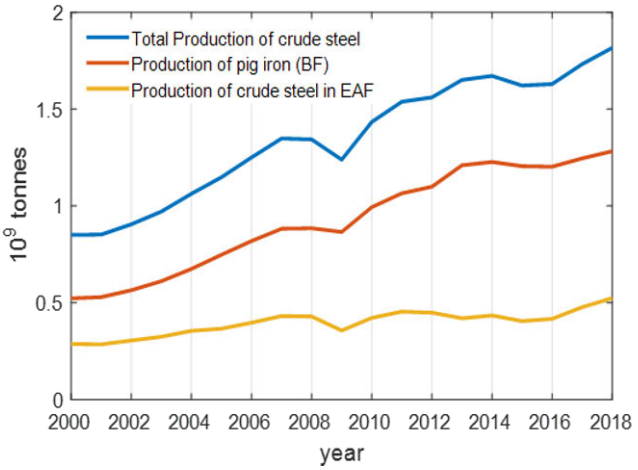

Figure 1. *Total global production of crude steel (blue) and produced by EAF (yellow) as well as iron produced via BF (red) - (worldsteel.org, 2020).*

The hearth plays an important economic and operational role in the performance and for the campaign length of the blast furnace so it has been the focus of extensive research work. Nonetheless, the hearth is a complex system involving several phases and characterized by many variables, making it challenging to describe appropriately by mathematical models. A particular problem is the lack of direct measurements of the internal conditions, so the reconstructed view of the internal state can only be verified indirectly. The state of the hearth and its drainage have been studied with different approaches and the models have contributed to a better understanding of the process, but some assumptions made may have to be revised to provide a better agreement between the simulated and observed behavior. The motivation behind the present work was to develop models and tools for an integrated assessment of the hearth state and a comprehensive use of operational data from the BF hearth.

The summary of the thesis includes a brief description of the blast furnace and the ironmaking process. Different studies connected to the hearth region are reviewed, focusing on methods and models that served as the basis for the present work. Finally, the models developed in this thesis are presented along with the main findings of the analysis that was undertaken.

2. Blast furnace and its operation

This chapter presents a brief overview of the ironmaking process (mainly inspired by the descriptions in Biswas, 1981; Omori, 1987; Cameron et al., 2020a; Geerdes et al., 2015; Yang et al., 2014) as well as a brief survey of relevant research work focused on the hearth region.

2.1 Overview of the process

The blast furnace is a unit process where molten (pig) iron is produced before it is refined into steel in the downstream processes. Essentially, the blast furnace is a large counter-current reactor where chemical reactions, heat and mass transfer occur in the presence of an iron oxide-containing raw material and a reducing agent at high temperatures provided by energy carriers. The blast furnace has a typical conical shape and it can be described in sections or zones.

In terms of inputs, the furnace is charged at the top with alternate layers of iron ore and coke while hot combustion air, blast, is supplied via tuyeres in the lower part of the furnace. Following the burden and coke descent from the throat, the materials are heated by the ascending gas and moisture is removed. Further down in the stack the slightly exothermic reduction reaction of hematite (Fe_2O_3) to magnetite (Fe_3O_4) starts in the presence of carbon monoxide and hydrogen at around 500-600 °C, producing CO_2 and steam released in the gas. Moving down and towards the center of the furnace, the oxygen removal goes further to produce wustite (FeO) at 600-800 °C. As the burden temperatures further increase, some of the wustite will be reduced to metallic iron (Fe), but the CO and H_2 content in the gas are not high enough to fully reduce the wustite. The ore starts softening between 1100 °C and 1150 °C in the region known as the cohesive zone, producing liquid iron and slag, which drip from the lower end of this region where the temperature reaches about 1400 °C. At this stage, the remaining wustite reacts with coke, or with the CO that appears in high concentrations due to the CO regeneration (Boudouard) reaction $C + CO_2 \rightarrow 2CO$, which starts as the temperature gets high enough to make coke reactive. From this zone downwards, coke is the only remaining solid material, through which the liquid iron phase and slag phase, arising from the gangue in the ore, dribble toward the hearth.

The zones in the blast furnace are characterized by their thermal and chemical state at any given moment of operation. Considering the burden from throat to the end of belly (cf. Fig. 2), a characteristic temperature profile of the furnace may show bigger temperature gradients in the horizontal direction than in the vertical one.

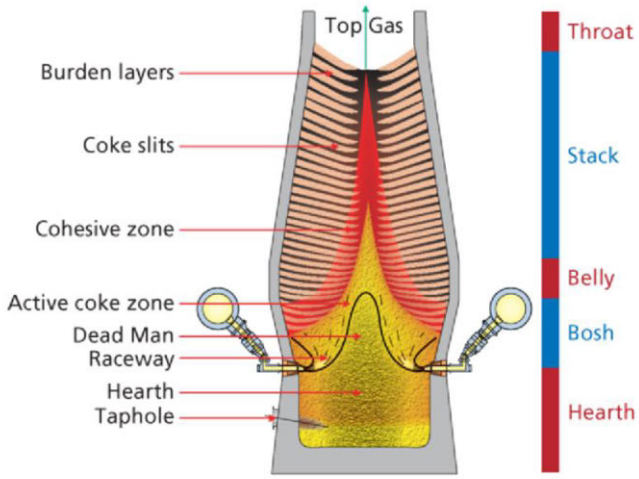

Figure 2. *Schematic of the blast furnace unit and its content (Geerdes et al., 2015).*

The reduction of the iron oxides requires a high temperature and reducing conditions. Energy is partly supplied as hot blast (1000-1200 °C) injected into the furnace via a tuyere system. The main source of energy is coke and hydrocarbons, where the latter by contrast to the charged coke are supplied from below by injection through the tuyeres. Today, the most common auxiliary reductant is pulverized coal. The combustion of coke and the auxiliary reductant occurs in front of the tuyeres at carbon excess, generating carbon monoxide and hydrogen gas at a flame of a temperature of 2100-2300 °C. As coke is consumed a void, raceway, is formed in front of each tuyere. The injection of pulverized coal makes it possible to decrease the coke rate substantially, but in order to ensure a high coal injection rate, the process should be well controlled.

Model calculations based on material and energy balances are used as key elements to guarantee that the conditions stay within feasible bounds. It is, for instance, important that the radial distribution of the solid and gas flows are well balanced in the furnace shaft to make the thermal and chemical conditions for the reduction reactions appropriate. These conditions can be affected by the burden distribution (Mitra & Saxén, 2015a). The more oxygen that can be removed from the burden while it stays in solid state, the better, which can be achieved by an adequate interaction between the burden and gas. For this, the burden permeability plays an important role. Monitoring the top gas composition is important to assess the efficiency of the process (de Castro et al., 2011). Figure 3 shows a typical mass balance of a blast furnace operating with pulverized coal injection (Yang et al., 2014). The thermal

conditions in the process, as well as key operation indices are reported in the figure as a result of material and energy balance calculations.

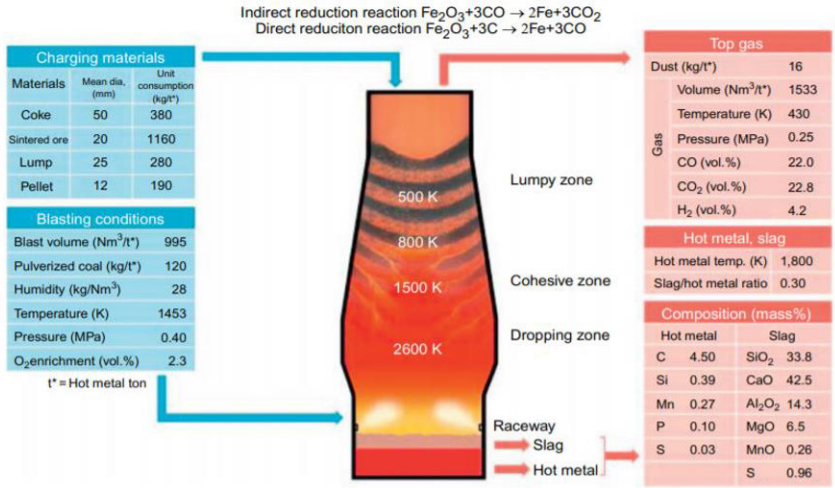

Figure 3. *Typical mass balance and temperature profile of a blast furnace operating with PCI (Yang et al., 2014).*

The productivity of the furnace depends mainly on the air supply. The production rate increases with the oxygen available. However, high gas supply drives up to the pressure drop, which can disrupt the burden descent and the heat balance. To decrease the gas velocity, the operating gas pressure is usually elevated. Thus, the highest productivity is achieved at maximum top pressure permitted and the top gas temperature is slightly above 100 °C with a given burden quality and fuel injection (Liu et al., 2018).

As iron and slag trickle down from the cohesive zone to the active coke zone, where the coke mainly flows towards the raceways, some carbon from coke is consumed to produce Fe_3C in a process called carburization. Both iron and slag descend through a coke bed that occupies the hearth known as the dead man and due to density differences slag accumulates on top of the iron layer at the bottom of the hearth before they are drained out of the furnace through the taphole(s). The dead man, i.e., the central part of the hearth coke bed, will be further described in Section 2.3.

2.2 Iron and slag production and properties

Hot metal is the desired product of the blast furnace process. However, the production of slag is inevitable. The chemical composition of both iron and slag is fundamental when it comes to the product specifications as well as to running the operation smoothly. The specifications are achieved by controlling or adjusting the raw material flow rates and their chemical composition. For instance, the burden composition is a determining factor

for the slag basicity, which, in turn, plays an important role for the sulfur content in the hot metal.

The iron content in hot metal produced (of about 945 kg Fe/tHM) depends on the thermal and chemical conditions, so it can slightly vary with time. The rest of the hot metal, from higher to lower concentration, consists of silicon, manganese, titanium, sulfur and phosphorus. Most of the silicon, titanium and sulfur in the charged and injected materials end up concentrated in the slag, while manganese and phosphorus report mainly to the hot metal. The complex chemical reactions and the temperature conditions in the lower furnace determine the distributions of these elements, which affect the quality of the product.

Besides having an effect on the quality of the hot metal, the composition of slag is a factor of concern since the properties of slag are important for the drainage of the liquid phases. The slag viscosity depends on its melting temperature, which varies with the composition, and mainly with the basicity. At temperatures close to the melting point of the main phases, solid crystals may exist which increase the apparent slag viscosity. As the slag composition can vary, the melting temperature also varies in a range, e.g., 1300-1450 °C. The composition also varies with the temperature, since the partition of several components between iron and slag are temperature-dependent. For instance, at a high thermal state of the furnace, the hot metal silicon content is high, which means a lower silica content of slag and hence increased basicity, which increases the slag melting temperature. This may increase the slag viscosity, which yields a lower outflow rate and an increase in the residual slag volume. The slag composition should be designed so small variations of hot metal silicon content do not lead to significant changes in the required slag temperature (Cameron et al., 2020c). Figure 4 shows the viscosity of slag for a range of basicity and temperature values.

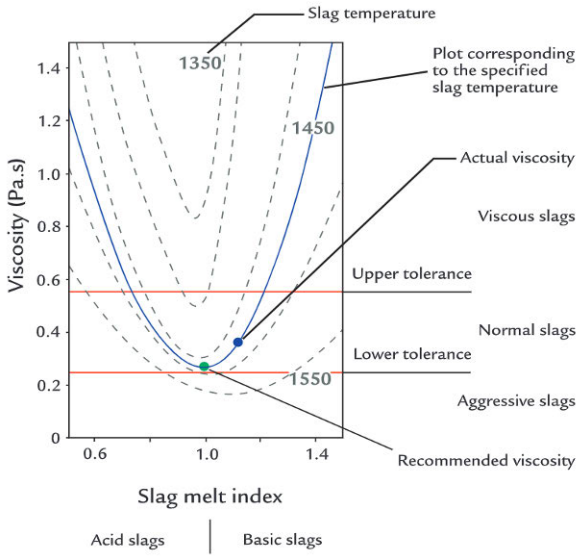

Figure 4. *Slag viscosity at different temperatures and basicity (Cameron et al., 2020c).*

In contrast, the iron melting temperature is considerably lower (about 1150 °C) and well below the average hearth temperature of about 1500 °C and thus its viscosity is a minor concern for the drainage. However, some studies suggest that the viscosity of molten iron increases with the concentration of silicon (Si) and titanium (Ti). The viscosity increase is particularly large at high Ti content at high temperature, about 1500 °C. Some investigators found indications that an increase of silicon and titanium detrimentally affects the taphole depth due to a coupling reaction between Si and Ti in the reduction of TiO_2 in the furnace (Matsui et al., 2006). Furthermore, the furnace temperature is more sensitive to the reduction rate of silicon than that of iron, so the hot metal silicon content is usually used as indicator of the thermal state of the blast furnace (Shi et al., 2011).

Liquid iron and slag densities are also noticeably different. The iron density (6.8-7.0 t/m^3) is more than two times larger than the slag density (2.4-2.6 t/m^3) allowing for an easy separation of the liquids both in the hearth and after they are drained out of the furnace. This stratification of the liquid phases has also an important role for the outflow order, as discussed later in the thesis.

2.3 Hearth and dead man

The hearth is the lowest part of the furnace located below the active coke zone and is the vessel where iron and slag accumulate before being drained. The length of furnace campaign is directly dependent on the durability of the hearth refractories and thus this region represents an essential part for the

furnace productivity and production economics. The hearth walls and bottom are constructed of carbon-based blocks and high-quality ceramics designed to endure the extreme thermal and chemical environment. Inevitably, throughout the campaign the hearth undergoes refractory wear. Severe hearth lining erosion is the cause of costly repairs, which are critical for safety reasons, and so monitoring the hearth lining is an important task to determine the hearth outlook when aiming for an efficient and productive campaign. A system of thermocouples is embedded in the lining in order to indirectly check the lining state. The hearth is also equipped with a cooling system around the steel shell to avoid overheating of the refractory materials. Different erosion models can be found in the literature that estimate the refractory wear and the formation of buildups or skull by tracing the isotherm of 1150 ^{0}C, the melting temperature of iron (Kurpisz, 1988; Swartling et al., 2010; Torrkulla & Saxén, 2000). Overall, the lining temperature profile can potentially reveal some dynamics of the system, indicate the performance of the furnace or even give some indication of the taphole state (Saxén et al., 2000; Swartling et al., 2012, Roche et al., 2017).

Regarding the hearth content, coke particles are the only solid material from the cohesive zone downwards. The coke slowly descends in the hearth along with its consumption by the carburization reactions and by reaction with the metals oxides in slag (SiO_2, MgO, Al_2O_3, MnO), forming a coke bed that extends from the level between the raceways to the bottom of the hearth. The core of this coke bed is referred to as the dead man due to the cone-shape region formed by the repose angle of the deposited coke particles (Yang et al., 2014) and as it was originally thought to be inactive. From here on, the term dead man is simply used to indicate the part of the porous coke bed situated in the hearth below the tuyere level. Figure 5 illustrates the content of the hearth including the dead man (Agrawal et al., 2019).

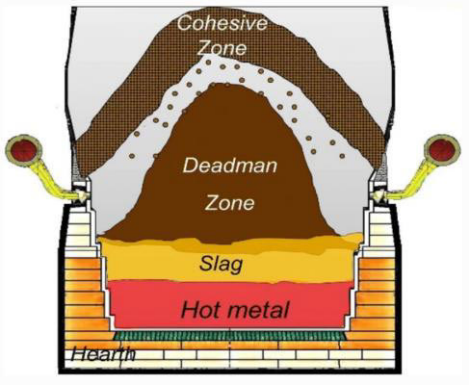

Figure 5. *Hearth and dead man illustration (Agrawal et al., 2019).*

Today, the important role that the dead man has in the process is well recognized. The action of the dead man can be assessed from the chemical and functional point of view. An appropriate dead-man state, in particular its permeability, provides an environment for a proper desulfurization and carbonization of the hot metal, and therefore it affects hot metal quality (Sun, 2005). From the operational standpoint, the dead man protects the hearth from excessive lining wear caused by the extreme thermal and chemical conditions inside the hearth: if the dead man is permeable, an excessive peripheral flow of the liquids can be avoided, which protects the walls from rapid wear. Additionally, the dead man affects the flow of both iron and slag though the hearth and out of the furnace, as discussed later in the thesis.

On the other hand, the carburization reported above can have a negative effect on the performance of the hearth. If the iron is almost carbon saturated as it flows through the dead man, it cannot consume coke fines, which may lead to a gradual clogging of the dead man (Nightingale, 2000).

2.4 Dead-man dynamics

The continuous production and the regular but intermittent drainage prompt volume fluctuations of iron and slag in the hearth. This promotes the coke renewal since the particles are gradually in motion, and some of them can enter the raceways from below. Furthermore, as mentioned above, the carbonization process also drives the renewal of the coke in the dead man as some coke is dissolved in the hot metal and also consumed to reduce residual FeO present in the slag (Sunahara et al., 1993). The total dead-man renewal is estimated to last about four weeks altogether, although the renewal rate varies depending on the hearth region. A higher carbon consumption rate is expected where the liquid flow is stronger and so the region in the periphery is believed to have a shorter renewal time, usually claimed to be in the order of a few days. In contrast, towards the center of the hearth the coke renewal is considerably slower.

An estimate of the total renewal rate can be obtained by considering the difference in the carbon content of the tapped iron and the iron entering the hearth. The reference blast furnace studied in this thesis, BF7 of Tata Steel Europe in IJmuiden, the Netherlands, can be taken as an example. BF7 is a large blast furnace with a hearth diameter of about 14 m and a hot metal production rate of about 9,000 t/d. Assuming the hearth coke to occupy a volume of 1000 m^3, with a bed voidage of 0.35 and a carbon content of 85% in the coke particles, and that the iron entering the hearth has a carbon content of 2.5% and a content of 4.5% at tapping, an average renewal rate of above 3 days is obtained, in general agreement with the numbers reported above.

The active nature of the dead man suggests a dynamic behavior where the bed porosity and coke renewal affect each other with an impact on hot metal

quality. A typical dead-man voidage ranges between 0.2 and 0.5 depending on the coke quality and distribution. Nonetheless, it occupies most of the space available in the hearth and so its role in the liquid drainage is fundamental (Babich et al., 2019).

The dead man is subjected to different forces that determine its state. The forces in balance are the upward forces that come from the buoyancy of the liquid phases in the hearth and the gas drag, while the downward forces acting on the dead man are the results of the burden weight, raceway conditions and liquid static and dynamic holdups (Upadhyay & Kundu, 2013). Because of the balance of the forces, the dead man can float in the iron bath or sit on the bottom of the hearth (Brännbacka and Saxén, 2003). Even though a floating state may keep the dead man active, it can disturb the gas and burden distribution in addition to exposing the bottom lining to potential wear. Many studies have suggested a partial floating dead man, which may arise when the channels with low flow resistance arise at the point where the bottom meets the sidewall (Vogelpoth et al., 1985; Huang et al., 2008). Figure 6 shows an illustration of the inner profile of a quenched hearth of a Japanese furnace, where it is evident that a coke-free zone in the peripheral part occurred during the operation. The carbon powder zone in the dead man center suggests the occurrence of a low permeability zone in the core.

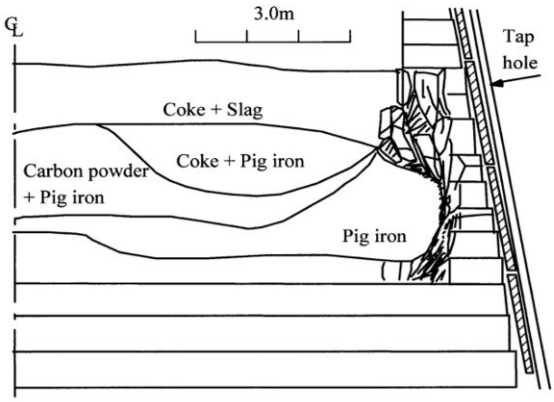

Figure 6. *Inner profile of a blast furnace hearth from a dissection study (Nouchi et al., 2003).*

Regions of low permeability or coke-free spaces force the liquid flow to circumvent the dead man creating a free flow channel around the hearth as the liquids are drained. This can lead to the dead man becoming inactive and induce excessive wear of the wall lining along with an uncontrolled formation/melting of buildups or skull. This state can also be caused by other factors or combination of them, including low production rate, low coke strength and particle size, long stoppages and lining erosion. It can lead to an even more severe erosion profile producing the so-called elephant-foot lining

erosion in the hearth (Torrkulla et al., 2002). The relation between the lining temperatures and the hearth fluid dynamics has been studied with CFD models that simulate both temperature and flow distribution of the phases in the hearth as well as the temperature profile in the refractory lining. These studies have revealed a rather unsettled flow in the hearth with velocity profiles affected by the tapping regime (Shibata et al., 1989; Guo et al., 2008; Shen., 2016; Vångö et al., 2019; Dong et al., 2019). A non-uniform dead man as well as an irregular hearth profile due to erosion have been demonstrated to affect the drainage. Thus, the notion of static and uniform hearth should be reconsidered and the dynamics of the dead man state be recognized. Evidently, the possibility of a compromised dead man is a serious issue that can be detected by indirect measurements such as lining temperatures and material consumption. Temporary or moderate variation in the hearth state that are inconsequential to the long-term operation may occur that could explain certain trends seen in the operation, in particular in the hearth drainage. In models explaining the behavior of the hearth, "well-established" values for the dead-man parameters (e.g., dead-man voidage, particle size) are often used without a strong justification, and the effect of these parameters, or gradual changes in them, has seldom been analyzed. In the opinion of the author, investigators should pay more attention to these issues.

2.5 Material distribution of the blast furnace

The blast furnace geometry and the continuous nature of the process give rise to the requirement of a suitable distribution of the phases in the process. As layers of ore and coke are charged at the top of the furnace, an appropriate radial distribution of the layers is important in order to ensure a well-distributed gas flow due to differences in permeability between ore and coke layers. Large and strong coke is often charged in the center of the furnace to promote a higher gas flow in this region and to provide a steady supply of good coke to the dead man. The burden distribution has an important role in controlling the cohesive zone level and shape and avoiding problems such as irregular burden descent and hangings. An irregular material distribution lower down in the furnace can have a detrimental effect on the flows in the active coke zone and to the dead man, affecting heat losses and possible asymmetry in the lining erosion. The operators rely on indirect measurements in order to estimate how effective the charging is and many models have been developed to simulate this process (Pettersson et al., 2005; Park et al, 2011;Mitra & Saxén, 2015b; Fu et al., 2015; Chibwe et al., 2020).

In addition to the burden, the materials and energy supply via the tuyeres are as important to guarantee a stable operation. The tuyeres are located at equal distance around the periphery of the blast-furnace bosh and each of them is theoretically accountable for an equal fraction of the total production rate. This holds true assuming constant temperature and composition of the

gas injected along with a balanced burden distribution. When PCI is used, an uneven supply of coal in one or more tuyeres changes the consumption of coke locally, and therefore, higher production rate will occur in certain sectors and lower in other. Moreover, if the flame temperature is compromised it affects the thermal balance and leads to asymmetry in the melting-zone level. Different systems are put in place to monitor and correct the coal injection not only to ensure a balanced production, but also safe operation (Geerdes et al., 2015; Helle & Saxén, 2003). Figure 7 illustrates some attributes of the system at different levels in the furnace that add to the complexity of the process.

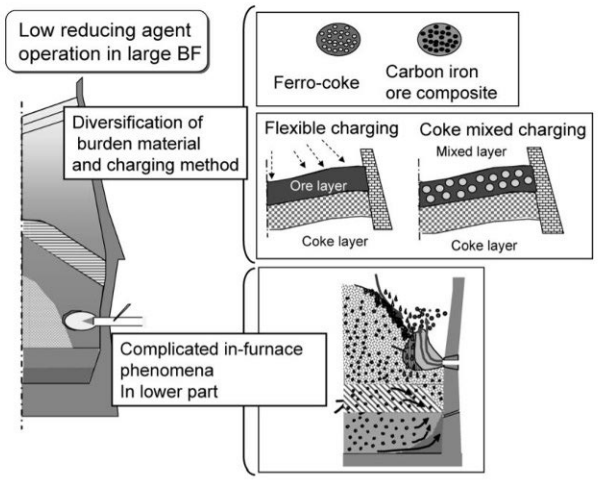

Figure 7. *Different attributes of the furnace process (Ueda et al. 2010).*

Minor or moderate imbalance can arise between different sides of the furnace for various reasons. Such imbalances may go unnoticed or unattended if they do not jeopardize the operation. CFD simulations of the transient multiphase flow in the furnace (e.g., Zhou et al. 2010, Naito et al., 2015, Bambauer et al., 2018) have indicated that flow conditions in the upper furnace may be affected by the state of the hearth, including the volumes of liquid in it. The large dimensions of today's furnaces and the differences in the flow regime in different zones induce a strong spatial distribution of the variables, which directly or indirectly affect the hearth state. Such deviations are potentially reflected in the hearth drainage as the tapping is the last phase of the ironmaking process. In the short term, the liquid levels inside the hearth fluctuate as iron and slag flow towards the taphole and the system approaches a new hydrostatic balance. In addition, the conditions in front of and in the draining taphole affect the drainage process. In summary, the hearth state is strongly affected by the conditions in other parts of the furnace, but also exerts influence on the conditions in those regions, which makes the system extremely complex and coupled.

2.6 Hearth liquid levels

Monitoring the level of the gas-slag interface is of utmost importance since an excessive elevation of the level may indicate a poor drainage and a high elevation also represents a severe safety risk and possible damage to the furnace. In such scenarios, prompt operational actions such as reduction of the production rate or modification of the tapping strategy are required even though they, in turn, can upset the operation. Unfortunately, there is no direct method for measuring the liquid levels in the blast furnace hearth as the region is inaccessible and the conditions are extremely hostile. Still, a tracking of the liquid levels in real time is an important task (Brännbacka and Saxén, 2001; Agrawal et al., 2016). Some potential issues that increase the liquid levels and could lead to an unstable operation are presented in Figure 8.

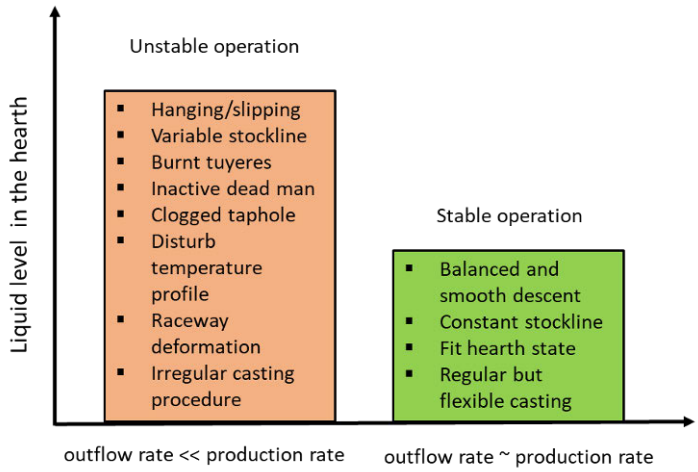

Figure 8. *Potential issues of an unstable operation and liquid level variation and stable one.*

In a stable operation state, the drainage rate balances the production rate, but as the tapholes do not drain at a constant speed some accumulation and depletion of liquids in the hearth always occur, but these are not sufficient to lead to the issues listed in Figure 8. When the total liquid level increases the buoyancy force increases, which can slow down the charging rate, increase the blast pressure and disturb the temperature profile of the hearth if the dead man floats (Torrkulla et al., 2002). High liquid level also can induce a deformation of the raceway deflecting the blast towards the wall and compromising the production and symmetry of the furnace operation.

To properly estimate the amount of slag and iron produced and drained is critical to track the liquid levels in the hearth. The continuous production with a periodical but flexible tapping strategy implies a likely inaccuracy in

the estimates. Furthermore, simplifications and assumptions in the drainage models may introduce additional errors to the estimates that can lead to unrealistic drift in the reconstructed liquid levels. In fact, even stochastic errors with zero mean will lead to drift upon integration, so drift is inevitable in any model, which calls for appropriate procedures to "correct" the estimated levels.

2.7 Taphole and tapping practice

A taphole represents an opening in the refractory sidewall and is a central part of the hearth operation as it is the connection through which the hearth pool of iron and slag is drained. The number of tapholes depends on the furnace size, but medium- or large-size furnaces have typically 2 to 4. In a standard operation, large furnaces operate with two or more tapholes that are alternated during the production. Under this operation state, one taphole is closed while another drains the accessible amount of iron and slag, and the operation then switches to the other, closing the one that operated, etc. Such back and forth switching between tapholes makes it possible to keep the liquid accumulation inside the hearth reasonable, also locally, even though the furnace continuously produces iron and slag.

A taphole is opened by drilling through the refractory at a specific location and it is closed after the drainage is ended by injecting malleable refractory clay through the hole by a clay gun, creating a plug. Alternating between two (or several) tapholes gives enough time for the clay injected to cure but still keeping at least one taphole open for most part of the operation. The drilling and plugging procedure has some functionality beyond creating an outlet for the furnace. For instance, the choice between different available drill diameters allows for controlling the liquid outflow rates. On the other hand, an improper drill positioning can break or expose part of the taphole to erosion. As to the material, when enough mud material is injected the taphole is rebuilt and extended, also forming a protecting region in front of the taphole inside the hearth known as the mushroom (cf. Figure 9). A longer taphole improves the contact between the taphole and the dead man, which maintains the flow through the dead man instead of along its periphery. Additionally, a longer taphole makes it possible to drain the hearth to a lower level due to the taphole angle and larger pressure drop. Conversely, some of the issues with extending the taphole to unreasonable length are the possibility of breaks causing water or gas leakage besides the high operational cost of refractory clay (Dash et al., 2001). It should, furthermore, be noted that the erosion of the inner end of the taphole that occurs during its operation consumes the mushroom, and it is not always possible to extend the taphole length by adding taphole clay due to unfavorable conditions at this location (Tsuchiya et al., 1998).

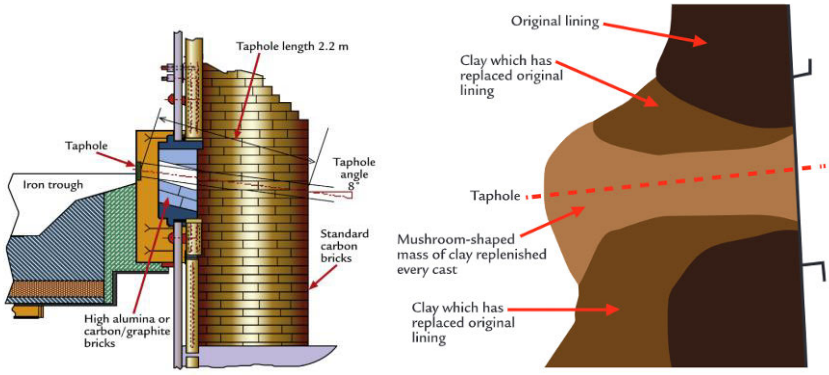

Figure 9. *Typical construction of a taphole (a) and illustration of formation the mushroom (b) (Cameron et al., 2020b).*

The extension of the taphole is considered also a suitable action to reduce splashy casting streams, which accelerates the refractory wear. Gas entrainment is the most significant cause of splashy casting among other factors, such as low drainage rate, taphole blockage and roughness. The taphole extension, however, it is only possible if the mushroom is stable and provides a holding space for the material. This stability can be achieved by shortening the raceway above the taphole (Tsuchiya et al., 1988; He et al., 2002).

The drainage is driven by the differences between the pressures that act on the liquids in the hearth and the atmospheric pressure in the casthouse. The quality of the refractory clay has a major role on the outflows, and particularly the endurance of the material to the thermal and chemical attack of the liquid phases that results in the enlargement of the taphole diameter during tapping (Nouchi et al., 2005). The associated erosion rate is an important parameter in the drainage modeling along with the surface roughness that determines the taphole shear stress. Since a majority of the pressure loss in the system occurs in the taphole, its conditions are central for the drainage, so the decisions concerning taphole sequencing and drill diameter are important. The operator expertise applied in following the casting routines and taking suitable actions in case of deviations is as important as the material and equipment used (Nightingale et al., 2001). However, some occasionally unavoidable external contingencies can disturb the operation. For example, a torpedo may not be placed on time, a delay due to cleaning work or equipment failure may occur, etc. Overall, the flexibility of the casting practice makes it possible to respond effectively to such issues, but it can upset the operation for the following taps.

2.8 Types of outflows and tap cycle

The tap cycle begins when the taphole is drilled open and ends when the taphole is plugged with refractory clay. The period between the outflow start of (any of) the liquid phases and the moment when the liquid outflow stops (usually as a result of an initiation of the plugging procedure) is from here on referred to as tap duration. The immiscible phases of iron and slag form a liquid interface in the hearth. Correspondingly, the slag phase floating on top of the iron is in contact with the raceway gas forming a gas-liquid interface. The taps can be classified based on the first liquid phase observed in the taphole: iron-first, slag-first and simultaneous flow, giving a rough indication of the location of the iron-slag interface in the hearth. The balance between the viscous forces and the gravitational forces governs the evolution of the drainage and the levels of both interfaces are expected to vary accordingly (Nishioka et al., 2005). A more detailed description of the evolution of the liquid interfaces is provided in Chapter 3.

Iron-first taps occur when the liquid interface is above the level of the taphole, so the drainage thus starts with iron-only flow. The liquid-liquid interface descends as the draining progresses and once it approaches the taphole (Liu et al., 2020) a two-liquid outflow is established. The time that elapses between when tap start and this moment is known as the slag delay. After this, a simultaneous outflow of the phases usually continues for the rest of the tapping even though the iron and slag shares in the outflow vary. Normally, this leads to a final state where iron is drained to levels below the taphole, which is made possible by the large pressure gradient in front of the taphole created by the viscous force of slag.

Conversely, slag-first taps occur when the liquid-liquid level is below the taphole. Since only slag flows out initially the iron volume in the hearth increases and the interface rises. Furthermore, the pressure gradient created by the slag outflow facilities a dragging of the iron-slag interface upwards until a two-liquid outflow is established. The low viscosity of iron provides less resistance to the flow compared with slag, which facilities this lifting effect. The iron delay associated with this outflow case can be interpreted as a negative slag delay.

The tap can also start with a simultaneous flow of both phases. This occurs when the liquid-liquid interface is in close proximity to the taphole level or sufficiently close so the tilting of the liquid interface occurs practically immediately after the taphole is opened. For all three types of outflow, the large pressure gradient and high superficial liquid velocity near the taphole lead to the tilting of the interface towards the taphole throughout the drainage, hence maintaining the two-liquid outflow. This effect allows draining iron from below the taphole, even enough to yield a slag-only outflow in the tap that follows from an alternating taphole.

Figure 10 presents the outflow rates of iron (red lines) and slag (blue lines) for six consecutive taps from BF7 of Tata Steel Europe in IJmuiden, the Netherlands, which is a large blast furnace ($d_{\mathrm{h}} = 14$ m) with three tapholes (TH1, TH2 and TH3). The outflows were normalized by dividing the outflow rate by the corresponding (estimated) production rate; thus, a normalized outflow rate of unity implies a balance between the inflow and outflow of the phase in question.

The period shows alternate tapping of tapholes TH2 and TH3, where the left panels show taps from TH2 with slag-first outflow and notable negative slag delay and the right ones taps from TH3 with iron-first outflow and short positive slag delay. On first inspection, the taps show similarities among the iron outflow patterns for a given taphole, but much less similarities as the outflows from the two tapholes are concerned. The drainage is also seen to differ with regard to the outflow to inflow ratio reached and tap duration.

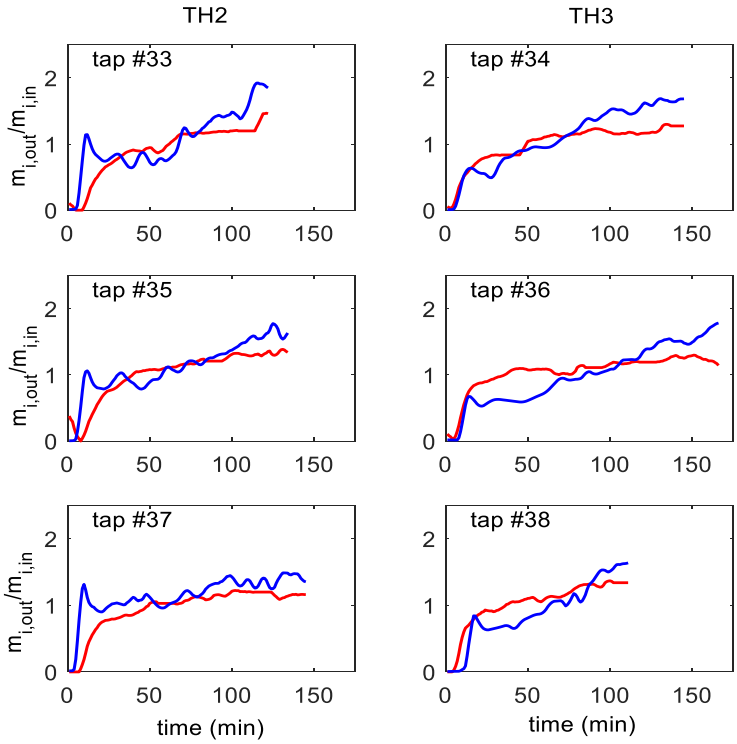

Figure 10. *Normalized iron (red) and slag (blue) outflow rates for six consecutive taps from the BF7 of Tata Steel Europe in IJmuiden, the Netherlands, studied in the present research work*

It is worth noticing that the slag-first taps presented in Figure 10 are qualitatively similar to the tap with negative slag delay in a large Japanese blast furnace (Chiba N^0 6) presented by Nishioka et al. (2005) and depicted

in the left panel of Figure 11. The slag drainage rate initially spikes to decrease to a minimum before gradually increasing again. Meanwhile, the iron drainage rate only increases slightly after the initial spike. This observation is also in agreement with the metal volume ratios presented by Nouchi et al. (2005) from the same furnace shown in the right panel of Figure 11.

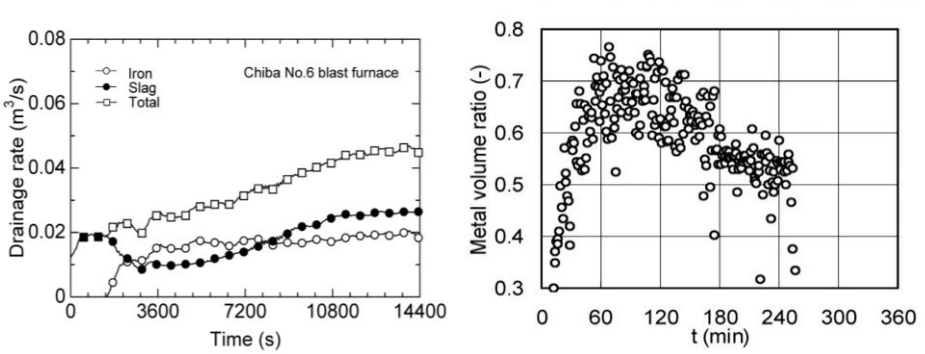

Figure 11. *Drainage rate of a tap from Chiba N^0 6 furnace, Nishioka et al. (2005) (left), and metal volume ratio from reference furnace, Nouchi et al. (2005)-(right).*

The maximum metal volume ratio in the outflow corresponds to the minimum drainage rate of slag during tapping, which coincidentally occurs about one hour after drainage starts in both panels of Figure 11. The balance of the pressure forces dominating the drainage varies during tapping exhibiting a similar pattern. However, a considerable degree of variation between the taps exists.

2.9 Casthouse arrangement and process data

Estimating the liquid levels accurately involves three central aspects: production rate estimates, assessment of the furnace internal state, and outflow rate measurements, where all three aspects are closely related. The instantaneous production rate is calculated from the analysis and quantities of the charged materials in combination with an oxygen balance for the gas phase, assuming the upper furnace to be in a quasi-stationary state. Oxygen is brought into the furnace with the burden as iron oxides, with its moisture and with the blast. On the other hand, oxygen leaves the furnace in the top gas mostly as CO_2 and CO, but also as H_2O. The oxygen balance based on blast parameters and the top gas analysis makes it possible to estimate the instantaneous production rate of iron and, assuming a fixed slag ratio, the production rate of slag. Iron and slag, once tapped, are collected in the through and separated by density differences to two flows in a runner system. The iron flows through a tilted channel into the torpedo/ladle where it can be weighed, while slag flows towards the granulation unit where the

amount of slag can be estimated either using the torque of the rotating granulation drum or a heat balance of water used for slag cooling. Figure 12 illustrates a typical cast house scheme for a three-taphole furnace.

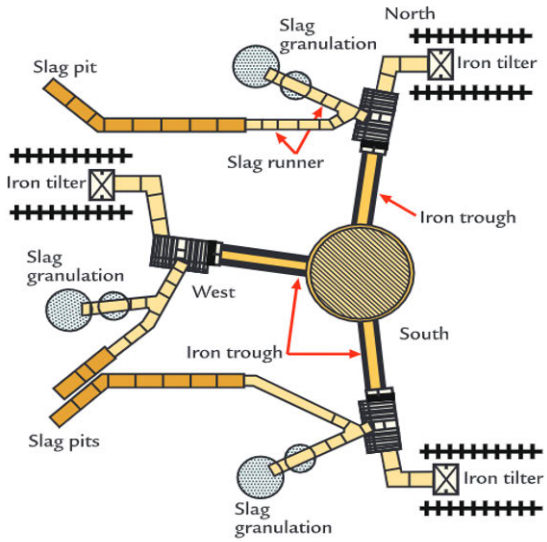

Figure 12. *Typical scheme of the casthouse of a blast furnace with three tapholes (Cameron et al., 2020).*

Estimates of outflow rates reconstructed from such data are presently the best available information about the drainage rates and constitute a source of useful information in order to describe the dynamics of the hearth liquids. The measurements allow corroborating the production estimates and deducing the remaining quantities in the hearth. Nonetheless, the outflow data also indicates a notable short-term variance during tapping and between different taps. Despite these problems, a general understanding of the hearth drainage has been gained based on such data, experimental work (Tanzil et al., 1984, Liu et al., 2020) and results of numerical simulations. Some mathematical models describing the evolution of the liquid levels and the outflow rates will be presented in Chapter 3. The operational data also provides the means to verify some assumptions about the drainage system and also to justify simplifications in the models. Even though a majority of the simulation studies aim to deepen the understanding of the process, the findings can be applied to develop tools that facilitate a monitoring of critical indicators, such as the liquid levels.

3. Drainage studies and hearth modelling

This chapter provides a brief description of some experimental work and mathematical models regarding the hearth drainage in terms of the interfaces and liquid levels as well as different approaches to model the hearth system.

3.1 Process interfaces, residual slag ratio and tap cycle

Early work conducted by Fukutake & Okabe (1976a, 1976b) studied the hearth drainage with experimental work consisting of a single liquid drained from a cylindrical packed bed with an opening in the base of the system. The main focus was to gain a better understanding of the slag drainage. The investigators correlated their experimental results with a dimensionless flow-out coefficient proposed in order to estimate the slag residual ratio or undrained volume of slag in a packed bed. However, this single-phase drainage model neglected the effect of the iron phase on the drainage. It was argued that the lower pressure gradient in the flow of iron would result in iron being drained first followed by iron and slag when the iron-slag interface has reached the taphole level. It was also suggested that the iron-slag interface would stay horizontal after it has descended to the taphole, staying stationary for the rest of the tap. (This would correspond to the case where the iron inflow is perfectly balanced by the outflow in the real process.) The dimensionless flow-out coefficient, F_L, introduced is given by

$$F_L = \left\{ 180 \frac{(1-\varepsilon)^2}{\varepsilon^3} \frac{1}{\emptyset^2 d^2} \frac{\mu}{\rho g} \right\} V_o \left[\frac{D}{H} \right]^2 \qquad (1)$$

where ε is the porosity of the bed, $\emptyset$ the particle sphericity, d the particle diameter, μ is the fluid viscosity, ρ is the fluid density, V_o is the fluid velocity, D the bed diameter, and H the initial height of the slag layer. The term in the parentheses represents the viscous part of the Ergun equation (Ergun, 1952). Some modifications of the flow-out coefficient have been reported over the years. Zulli (1991) modified the expression to account for the effect of iron being drained below the taphole, while Bean (2008) corrected the expression even further to account for the variation of outflow rate.

Tanzil et al. (1984) conducted experimental work to study the effect of the iron phase on the drainage and the validity of the hypothesis of a steady and horizontal liquid-liquid interface. The experimental equipment consisted of a two-dimensional Hele-Shaw model, a two-plate system that can be demonstrated to perform analogously to a packed bed. The system allowed for identifying and tracking both interfaces and the local behavior at the end of the drainage. Air, a glycerol-water mixture and mercury were used as the fluids corresponding to the furnace gas, slag and iron, respectively. The

investigators observed that a one-liquid outflow occurred when the liquid interface is either above or below the level of the exit. Once the liquid-liquid interface reached the taphole a two-liquid outflow was established and as the drainage continued this interface tilted downwards away from the taphole and the heavier phase was drained from below the outlet level. The results also showed that the interface between the air and the lighter phase tilted down towards the taphole after some time, finally ending the stable draining of the liquids. The two-liquid experiment provided justification for a significant correction of the slag residual ratio observed in the one-liquid experiments. However, at low values of the flow-out coefficient (for glycerol) associated with low drainage rates, the pressure gradient was low, and therefore similar results were obtained for both types of experiments (cf. Figure 13). On the other hand, at a higher flow-out coefficient, the viscous forces are sufficient to overcome the gravitational ones and the generated pressure gradient allows a significant volume of mercury to be drained below the outlet level (despite the high density of the phase).

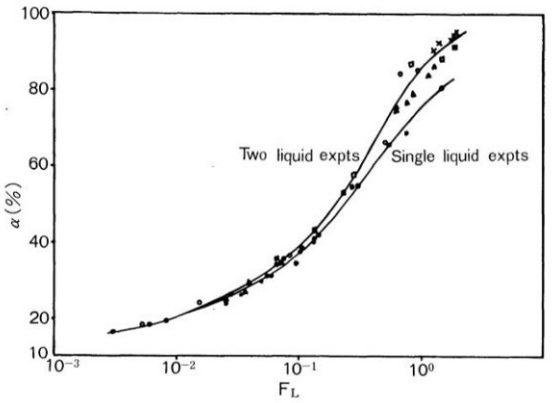

Figure 13. *Comparison of residual glycerol (analogous to slag) ratio measured from single- and two-liquid experiments (Tanzil et al., 1984).*

These findings indicated that a two-liquid approach better describes the drainage and that the distortion of the interfaces occur. It was argued that the viscous forces in balance with the gravitational forces in the vicinity of the outlet governs the drainage while the gravitational forces are more dominant away from the outlet, inducing interface distortion. For the real system in the blast furnace, a similar reasoning is given of why it is possible to drain iron to a level below the taphole. Figure 14 illustrates the interfaces at the end of the drainage for the system of gas (G-phase), slag (S-phase) and iron (I-phase), where D is the diameter of the bed while H_s and H_i express the distance from the taphole level to the overall slag and iron levels, respectively.

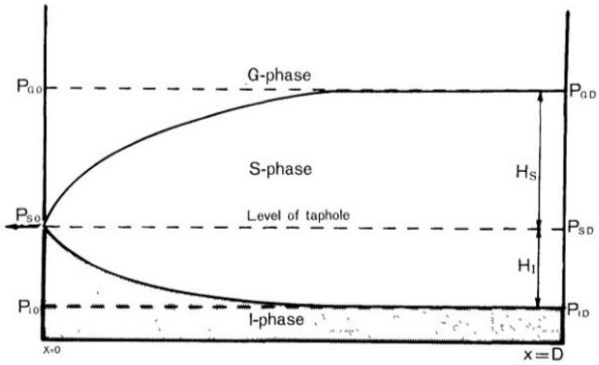

Figure 14. *Schematic of the distortion of the interfaces at the end of drainage (Tanzil et al., 1984).*

Additionally, Tanzil et al. (1984) derived an asymptotic ratio related to the ratio of the residual volumes of the two fluids after drainage according to

$$\frac{H_I}{H_S} = \frac{\rho_S}{\rho_I - \rho_S} \tag{2}$$

where ρ_S and ρ_I are the densities of slag and iron, respectively. Calculating this ratio for the iron-slag system yields that 41% of the total slag volume left after drainage is below the taphole. The two-liquid model reduced the errors associated with the simplification of a single-liquid outflow and stationary interface at taphole. The simultaneous flow and the interface bending are recognized as important features when estimating the liquid levels in the hearth. The proposed expression for residual slag ratio also applies to a three-dimensional system such as the blast furnace hearth. Yet, the fluid flows in the hearth system as well as the pressure profile of the actual system are not taken properly into account. Different attempts to provide a better fitting of the flow-out coefficient are based on experimental settings quite far from those in the blast furnace hearth system and, e.g., neglect possible changes in the conditions in front of the taphole.

In a later work, Tanzil and Pinczewski (1987) developed a drainage model based on their previous finding. The pressure distribution of each liquid phase is solved in the two-dimensional model. It is assumed that the coke bed is homogeneous and isotropic and that the flow within the bed is laminar. The model accounted for the simultaneous fluid outflow previously proposed and it was compared with the results of the two-liquid experiments, as well as with measurements from a large furnace with a high production rate. The results indicated a good estimation of the liquid levels based on the slag residual ratio proposed. However, the model failed to reproduce the variation of iron flow rate seen in the reference furnace, and, in particular,

the initial rapid increase in it. Thus, the two-dimensional approach may be insufficient to model the pressure distribution of the actual system.

Nishioka et al. (2005) carried out a study of the drainage with a similar two-dimensional experimental equipment, but using silicon oil and water as the phases corresponding to slag and iron, respectively. The liquid interface and the air-silicon interface were tracked throughout the drainage. Similar results to those of Tanzil et al. were reported for the cases of an initial liquid-liquid interface above or below the taphole. After a certain time of a single-phase outflow, a simultaneous flow of both phases followed, keeping the local liquid-liquid interface at taphole level. Thus, the heavier liquid, water in this case, was drained below the taphole as the drainage progressed. It is also worth noticing from the results of both Nishioka et al. and Tanzil et al. that a high outflow rate, deduced from the reported time and distance travelled by the interface in the experimental results, occurs during the initial single-phase outflow rate. However, little was said about the outflow rate variation, possibly due to experimental limitations. Figure 15 shows results of the experiments by Nishioka et al. with an interface below and above the outlet at the beginning of the drainage. The figure also shows the calculated location of the interfaces in time by solving the momentum equation in a two-dimensional numerical model.

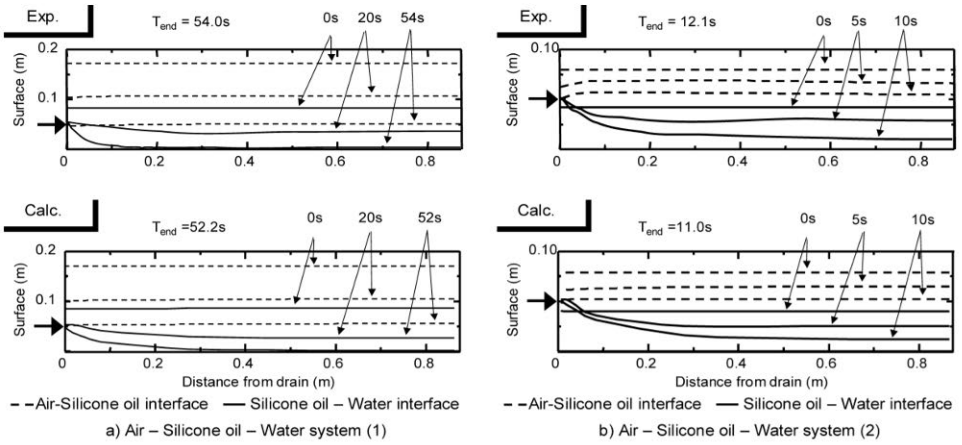

Figure 15. *Experimental and calculated location of the interfaces of the air, silicon oil and water system (Nishioka et al., 2005).*

Such experimental work provided the basis for different assumptions about the hearth system that have been applied in several mathematical models proposed later in the literature. In the following section, the modelling of the system is briefly summarized with a series of relevant studies on the topic.

3.2 Effect of in-furnace conditions in a symmetric hearth

This section presents some drainage models and their sensitivity with respect to main hearth parameters that are known to have an effect on the drainage. These modeling studies are based on basic concepts of fluid dynamics to describe the flow through a packed bed.

Based on experimental work, Nishioka et al. (2005b) developed a mathematical three-dimensional model based on the Navier-Stoke equations and solved by a finite difference method. The model estimates the position of the interfaces of iron-slag during tapping. The interaction between the coke bed and the fluids, $\bar{S}$, was derived from the Kozeny-Carman equation

$$\bar{S} = 180\frac{\mu}{\rho}\frac{(1-\varepsilon)^2}{d_p^2\varepsilon^3}\bar{u} \tag{3}$$

The taphole was modeled as a pipe with diameter, D, and length, L. The total drainage of iron and slag was defined as

$$\bar{u} = \sqrt{\frac{\Delta P D}{2 f \rho L}} \tag{4}$$

where ΔP is the pressure drop in the taphole and the friction factor in the taphole, f, is given by an expression calculated considering the surface roughness of the taphole, the taphole diameter, and the Reynolds number. Similar conditions to their reference blast furnace (Chiba N°6) were applied to the model and the results showed that both interfaces stay tilted towards the taphole with a more pronounced bending by the end of the tap. The left panel of Figure 16 shows results for five consecutive taps in quasi-steady state. These findings, even though more sophisticated, are in agreement with the hypothesis by Tanzil et al. where a distortion of both interfaces occurs as the results of the varying pressure balance terms during the drainage. The right panel of Figure 16 presents a comparison between the simulated base case of a uniformly packed bed with 30 mm of coke particles and a void fraction of 0.3, and presumably a typical outflow pattern from their reference furnace. Even though the overall agreement is good, the model still shows a quite poor fit of the iron and slag drainage rate of the reference furnace at the beginning of the tapping.

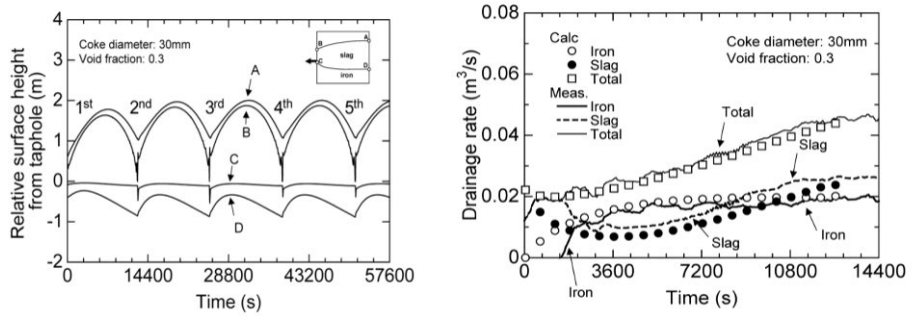

Figure 16. *Distortion of iron and slag interface for simulated consecutive taps (left) and comparison of calculated drainage rate and measured one from Chiba N° 6 blast furnace (Nishioka et al., 2005a).*

A more extensive study of the effect of the in-furnace parameters was presented in Nishioka et al. (2005b) where different cases of the hearth conditions were evaluated with the simulation model. Figure 17 shows the effect of some parameters on the maximum level of the gas-slag interface reached during tapping. Here, the dead-man permeability as well as the slag viscosity were focused upon. The results showed, not surprisingly, that by increasing the void fraction and the particle diameter the maximum level dropped since the change increases the liquid capacity of the bed. By increasing the slag viscosity the level rose, which is expected from the Kozeny-Carman equation (Equation 3). The study of dead-man permeability considering different distributions of the coke diameter, permeability zones and coke-free space, showed that the permeability conditions in the periphery govern the drainage patterns for iron and slag (not shown).

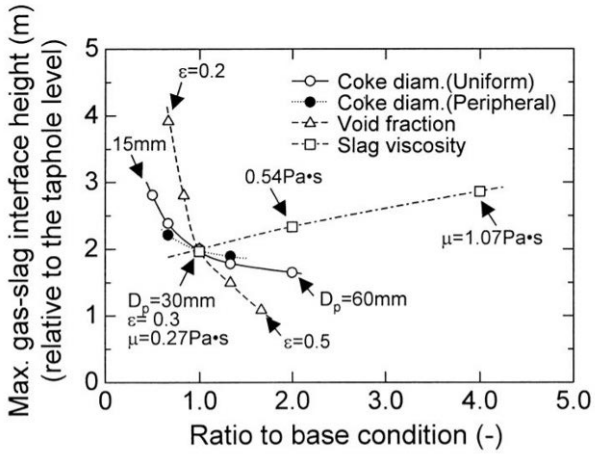

Figure 17. *Effect of some in-furnace conditions on the gas-slag interface level using a mathematical model (Nishioka et al., 2005b).*

Niskioka et al. studied the effect of the coke diameter at constant void fraction on the liquid level, reporting a larger volume of undrained slag and larger volume of drained iron when the coke diameter was decreased. According to the results, by decreasing the permeability of the bed the drainage of slag gets poor, increasing its residual volume while iron is drained below the taphole lowering its level considerably. The effect of the hearth permeability was further studied by Iida et al. (2009) with a mathematical model developed with the working hypothesis of a low-permeability zone in the hearth. The model applied a simplified expression of the share of iron in the outflow that depends on the relative overall level of the iron-slag interface proposed by Nouchi et al. (2003), see next paragraph. The cases studied resemble a partially inactive hearth and dead-man asymmetry; for all cases the slag level shows up to twice the fluctuation that the model predicts for the base case with a dead man with "normal" and uniform permeability.

Nouchi et al. (2003, 2005) conducted a comprehensive study using a two-dimensional experimental scheme consisting of a half cylinder-shaped vessel filled with plastic beads to create a packed bed. Hydrochlorofluorocarbon (HCFC), liquid paraffin and nitrogen gas were used as the phases resembling iron, slag and furnace gas, respectively. An alternate tapping procedure was followed by sampling the liquids through valves located in opposite sides of the equipment.

The results, presented in the left panels of Figure 18, showed that HCFC drainage rate gradually increased for half of the tapping to then stabilize at a rate higher than the inflow rate. The paraffin drainage velocity, however, initially spiked and then after a period of small variation increased again gradually until the end of tap. The experimental results seemed in agreement with the general drainage pattern from a reference furnace. However, a good deal of variation is noticed in their data set (cf. right panel Figure 11). The valve opening was increased to evaluate the effect of different taphole diameters resulting in shorter tapping length and lower slag level in the hearth, and obviously also to mimic erosion of the taphole.

Nouchi et al. (2005) studied the effect of concentric low-permeability zones of 50% and 80% of the diameter of the hearth-like system. The right panels of Figure 18 present the phase ratio and levels for the cases. The most significant effect was the poor paraffin (slag) drainage and some notably different patterns of the HCFC outflow ratio. These results are in general agreement with what Nishioka et al. found concerning the important role of the peripheral permeability on the drainage rate pattern of iron and slag.

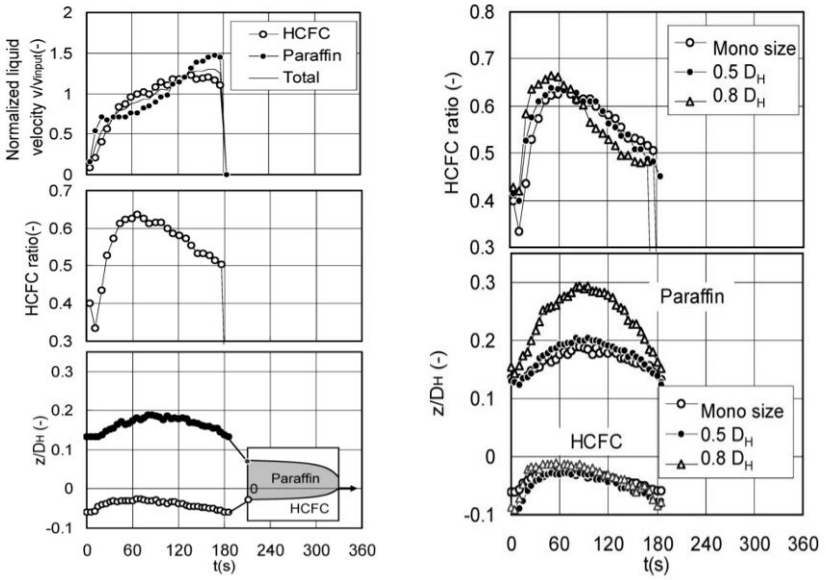

Figure 18. *Liquid velocity, HCFC ratio and liquid levels of nominal experimental (Left) and HCFC ratio and liquid levels of experiments with concentric low permeability zones (right) (Nouchi et al., 2005).*

Regarding the model, the pressure drop of the slag in the dead man (ΔP_{flow}) along the liquid-gas interface (vdt) was described by the Kozeny-Carman equation according to

$$\Delta P_{\text{flow}} = 180\mu_{\text{slag}} \frac{(1-\varepsilon)^2}{d_p^2 \varepsilon^2} v(vdt) \tag{5}$$

and the acting hydrostatic force is expressed as hydraulic pressure,

$$\Delta P_{\text{flow}} = \rho_{\text{slag}}\, g\ \sin\theta\ (vdt) \tag{6}$$

where θ is the angle of inclination of the slag interface. Assuming an equal angle of inclination for both the experiments and the real BF hearth, some scale factors were derived. An expression for the end level of paraffin (slag phase) was also presented as

$$z_{\text{p}} - z_{\text{tap}} = \frac{k_{\text{h}} D_{\text{H}}}{180} \sin\theta = k_{\text{h}} D_{\text{H}} \frac{\mu}{\rho g d_p^2} \frac{(1-\varepsilon)^2}{\varepsilon^2} \frac{v_{\text{total}}}{S} \tag{7}$$

where $z_{\text{p}} - z_{\text{tap}}$ is the level of paraffin above the taphole, k_{h} is a dimensionless arbitrary coefficient, D_{H} the diameter of the hearth system, v_{total} the total volumetric drainage velocity and S the hearth cross-section area. The arbitrary coefficient was defined to scale the experimental results to the blast furnace calculations. This represents another attempt to find a

better tap-end condition than the one provided by the slag flow-out coefficients explained above.

The left panels of Figure 19 show their results corresponding to different openings of the control valve equivalent to different taphole diameter or initial drainage velocity. The right panels present cases with a concentric low-permeability zone corresponding to the experimental results shown in the right panels of Figure 18.

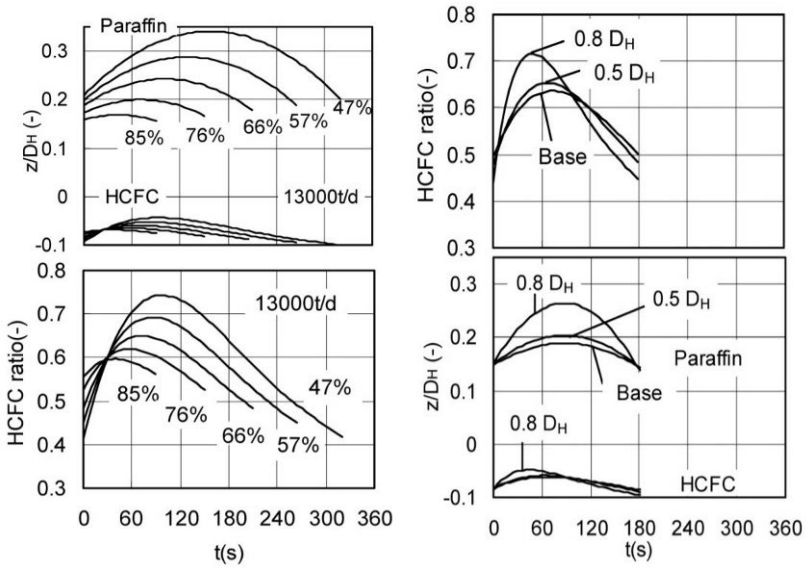

Figure 19. *Effect of initial outflow opening or initial drainage velocity (left) and the presence of concentric low permeability zones (right) (Nouchi et al. 2005).*

The results indicated that changes in the taphole conditions produce various outflow patterns that differ from one another even more than the patterns produced for cases with different concentric low-permeability regions. The differences between the cases are evident with respect to tap duration, outflow pattern (HCFC ratio) and residual slag ratio.

Vångö et al. (2019) presented a CFD-DEM model that attempted to model the drainage pattern and the liquid velocities in a dead man also with a concentric low permeability zone, but further considering the buoyancy effect and an eroding taphole. Even though a large number of parameters were considered in the model, the high computational burden of the approach limits the number of cases that can be studied with the technique.

The literature also presents different grossly simplified simulation concepts of the blast furnace hearth, where basic concepts of fluid dynamics are applied to evaluate specific aspects, such as hearth geometry, sump depth, production rate, slag ratio, and tapping time (Brännbacka et al., 2005).

Shao and Saxén (2011) developed a model with similar scope by taking into account fully stratified phases in the dead man and taphole. The taphole was modelled as a pipe of certain inclination where the shear stress of each phase contributes to the pressure balance. The friction factor for each phase, λ_{liq}, was estimated with the Colebrook equation (Colebrook et al. 1937) for turbulent flow for Re > 2300

$$\frac{1}{\sqrt{\lambda_{\mathrm{liq}}}} = -2\log\left(\frac{2.51}{\mathrm{Re}\sqrt{\lambda_{\mathrm{liq}}}} + \frac{\delta}{3.7}\right) \tag{8}$$

and for laminar flow (Re < 2300)

$$\lambda_{\mathrm{liq}} = \frac{64}{\mathrm{Re}} \tag{9}$$

where δ denotes the taphole roughness and Re the Reynolds number. The pressure drop in the bed for each phase ($\Delta P_{\mathrm{dm,liq}}$) was derived from the Kozeny-Carman equation with a correction factor based on the hearth geometry and the share of the liquid phases in the taphole

$$\Delta P_{\mathrm{dm,liq}} = 180\frac{\mu_{\mathrm{liq}}(1-\varepsilon)^2}{\pi(\xi D_{\mathrm{p}})^2\varepsilon^2}\left(\frac{1}{R_{\mathrm{th}}} - \frac{1}{R_{\mathrm{h}}}\right)\left(\frac{D_{\mathrm{liq}}}{D_{\mathrm{ir}} + D_{\mathrm{sl}}}\right)^3 \dot{V}_{\mathrm{liq}} \tag{10}$$

where R_{th} and R_{h} are the taphole and hearth radius, respectively. D_{liq}, D_{ir} and D_{sl} are the equivalent diameters of each phase in the taphole. The authors reported that an improvement of the bed permeability in terms of higher void fraction and larger coke diameter lowers the tap-end level of slag. The study also suggested that a larger pressure drop in the bed results in iron being drained to lower level. The model, however, only considered uniform bed conditions that are unlikely to occur, in particular near the taphole entrance (Shao, 2013).

When developing a model aside from taking into account a sufficient number of variables it is also important to consider different system indicators or responses. Brännbacka et al. (2005) presented a model to evaluate the effect on the slag delay of some key variables such as bed porosity, hearth diameter, liquid production and tapping strategy. Even though the model considered a simplified tap cycle, the calculations showed significant variation of slag delay under different states of hearth buoyancy. Moreover, the slag delay estimates were correlated with those from two Finnish blast furnaces. The study identified the slag delay as a relevant indicator of the hearth state and liquid levels. However, to better describe the hearth drainage a more detailed description of the pressure loss is required.

From the studies described above, it can be concluded that uniform or symmetric hearth conditions in the models can reproduce some general

characteristics of the drainage, but the descriptions cannot appropriately reproduce certain outflow patterns seen in the real furnace. In the following section, the possibility of asymmetry in the system is addressed.

3.3 Hearth asymmetry and modelling of hearth dynamics

The studies presented thus far were aimed at capturing the main characteristic of the hearth drainage and to evaluating the system behavior under different conditions. This section presents studies that address the dynamics of the hearth by modeling the systems under assumptions other than those based on a uniform, symmetric and static hearth description.

Several authors have studied the possible correlation between the in-furnace state and the hearth temperature. Iida et al. (2008) pointed out some correlation between tap duration and hearth temperature. The authors showed some rather loose correlation of a longer tap with higher bottom temperature from an extensive data set from two blast furnaces, even though both variables fluctuated significantly. Sawa et al. (1992) pointed out that the heat transfer coefficient between molten iron and the lining was too large to induce a significant skull formation, and that (short-term) lower temperatures in the refractory lining were more likely an indication of the formation of a low permeability zone. With respect to the dead-man permeability, Post et al. (2005) suggested that some of the coke consumption and its dissolution in molten iron occurs unevenly in the hearth, which can lead to a local increase of the coke-bed void fraction, particularly in the vicinity of the taphole. These hypotheses essentially underline the possibility of a changing and non-uniform dead man.

Iida et al. (2009) recognized that an oversimplified view of the hearth is insufficient for explaining the actual drainage measurements. The authors developed a model consisting of a packed coke layer and a taphole. A coke filter in front of the taphole was considered to model the coke bed in contact with the taphole. The carbon dissolution into molten iron during tapping was taken into account by a mass-tranfer expression affecting the state of the coke filter. The drainage rate was controlled in the model by the passing speed through the filter and the taphole. The pressure drop in the coke filter was derived from the Kozeny-Carman equation and the pressure drop in the taphole by the Darcy-Weisbach equation. Figure 20 shows a schematic of the model. The taphole length was assumed to be $L_2 = 3.5$ m while the resulting coke-filter length, which was subject to adjustment since the model was sensitive to it, was found to be only $L_1 = 8$ cm to make the model match the observed draining characteristics. The high pressure drop in the filter is a result of its one-dimensional treatment, where the liquid has the same velocity as in the taphole.

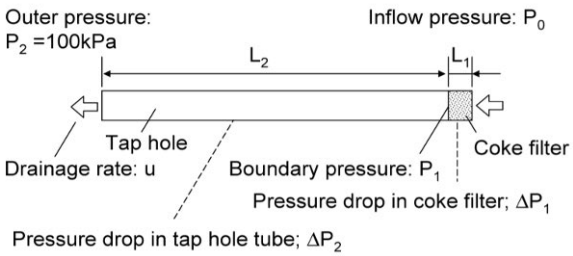

Figure 20. *Schematic of the mathematical model of Iida et al. (2008).*

The rate of dissolution of coke was based on the studies by Sunahara et al. (1992) and Sun et al. (2005) and was expressed to yield the void fraction in the coke filter by assuming that the coke particles in the filter stay at fixed positions and only shrink, thus influencing the drainage rate. Based on the observed and calculated drainage, which indicated shorter tap duration with lower iron saturation, the authors hypothesized that a low degree of carbon saturation in the molten iron indicates the presence of a low-permeability zone. They argued that a low-permeability zone results in a shorter time from the moment when the liquids drip into the hearth until they reach the taphole. Moreover, it was claimed that the conditions in front of the taphole are as relevant as the taphole diameter or taphole enlargement (i.e., erosion) rate when it comes to controlling the total drainage rate, but little was said about the difference between iron and slag drainage rate during tapping. Figure 21 shows the calculated tap duration against the erosion rate of the taphole diameter and the initial void fraction of the coke filter at different saturation of iron entering the filter. A broad range of tap durations are produced by the model, just like observed in the real system.

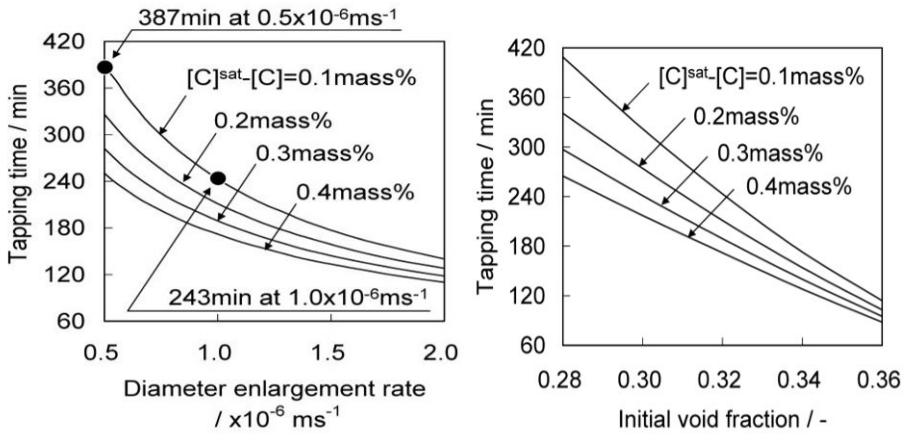

Figure 21. *Calculated tapping time for different taphole diameter enlargement rate (left) and initial void fraction (right) at different molten iron saturation (Iida et al., 2008).*

Iida et al. (2009) expanded their previous work by incorporating an alternate tapping model, as described by Nouchi et al. (2005), in their model of the taphole and coke-filter system. It included a non-uniform distribution of iron and slag inflows based on the concept of low permeability zones proposed by Watakabe et al. (2000). With respect to the dead man, a vertical plane of low permeability was considered, dividing the hearth into two sections, one for each taphole. Even though the plane prevents slag from permeating between the sections, metal was allowed to flow below it. This assumption limits the volumes available to drain in each section since it allows the descent of the slag interface in the draining section at a higher rate and the pressure balance becomes different between the two sections. This fundamentally changes the drainage rate and the iron/slag share during tapping and between taps.

Unequal conditions between the tapholes with a low-permeability zone in the hearth were tested in the model. The results were compared with operational data corresponding to 100 days of production of a blast furnace in Japan, which showed significant differences between tapholes in terms of daily average liquid quantities and daily tapping time as well as the carbon content in hot metal and FeO in the slag. The model was able to reproduce the general behavior of the drainage. However, it failed to reconstruct the initial part of the drainage.

The case that considered a vertical low-permeability wall (VLPW) that divided the hearth into two fixed sections of different size yielded uneven amounts of iron and slag between the tapholes, similar to the imbalance seen in the data. The model also anticipated that such a hearth state would yield a significant variation of the slag level. Figure 22 shows the unbalanced drainage between the two tapholes from the multi-taphole furnace studied. The taps are fairly disperse, but a distinction between the tapholes is noticed. The figure also shows the calculated iron and slag drainage rate for each taphole for the case of a VLPW at the TH1 side and a higher carbon saturation for the TH2 side. Figure 23 depicts the calculated slag-gas interface levels for the case with and without VLPW. The results show that the presence of a VLPW not only significantly affects the liquid level but also the tap duration.

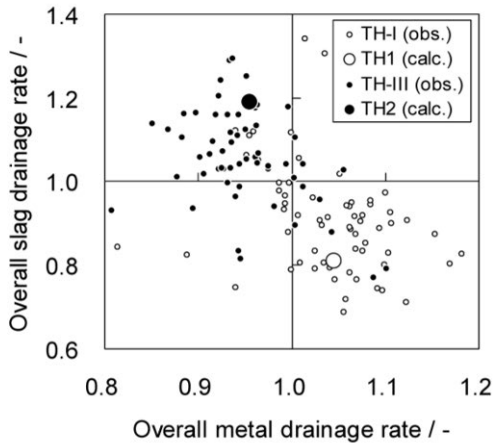

*Figure **22.** Overall iron and slag drainage rate from two tapholes from the reference BF and calculated average from the case of VLPW and different liquid phase content (Iida et al., 2009).*

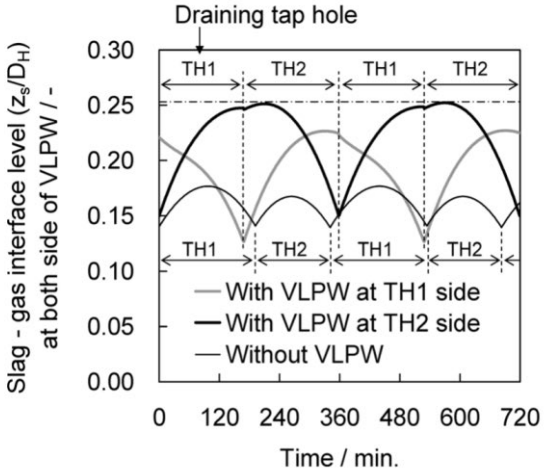

***Figure 23.** Simulated slag level for different cases of VLPW (Iida et al., 2009).*

The discrepancies between the model results and the practical findings might be due to invalid assumptions about the flow between the sections. Nonetheless, the study addressed the imbalance observed between tapholes with a comprehensive evaluation of the hearth system that included the taphole, dead man and composition of iron and slag. This approach provided insight into the conditions in a blast furnace hearth in a non-uniform state and the implication of it on the liquid levels.

Saxén (2015) made a similar approach with respect to dead-man asymmetry in a simple hearth model. The work described the quasi-

stationary drainage of a two-taphole hearth system with a vertical low-permeability zone and a dead man that possibly floats. The low-permeability zone proposed divides the hearth in two pools, but contrary to the work conducted by Iida et al. (2009) the flow of iron and slag between the pools was permitted and controlled by cross-flow coefficients. The flow was defined as driven by the pressure difference of the phases between the pools.

The model flexibility allowed studying the permeability of the coke bed on a broader extent. The findings suggested that a partially floating dead man lowers the slag level as well keeps the iron-slag interface close to the taphole level, shortening the slag delay. Moreover, the slag delay shortened when the iron flow between the pool improved or when the slag flow decreased. Conversely, the residual slag in the hearth varied little at different rates of flow cross-pool communication. The dead-man buoyancy and the pool communication had a significant effect on the slag delay but modest effect on the slag end level, to achieving that, a range of different outflow patterns must occur as reported by other authors (Iida et al., 2009; Torrkulla et al., 2002; Brännbacka, 2003).

In a more recent work, Post (2019) studied different hearth profiles and local hearth conditions by developing a dissolution model and a coke-bed packing model. The 3D CFD simulations without considering dissolution and under different cases of liquid inflow distribution showed that in the region near the taphole the liquid flow (streamlines) converges in the taphole from all directions. Far from taphole the formation of vortices and flow in the periphery occurred. The considerably higher flow velocity near the taphole indicate that a detailed description of the pressure loss in the coke bed is required when modeling the hearth.

When carbon dissolution was considered the coke volume fraction varied depending of the hearth region. Figure 24 shows the voidage distribution corresponding to the system in steady state. Due to the velocity profile and flow path, a coke-free zone was formed in front of the taphole and near the wall and corners were the high flow velocity promoted carbon dissolution. As the formation of these zones depends of a particular flow distribution it can be inferred that in multi-taphole furnaces considerable differences in size and shape of the cavity in front of tapholes may arise. The results implied the possibility of different degrees of contract between the dead man and the taphole, which also makes necessary a revision of the modeling assumptions when describing the hearth state.

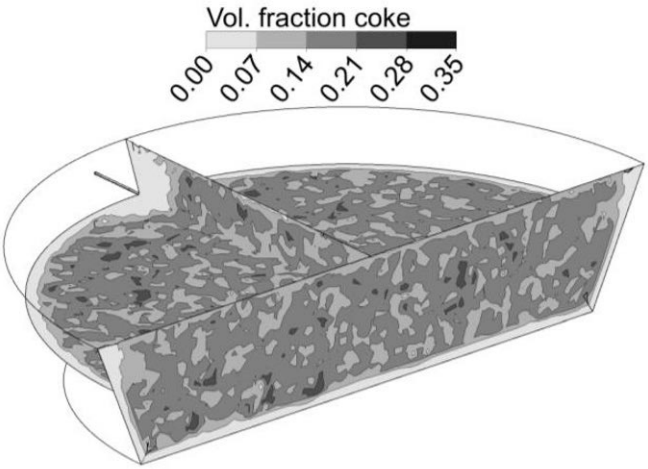

Figure 24. *Residual coke volume at steady state for a simulation considering carbon dissolution (Post, 2019).*

3.4 On-line models and applications

The harsh environment in the blast furnace hearth makes it impossible to directly measure the liquid levels, so instead the problem has to be tackled by other techniques if on-line estimates are desired. The most obvious way is by stating balance equations for the hearth liquids and solving these with respect to the levels. Besides mass balances, discussed briefly at the end of this subsection, several indirect techniques are available to estimate the levels of the liquids in the hearth. These include measurements of electromotive force (emf) or furnace expansion with strain gauges at the furnace shell (Hattink et al., 2008), and the injection of pressurized nitrogen via an unused taphole (Desai, 1993; Danloy et al., 1999).

The electrical potential difference, or electromotive force, measured by electrodes attached to the furnace shell is claimed to arise due to chemical reactions in the hearth in combination with the different conductivities of metal, slag and lining material (Dorofeev & Novokhatskii, 1984). As a continuous signal, it has the advantage to being available on-line, but the emf often shows serious drift and noise, so an application of it for liquid-level estimation is not straightforward. It has further been found to depend on the thermal state of the system, which complicates its application in practice. Many "promising applications" have been reported in the literature, but most investigators only provide illustrations of a few taps, and usually fail to report how drift in the signal could be addressed to provide useful information in real time and not only in retrospect. The paper by Ito et al. (2014) is among the few detailed and serious attempts to address the problems associated with the use of emf for liquid level prediction. These authors applied the

technique to a Japanese furnace and the estimated levels around the circumference, suggesting that the iron and slag content was distributed non-uniformly in the hearth. The method, however, only seemed to provide a general correlation between production and liquid level and neither the fluctuation during the tap cycle nor the influence of the hearth state on such imbalance were addressed (Ito et al., 2014). Gomes et al. (2016) approached the problem by a data-driven prediction of the liquid levels based on emf signals, using information about the cyclic behavior in a time series model of ARIMA type, also considering neural networks for non-linear prediction. These authors carried out a detailed study of the characteristics of the emf signals, but finally only predicted the emf without coupling it to estimated liquid levels. Furthermore, the model used is based on detected periodicity of the signal, which means that the predictor has little chance to perform well if the duration of the tap cycle changes.

Saxén & Brännbacka (2005) developed a mathematical model to track the iron and slag levels in the hearth in real time as well as predicting the end of the tap based on "measurements" of the liquid outflows (reconstructed from iron levels in ladles and slag flow to the granulation drum) as well as on-line estimates of the production rate. The model included a filtering procedure for preventing excessive drift in the level estimates. In an attempt to improve the accuracy of the model, emf signals were incorporated in the estimation procedure as additional information. Figure 25 shows some results of the approach, which hold some promise for future application, but the method needs further refinement to demonstrate its generality.

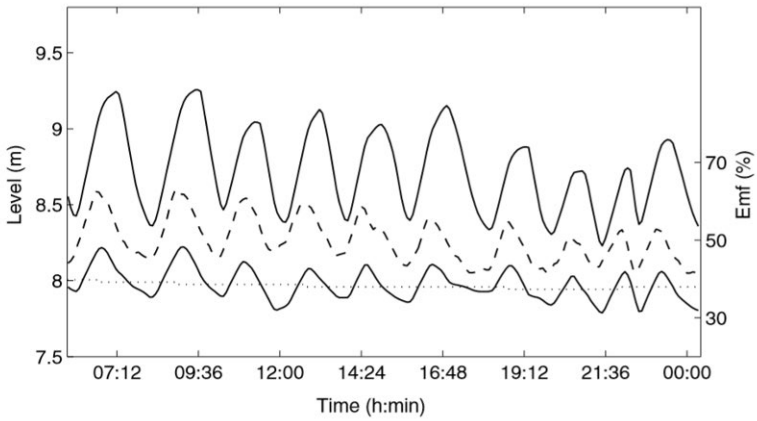

Figure 25. *Estimated slag level (upper line) and iron level (bottom line) with partially floating dead man and the (scaled) emf signal (dotted line), Saxén & Brännbacka (2005).*

An additional concern when developing tools to be used on day-to-day basis in the cast house is how fast the estimates are obtained. The model must be

able to process the available information conveniently so appropriate actions could be taken in time, if necessary. Consequently, a trade-off between a detailed description and the computational time is required.

3.5 Conclusions

The drainage of the furnace hearth has been studied with experimental settings analogous to the real system and the tapping procedure has been mimicked in innovative ways. Yet, the hearth is a complicated system and a simple experimental setting often lacks the required complexity to provide sufficiently detailed information about the hearth drainage. Nevertheless, the findings of the experimental models have supported the development of mathematical models that have deepened the understanding of the process, in particular how the iron-slag and the slag-gas interfaces develop during the drainage. The analysis of the operational data included in some studies revealed the intricacy of the process. Due to the simplifications and assumptions in the models, the liquid drainage rate predicted by different models usually showed a modest fit to iron and slag outflows measured in real blast furnaces. Nonetheless, monitoring and control of the material and energy balance in the furnace remains important to ensure a safe and efficient operation.

To study the hearth most authors have described the processes with a set of mathematical expressions based on principles of fluid dynamics. The taphole conditions and the dead-man state, in particular its permeability, have been identified as central aspects for the drainage. However, the changes that both the taphole and dead man undergo during each tap and along the campaign have not been clearly identified. Due to the lack of direct measurements, the validity of the models still depends heavily on appropriate assumptions and simplifications.

4. Models developed in this thesis

This chapter briefly describes the models developed in this thesis, including the main assumptions made, central equations, key findings as well as a brief interpretation of the results. The chapter is divided in three sections: Section 4.1 presents a study of the liquid outflow data, Section 4.2 introduces two off-line models, while Section 4.3 presents an on-line model.

4.1 Process data analysis and outflow classification

Drainage data of a blast furnace, i.e., outflow quantities or rates, are one of the most reliable sources of information about the production and accumulation/depletion of iron and slag in the hearth. Even though an extensive amount of tap data is available throughout the campaign, the unprocessed data is corrupted by noise and drift so to make it useful it has to be carefully filtered and interpreted.

The process data for this thesis was gathered from blast furnace N° 7 (BF 7) of Tata Steel Europe, The Netherlands. This blast furnace has a hearth diameter of 14 m and counts with three operating tapholes, here labeled TH-1, TH-2 and TH-3 as shown in the left part of Figure 26. The data analyzed consists of two data sets, Data set 1 and Data set 2, of three and six months worth of measurements of liquid outflow rates, respectively. The iron outflow rate was obtained from torpedo weighing while the slag outflow rate was estimated based on measurements from the granulation unit, both as one-minute averages. Using the casthouse records each tap was identified. Figure 26 also shows the tapping schedule during these periods as part of the casting strategy of alternate tapholes. The solid-line rectangles indicate the periods described in Section 4.1 and the dashed-line rectangles represent additional periods studied in Paper I.

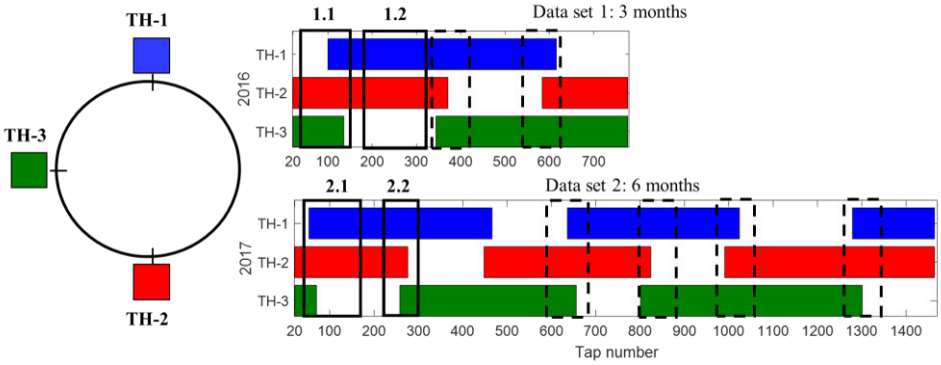

Figure 26. *Taphole location in the reference furnace (left) and operating periods of the tapholes for the Data set 1 (right top) and Data set 2 (right bottom). The sub-periods studied in following sections are also indicated.*

A tool was developed in order to compress and classify the taps according to the outflow patterns by applying principal component analysis (PCA) to the available data. This method allows reducing the dimensionality of the data by transforming a multi-variable data into another coordinate system with few variables or components. The method reports the percentage of total variance explained by each component and so taking into account a few components might be enough to describe the essential part of the data with sufficient accuracy. Therefore, the components can replace the original data (Kourti, 2009; Bartholomew, 2010). Since PCA is scale-dependent, the tap outflow rates were normalized by calculating the slag share defined as

$$S_{\mathrm{slag}}(i) = \frac{m_{\mathrm{slag}}(i)}{m_{\mathrm{iron}}(i) + m_{\mathrm{slag}}(i)} \tag{11}$$

where i denotes the time, while $m_{\mathrm{iron}}(i)$ and $m_{\mathrm{slag}}(i)$ are the corresponding mass flow rates of iron and slag, respectively. The tap duration was normalized by down-sampling S_{slag} to ten average points. This information preprocessing guaranteed that essential features of the outflow patters were retained, and that single "outliers" did not play an important role for the classification.

Figure 27 shows some examples of the pre-processing of the samples, including a slag-first tap (# 371) and an iron-first tap (# 596). The left panels show the original outflows, the center panels show their corresponding outflow normalization applying Equation 11, and the right panels finally show their 10-point normalization along with their reconstruction using the PCA results.

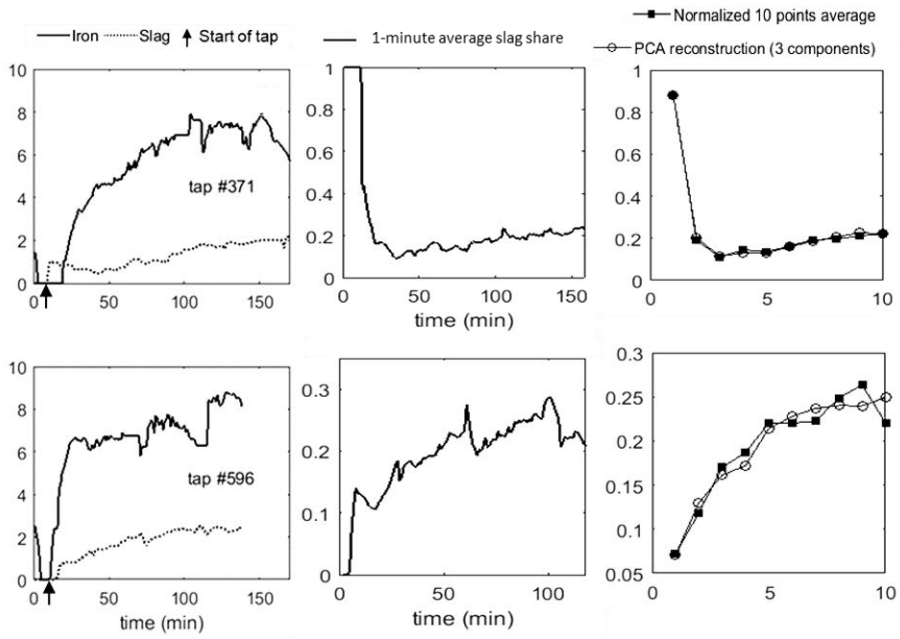

Figure 27. *Examples of liquid outflow patters from the Data set 2 (left panels), with their corresponding slag share (middle panels) and discretized 10-point patterns (solid squares) and PCA reconstruction (open circles) in the right panels.*

The method was applied to each data set yielding for each sample values in the principal component coordinate system. The normalized outflow patterns corresponding to the limits of the main component domain were then constructed. These patterns represent the limits of the components in the original data, as shown in Figure 28. After studying the results, it could be hypothesized that the first component (C1, top panels) largely reflects the initial stages of the tap, i.e., indirectly the slag delay, where a value near zero corresponds to iron-first and near one to slag-first drainage. The second component (C2, middle panels) captures mainly the overall level of the slag share. The fourth component for Data set 1 (C4) and third components for data set 2 (C3) represent the trend in the slag share during tapping. Thus, the method has identified three main drainage characteristics in both data set separately: the proximity of the iron-slag interface to the taphole when it is opened (C1), the iron and slag mass distribution (C2) and typical outflow rate progression (C4, C3), also discussed by other authors (cf. Figure 11 and 23). The panels in Figure 28 also show the percentage that each component contributes to the representation of the data. It is worth noting that C2 does not only reflect the overall slag ratio, which in the blast furnace depends on the burden composition and rate of reductants, but also on the distribution of the slag between the tapholes, as discussed in Section 3.3.

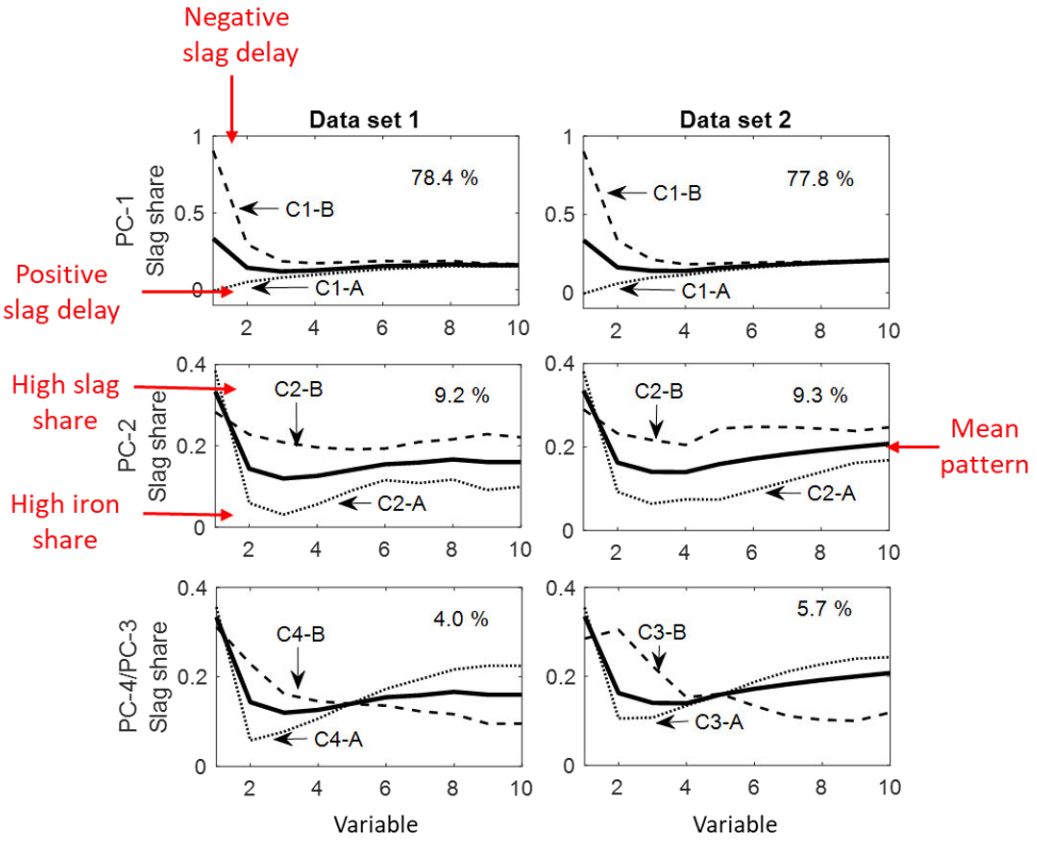

Figure 28. *Slag share ranges represented by the principal component for Data set 1 (left panels) and Data set 2 (right panels). Solid lines represent the mean pattern, dotted lines the lowest values (labelled A) and dashed lines the highest (labelled B).*

The right panel of Figure 29 shows the position of all outflow samples regardless of taphole in the 3-dimensional principal component space (C1, C2, C3) corresponding to Data set 1. The left panels show the equivalent patterns of the mean values for each taphole. At first inspection of the distribution of the data points, the difference between tapholes is apparent suggesting an uneven distribution of the liquids expected in a large hearth with multiple tapholes. This effect was also pointed out in studies by Iida et al. (2008), Nouchi et al. (2005) and Nishioka et al. (2005b).

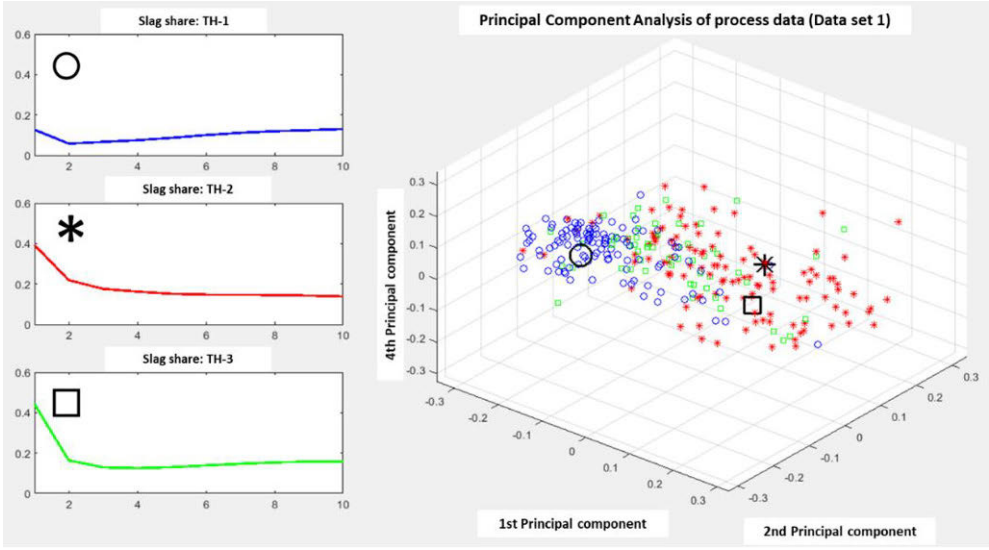

Figure 29. *Three-dimensional representation in the principal component coordinates of the sample points from Data set 1 (right) and the 10-points outflow pattern corresponding to the mean pattern for each taphole (left).*

As some distinctive patterns between tapholes emerge, the occurrence of them along the evaluated periods was also of interest. A 20-point moving average of the selected principal components was applied (representing roughly two days of production) for each taphole. This post-processing criterion yielded a quasi-time evolution that even if it lacks the accuracy to provide detailed information about the system from tap to tap can give some indication of how the system responds to changes in the liquid distribution and volume fluctuation. Figure 30 shows the evolution of C1 vs C2 for two periods of each data set (cf. Figure 26). A study of several other periods can be found in Paper I. The limits of the figure's plane correspond to the outflow patterns illustrated in Figure 28 for each component and the plane center represents the *mean pattern* also indicated in Figure 28. The tapholes displayed significant differences in terms of slag delay and slag share, in particular when a taphole was taken into operation (Period 1.1 and 2.1). Conditions such as the mushroom size and dead-man permeability in front of an inactive taphole are expected to be different from one that has been in operation for several taps. After some taps the "new" taphole operation often shifted towards the *mean pattern* while the other taphole shifted to compensate for the imbalance either by drifting apart (Period 1.1) or converging to a similar pattern (Period 2.1). It was found that the drainage system as a whole can reach a balanced drainage (Period 1.2) but can also maintain an imbalance seen in the slag delay and/or the liquid distribution (Period 2.2).

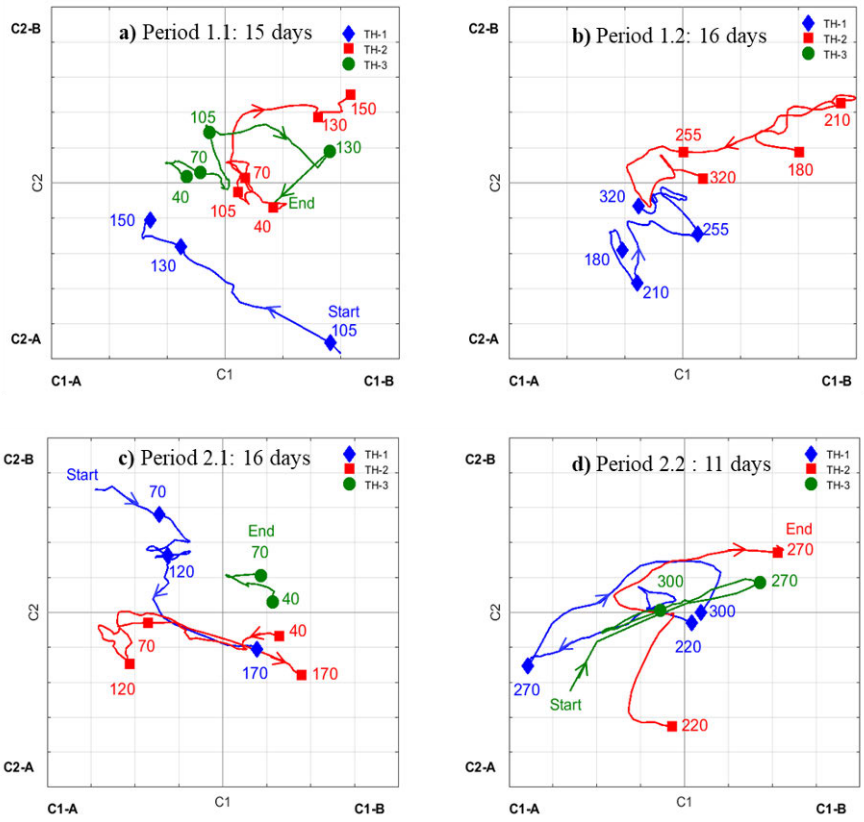

Figure 30. *First vs. second principal components (C1,C2) corresponding to Period 1.1 and 1.2 from Data set 1 (top panels) and Period 2.1 and 2.2 from Data set 2 (bottom panels).*

The additional component considered for each data set, C3 and C4 (cf. Paper I) captured a characteristic feature of the drainage where the slag outflow decreases to a minimum to then increase steadily, as reported by other authors (Nouchi et al., 2005; Nishioka et al., 2005; Iida et al., 2009). However, no clear evidence of correlation with the process data was found besides that an early low slag drainage leads to a higher slag outflow by the end of the tap and that a somewhat uniform distribution of slag during tapping results in a longer tap duration. Overall, the complexity of the drainage system was noted and the results indicated that each taphole displays distinctive outflow characteristics that may be the results of a changing liquid distribution due to local conditions. The quasi-time evolution of the outflows in the component space along the equivalent pattern is illustrated by the video provided in Roche (2020).

4.2 Off-line models and evaluation of hearth conditions (Paper II and III)

The outflow classification previously described revealed distinctive outflow patterns among operating tapholes as well as the dynamic nature of the process. In this section, two off-line models aiming to track iron and slag levels in the hearth by addressing the key findings are summarized. Paper II presents a model focused on the liquid pool dynamics to describe and explain the observed liquid distribution. For the case of simplicity, a parametric approximation of the liquid outflows was introduced to consider the deviations observed in Paper I. By contrast, Paper III presents a model mainly focused on the conditions at and in the taphole, considering both gravitational and viscous forces. In both studies, the models were evaluated in terms of the slag delay, tap duration, liquid levels, as well as a comparison with the process data (Data set 1 in Figure 25) from the reference furnace.

Both models are based on the following main assumptions:

1. The volumes of iron and slag in the hearth are characterized by overall levels, z_{ir} and z_{sl}.
2. The hearth is cylindrical and its diameter (d_{h}) as well as the dead-man voidage (ε_{h}) are given.
3. The dead man sits on the hearth bottom.
4. The inflow rate of iron to the hearth, $\dot{m}_{\mathrm{ir,in}}$, and the slag (mass) ratio, γ_{in}, are given.
5. Two tapholes are alternated with an inter-cast time, t_{pl}, during which both tapholes are closed.
6. Simple conditions are applied to determine the phases that initially flow out when the taphole is opened.
7. The tapping ends when the gas-slag interface locally bends down to the taphole.

4.2.1 Two-pool model with fixed outflow rates (Paper II)

Model assumptions and parameters

The apparent liquid distribution was tacked by assuming a hearth divided into two pools with individual levels of iron ($z_{\mathrm{ir}}^{(j)}$) and slag ($z_{\mathrm{sl}}^{(j)}$) where j indicates the pool number. A novelty of the model is to consider pools of varying size (from an initial area share of $s_{\mathrm{min}}^{(j)}$) as the dead-man in front of the operating taphole has access to higher liquid volumes during tapping. This assumption is supported by observations that indicated a rather extreme liquid share in tapholes when entering operation, as discussed in section 4.1, as well as by the fact that taps with an initial iron outflow rate clearly below the production rate could drain iron and slag simultaneously. The permeability between the pools is governed by the hydrostatic pressure

of the two pools and controlled by iron and slag communication factors, φ_{ir} and φ_{sl}. Figure 31 illustrates these particular assumptions: on the left a vertical view of the hearth shows the main variables as well as the hearth pools (here of equal size) and with taphole TH1 open. In the right panel, an example of pool size growth is presented, where Pool 1 increases in size from representing 40% of the total cross-sectional hearth area at the initial time, t_{min}, to 60% at a later time moment, t_{pool}.

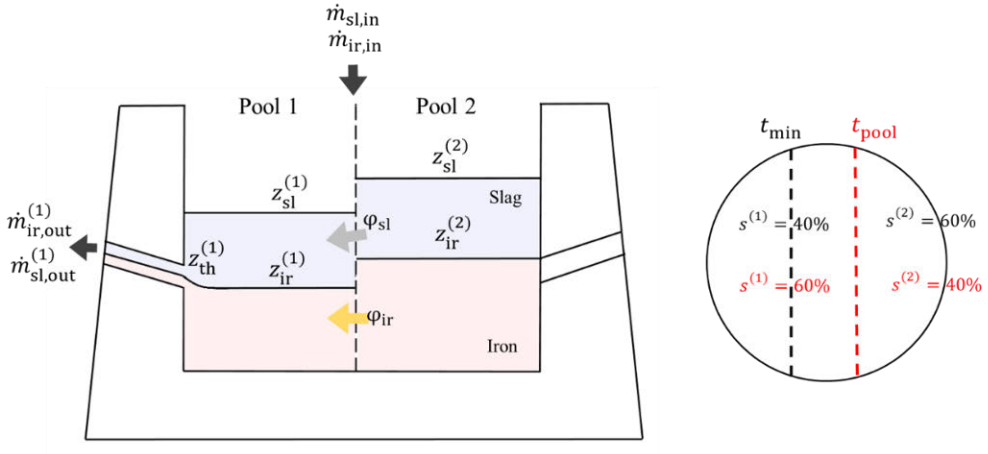

Figure 31. *Vertical cross-section of two-pool blast furnace hearth with Pool 1 draining, main variables and parameters of the model are indicated (left). Horizontal cross-section illustrating the draining pool growth from 40% to 60% of the area.*

The liquid levels in the pools are expressed by the differential equations

$$\frac{\mathrm{d}z_{\mathrm{ir}}^{(j)}}{\mathrm{d}t} = \frac{s^{(j)}\dot{m}_{\mathrm{ir,in}} + \sum_{i\neq j}\dot{m}_{\mathrm{ir}}^{(ij)} + \delta_{j,j^*}\dot{m}_{\mathrm{ir,out}}}{\rho_{\mathrm{ir}}A^{(j)}\varepsilon} \tag{12}$$

$$\frac{\mathrm{d}z_{\mathrm{sl}}^{(j)}}{\mathrm{d}t} = \frac{\mathrm{d}z_{\mathrm{ir}}^{(j)}}{\mathrm{d}t} + \frac{s^{(j)}\dot{m}_{\mathrm{sl,in}} + \sum_{i\neq j}\dot{m}_{\mathrm{sl}}^{(ij)} + \delta_{j,j^*}\dot{m}_{\mathrm{sl,out}}}{\rho_{\mathrm{sl}}A^{(j)}\varepsilon} \tag{13}$$

where the first term in the numerator on the right-hand-side expresses the liquid inflow (from above) to the pool, the second is the cross-flow between the pools, while the third is the outflow if this is the pool that is being tapped (j^*). The Kronecker delta is defined as $\delta_{j,j^*} = 1$ if $j = j^*$, else $\delta_{j,j^*} = 0$.

The outflow parametrization is based on the findings presented in Section 4.1. The left panel of Figure 32 shows the *mean pattern* of Data set 1 presented in Figure 28 along its linear approximation of two segments. This was expanded to individual approximations for the outflow of iron and slag,

as illustrated in the right panel of Figure 32. The latter panel also shows the outflow model parameters, including the initial ramp-up time, Δt_{i}, initial outflow rate, $\gamma_{i,\mathrm{start}}$, and the angle expressing the outflow growth after the initial ramp-up period, θ_{i}, for i = ir, sl. The outflow parametrization is explained in the Appendix of Paper II.

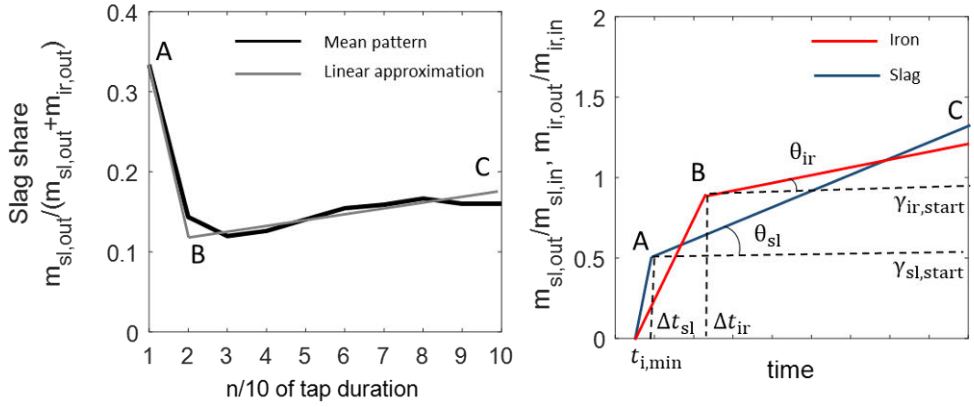

Figure 32. *Mean slag share pattern corresponding to Data set 1 and its linear approximation by two segments (left), and iron and slag outflow parametrization for the present model.*

Tap cycle criteria

A "fuzzy" region around the taphole Δz_{th} was defined to determine the liquid phase seen in the beginning of the tap (cf. Figure 33). When the iron-slag interface is within this region, iron and slag flow out simultaneously. When above or below, the tap starts with only iron or slag, respectively, and once the overall interface reaches the fuzzy region, two-phase drainage is established. This region is considered to account for the uncertainty of the conditions in front of the taphole (where the drill possibly breaks the inner wall) and the probability that both phases would flow out if the interface is "close enough" to the taphole level. The lifting of iron from below the taphole in the beginning of the tap is defined to be proportional to the slag outflow, but bounded to a maximum lifting height, Δz_{lift}.

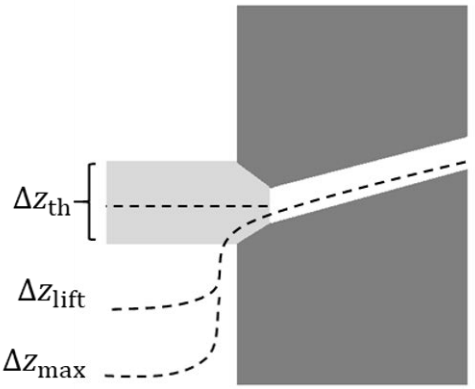

Figure 33. *Illustration of the adjustable region around the taphole to determine the type of outflow (Δz_{th}) as well as the maximum iron lifting at the beginning of the tap (Δz_{lift}) and the maximum depth that iron can reach at any time (Δz_{max}).*

Different investigators have proposed expressions for the flow-out coefficients to calculate the end of the tap based on experimental work and assuming nominal flow through a uniform packed bed. However, when it comes to the real system such conditions may not apply due to inhomogeneous dead-man permeability that can also change with time. In the present model the tap-end conditions was expressed as a function of the slag outflow of the draining pool, j^*. The tap is taken to end when

$$z_{\mathrm{sl}}^{(j)} - z_{\mathrm{th}}^{(j)} < \omega \frac{\dot{m}_{\mathrm{sl,out}}^{(j)}}{\rho_{\mathrm{sl}} A^{(j)} \varepsilon_{\mathrm{h}}} \tag{14}$$

where ω is a model parameter and ε_{h} is the dead-man voidage. Similar to the out-flow coefficients reported in the literature, the level at tap end is proportional to the slag outflow, but Equation 14 represents a simpler expression. The condition for the final iron level in the draining pool was inspired by the asymptotic expression 2 derived by Tanzil et al. (1984)

$$\Delta z = \min\left(\frac{\rho_{\mathrm{sl}}}{\rho_{\mathrm{ir}} - \rho_{\mathrm{sl}}} (z_{\mathrm{sl}}^{(j^*)} - z_{\mathrm{th}}^{(j^*)}), \Delta z_{\mathrm{max}} \right) \tag{15}$$

where Δz_{max} is a model parameter that defines the maximum depth from the taphole that the iron-slag interface is allowed to reach (cf. Figure 33).

Key findings and analysis

A sensitivity analysis was conducted with respect to the pool communication of iron and slag as well as the pool size. The evolution of the liquid levels of

both pools was studied after a quasi-stationary state was reached. Figure 34(a) shows the base case for pools of equal size based on the model parameters that resulted from the data analysis (cf. Figure 32) and the overall drainage characteristics, i.e., tap duration and slag delay. In the figure, the horizontal line depicts the level of the tapholes, while the levels of the draining pool are shown by green (Pool 1) and red (Pool 2) markers, and the level in the non-draining pool is presented by black markers. Figure 34(b) shows the case with a dynamic growth of the draining pool from 40% to 60% of the cross section (cf. right panel Figure 31) while the other pool shrinks accordingly. The liquid interface stays relatively close to the taphole as more iron flows from the adjacent pool to the draining pool, extending the tap duration compared to the base case. Figure 34(c) and Figure 34(d) show cases with poor iron and slag communication between pools of same size, respectively.

Poor liquid flow through the hearth can be caused by the existence of different dead-man voidage regions between parts of the hearth, which would induce permeability and pressure profiles, and therefore, imbalanced liquid distributions. A poor coke-size distribution, e.g., including coke fines or solidified material, may lead to a dead-man with low-permeability zones that inhibit the flow of particularly slag due to its higher viscosity. On the other hand, in the lower part of the hearth the occurrence of coke-free zones can lead to an inactive dead-man core, limiting the iron flow through the dead man. Figure 6 in Section 2.4 presented an illustration of the inner state of the quenched hearth of a Japanese furnace, where the different zones identified suggest not only a distribution of permeability, but also asymmetry in the hearth.

Regarding the results, a poor iron communication gives rise to a higher slag level in the draining pool, thus delaying the end of the tap. The high iron level in the non-draining pool results in a long positive slag delay in the following tap. In the case of a poor slag communication (Figure 34(d)) were the slag column of the non-draining pool is high, the system compensates with a higher cross-pool flow of iron, draining more iron and ending the tap with a lower iron level in the non-tapping pool. This results in a clearly negative slag delay for the following tap.

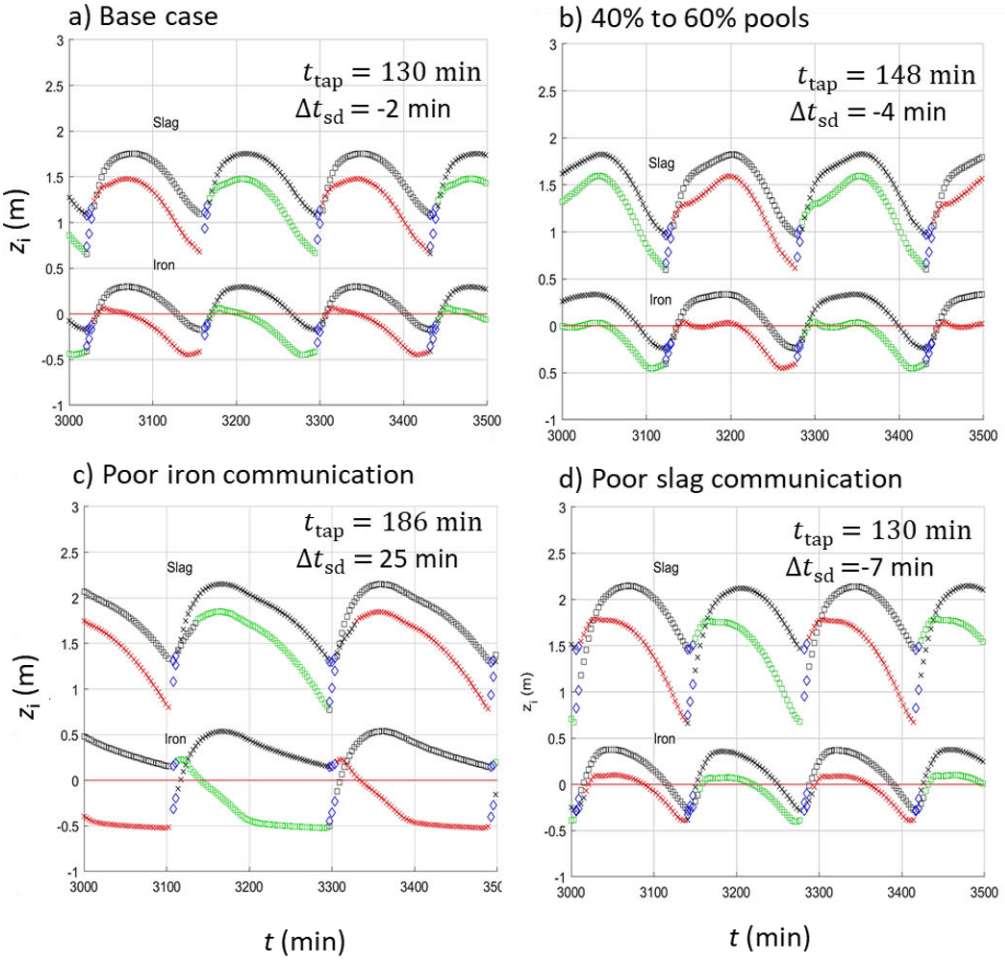

Figure 34. *Liquid levels for the base case of the model of Paper II with two pools of equal size (a), a dynamic growth of the draining pool from 40% to 60% (b), poor iron communication (c) and poor slag communication (d). The horizontal line depicts the level of the tapholes, levels of the draining pool are shown by green (Pool 1) and red (Pool 2) markers, while the levels in the non-draining pool are presented in black.*

As presented in Section 4.1 the drainage data from the reference furnace showed a significant degree of variance, where the operating tapholes showed opposite outflow characteristics with respect to slag delay, tap duration and liquid distribution. To evaluate these observations, a comparison with the model response was conducted. The top panel of Figure 35 depicts the slag delay of 20 consecutive taps from alternate tapholes (Data set 1), where TH3 taps showed only slag in the beginning of the tapping, while TH1 showed mostly a short (positive) slag delay or simultaneous outflow—

except for a single tap with a long slag delay (#586) due to a longer inter-cast time. In an attempt to reproduce this type of drainage, a stochastic evaluation of the tap-end parameter, ω, in Equation 14 was conducted, by selecting the value of this parameter from a normally distributed random number with a mean set as the nominal value for the parameter in the model. The middle and bottom panels of Figure 35 show the simulated tap duration and slag delay, respectively, of a set of consecutive taps given asymmetric and dynamic pool sizes. The pool growth during drainage was set from 20% to 50% for Pool 1 and — as a complement — from 80% to 50% for Pool 2. The results are seen to resemble the behavior of the depicted period from the actual furnace, suggesting that the variance observed in the data may be caused by the unknown conditions in front of the taphole, which affect the moment when the tap ends. This has been stressed by other investigators in the literature (e.g., He et al., 2002).

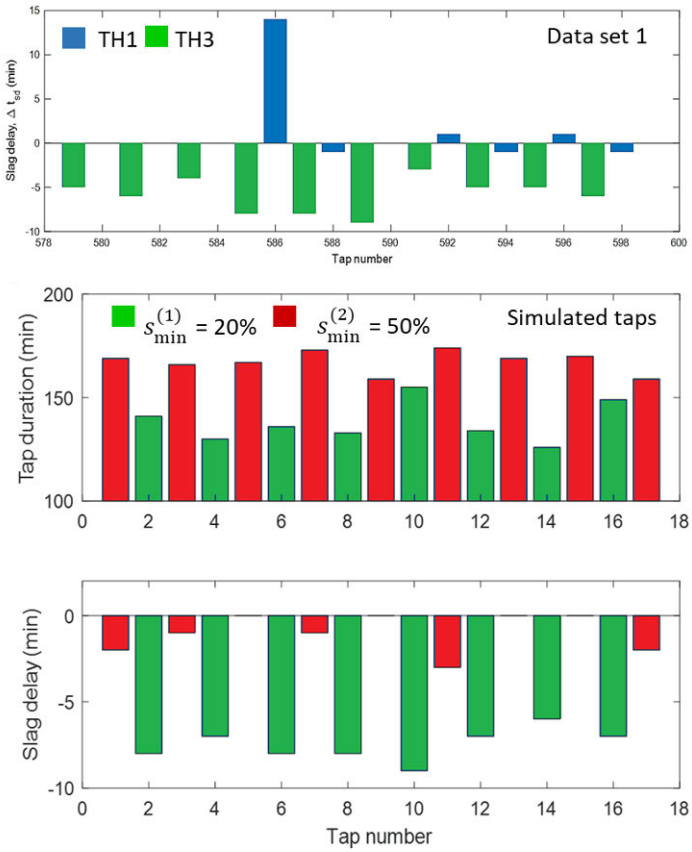

Figure 35. *Consecutive taps from Data set 1 with different outflow between tapholes (top), as well as tap duration (middle) and slag delay (bottom) for simulated case of asymmetric and dynamic pool size.*

Overall, the model allowed for an evaluation of hearth states with respect to permeability. A sensitivity analysis of the liquid pool communication and pool size yielded results in agreement with practical findings from the reference furnace. The simulated cases indicated that the observed liquid imbalance in the furnace could arise from different asymmetric and dynamic permeability profiles in the dead man. Moreover, the stochastic evaluation of the tap-end condition indicated that the taphole conditions and the local conditions in the regions near the taphole might explain the variance of the drainage patterns for a particular dead-man state. Suitable values for the model parameters were assumed (cf. Figure 33), but a deeper analysis of these conditions is still required.

4.2.2 Single-pool model based on fluid dynamics (Paper III)

The model presented in Paper III was designed to more appropriately describe the evolution of the iron and slag levels in the hearth as well as the drainage of the phases by stating and solving equations for the fluid dynamics involved, still avoiding a detailed (CFD-like) treatment to reduce the model complexity and make it fast. Like in the reference furnace and the treatment in Paper II, an alternate tapping strategy was applied.

Differential equations for the liquid levels are expressed by analogy to Equations 12 ad 13, but since this is a one-pool model, $i = j = j^* = 1, s^{(j)} = 1$ and thus $A^{(1)} = A_\mathrm{h}$. The iron and slag outflow, $\dot{m}_\mathrm{in,out}$ and $\dot{m}_\mathrm{sl,out}$, are expressed by a pressure balance between the in-furnace and the surrounding house cast pressure conditions. The balance considers both the resistance of the dead man and the taphole. The left side of Figure 35 illustrates the blast furnace hearth and the main variables in the model, where p_0 is the atmospheric pressure and p_gas is the in-furnace gas pressure. Expressions for the pressure at the slag-gas (z_sl) and iron-slag interfaces (z_ir) far from the taphole were derived as

$$p_\mathrm{g} = p_\mathrm{th} - g\rho_\mathrm{sl} z_\mathrm{sl} + \Delta p_\mathrm{bed,sl} + \Delta p_\mathrm{ent,sl} \tag{16}$$

$$p_\mathrm{g} + g\rho_\mathrm{sl}(z_\mathrm{sl} - z_\mathrm{ir}) = p_\mathrm{th} - g\rho_\mathrm{ir} z_\mathrm{ir} + \Delta p_\mathrm{bed,ir} + \Delta p_\mathrm{ent,ir} \tag{17}$$

$$p_\mathrm{th} = p_0 - g\rho_\mathrm{mix} l_\mathrm{th} \sin\alpha_\mathrm{th} + \Delta p_{\mathrm{th},j}; \qquad j = \mathrm{ir, sl, mix} \tag{18}$$

where p_th is the pressure in front of the taphole, and the pressure losses in the dead man ($\Delta p_{\mathrm{bed},j}$) and at the entrance of the taphole ($\Delta p_{\mathrm{ent},j}$) are discussed later. The right side of Figure 36 illustrates an entrance void in front of the taphole and how the dead man extends in the hearth from a minimum radius defined from the taphole entrance (r_min) to the hearth radius (r_h).

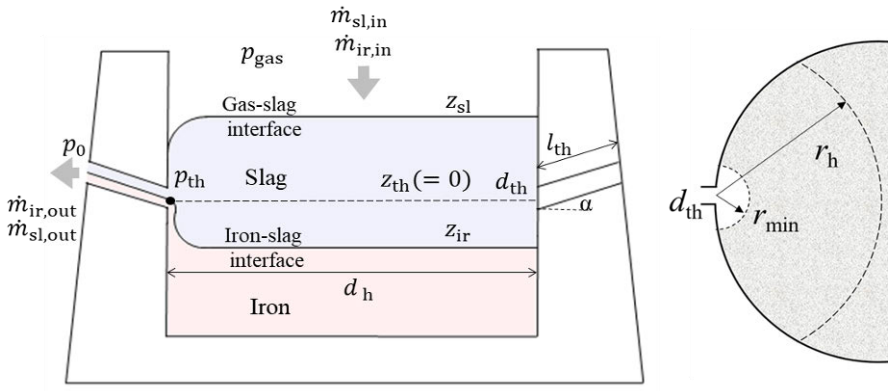

Figure 36. *BF hearth and its main variables and parameters in the model (left) and top view illustrating region for integration of bed pressure loss (right).*

Considering the findings by Post (2019) concerning the formation of a coke-free zone in front of the taphole illustrated in Figure 24 as well as the liquid flow and velocity profile, the pressure drop of the liquids in the dead man was derived from the Ergun equation (Ergun, 1952). Giving the local average velocity, and assuming a flow cross-section area of a hemisphere, the pressure drop was integrated from r_{min} to r_{h}, yielding

$$\Delta p_{\mathrm{bed},j} = 150\frac{\mu_j(1-\varepsilon)^2}{2\pi(d_{\mathrm{c}}\Phi)^2\varepsilon^3}\left(\frac{1}{r_{\mathrm{min}}}-\frac{1}{r_{\mathrm{h}}}\right)\dot{V}_j + 1.75\frac{\rho_j(1-\varepsilon)}{12\pi^2(d_{\mathrm{c}}\Phi)\varepsilon^3}\left(\frac{1}{{r_{\mathrm{min}}}^3}-\frac{1}{{r_{\mathrm{h}}}^3}\right){\dot{V}_j}^2; \qquad j=\mathrm{ir,sl} \tag{19}$$

The first term of the expression, which is proportional to the outflow velocity, considers the viscous forces while the second one, proportional to the square of the velocity, represents the inertial forces. Nouchi et al. (2003), Nishioka et al. (2005), Iida et al. (2009) took into account only the viscous forces in their studies, which represents an oversimplification of the system considering the estimated high liquid velocity particularly in the vicinity of the taphole.

In the case where only one phase (iron or slag) flows out, the entrance loss was written as

$$\Delta p_{\mathrm{ent},j}^{(1)} = k_{\mathrm{ent}}\frac{\rho_j}{2}u_{\mathrm{th},j}^2 \tag{20}$$

where k_{ent} is an entrance-loss factor and $u_{\mathrm{th},j}$ is the velocity in the taphole. In case of simultaneous outflow of iron and slag, another entrance-loss term ($\Delta p_{\mathrm{ent},j}^{(2)}$) was considered since the flow of the first phase that flows out constrains the second one:

$$\Delta p_{\mathrm{ent,ir}}^{(2)} = k_{\mathrm{up}} \frac{\rho_{\mathrm{ir}}}{2} \left(\frac{\dot{V}_{\mathrm{ir}}}{A_{\mathrm{up}}} \right)^2 = k_{\mathrm{up}} \frac{\rho_{\mathrm{ir}}}{2} u_{\mathrm{up}}^2; \qquad z_{\mathrm{ir}} \leq 2d_{\mathrm{th}} \tag{21}$$

$$\Delta p_{\mathrm{ent,sl}}^{(2)} = k_{\mathrm{down}} \frac{\rho_{\mathrm{sl}}}{2} \left(\frac{\dot{V}_{\mathrm{sl}}}{A_{\mathrm{down}}} \right)^2 = k_{\mathrm{down}} \frac{\rho_{\mathrm{sl}}}{2} u_{\mathrm{down}}^2; \quad z_{\mathrm{ir}} \geq 2d_{\mathrm{th}} \tag{22}$$

Figure 37 illustrates the procedure to check whether iron starts flowing out and the liquid interface bends upwards at the taphole and iron flows from below. The cross-section area A_{up} is calculated based on the geometry. Likewise, for slag a similar procedure was followed. The overall entrance loss is given by

$$\Delta p_{\mathrm{ent},j} = \max(\Delta p_{\mathrm{ent},j}^{(1)}, \Delta p_{\mathrm{ent},j}^{(2)}) \tag{23}$$

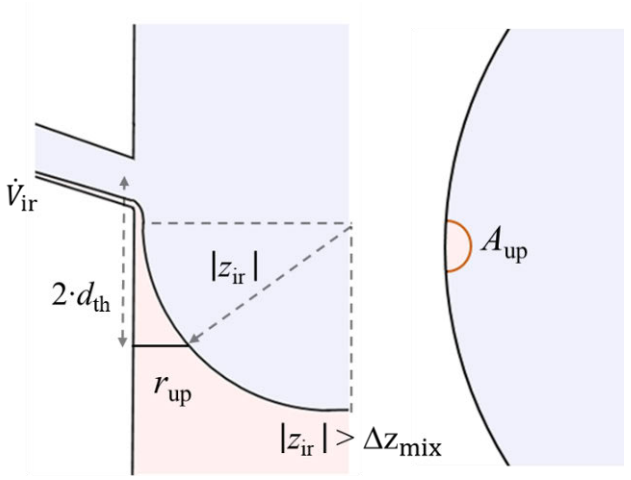

Figure 37. *Definition of the geometry for estimating the entrance loss for iron for the case where the overall iron level is below the taphole. Vertical cross-section (left) and horizontal cross-section (right).*

The pressure loss in the taphole was expressed by the equation for the losses in a rough pipe. The taphole diameter (d_{th}), length (l_{th}), angle of inclination (α_{th}) and erosion rate (e_{th}) were given for each taphole. For the case where iron and slag flow out simultaneously, ρ_{mix} and μ_{mix} were obtained as mean

values based on the volumetric shares of the two phases. The taphole friction factor was calculated with Equations 8 and 9.

The geometric parameters (hearth diameter, taphole length and diameter), as well as production rate, overall slag ratio and blast pressure were estimated from typical values of large blast furnaces. The material properties such as iron and slag densities and viscosities, taphole roughness, coke particle size and shape factor, as well as bed voidage were taken from values used in similar numerical studies found in the literature. Table 1 presents the model variables and parameters and the values considered for the base case. A more detailed description is given in Paper III.

Table 1. Conditions and model parameters for the *base case*.

Variable or parameter	**Value**	**Unit**	**Variable or parameter**	**Value**	**Unit**
$\dot{m}_{\mathrm{ir,in}}$	11000	t/d	l_{th}	3	m
γ_{sl}	0.2	-	$d_{\mathrm{th,ini}}$	0.064	m
ρ_{ir}	6700	kg/m^3	e_{th}	$3.3{\cdot}10^{-6}$	m/s
ρ_{sl}	2400	kg/m^3	ξ	0.003	m
μ_{ir}	0.006	Pa·s	p_{gas}	$3.2{\cdot}10^{5}$	Pa
μ_{sl}	0.35	Pa·s	p_0	$1.01{\cdot}10^{5}$	Pa
d_{h}	14	m	t_{pl}	6	min
ε_{h}	0.35	-	ε	0.35	-
d_{c}	0.035	m	k_{ent}	0.05	-
Φ	0.6	-	k_{up}	0.05	-
ε	0.35	-	k_{down}	0.05	-
r_{min}	0.1	M	α	10	°
β	0.01	-	Δz_{mix}	$3d_{\mathrm{th}}$	m

Tap cycle criteria

An alternate tapping strategy similar to the one of the reference furnace was simulated with particular taphole conditions for each taphole. After the inter-cast period, one taphole is opened and the vertical level of the iron-slag interface, z_{ir}, was used to determine the initial phase(s) to flow out: only iron flows out if $z_{\mathrm{ir}} \geq z_{\mathrm{th}} - d_{\mathrm{th}}/2$, only slag if $z_{\mathrm{ir}} < -\Delta z_{\mathrm{mix}}$ and otherwise both iron and slag. A revision is undertaken in the next time step based on the previous solution. In case of initial iron-only flow, an *ansatz* is made that also slag starts flowing out at a given volume flow rate and the pressure balance of the slag phase in the hearth is solved with respect to the static pressure in front of the taphole, p_{th}. If the value is higher than the taphole pressure determined in the previous solution, simultaneous outflow of iron and slag is assumed to occur. A corresponding procedure is followed in the case of slag-only flow. This makes it possible to describe both negative and positive slag delays at the beginning of the tap.

In the model, the tap end is defined as the time when the gas-slag interface can locally bend down to the taphole. This requires that the pressure loss of slag in the bed and the taphole entrance together balance the head of the slag layer according to

$$\Delta p_{\mathrm{bed,sl}} + \Delta p_{\mathrm{ent,sl}} \geq \rho_{\mathrm{sl}} g z_{\mathrm{sl}} \qquad (24)$$

When this condition is satisfied, the taphole is plugged and after the inter-cast time has passed the other taphole is open and the procedure is repeated.

Key findings and analysis

The effect of some in-furnace parameters was evaluated to gain a better understanding of the primary factors that affect the drainage process. The results are compared with practical findings from the reference furnace. The *base case* was based on the findings in Paper I and Paper II as well as the typical values found in other numerical studies of the blast furnace hearth (cf. Table 1). The left panels of Figure 38 show the outflow pattern for the *base case* and the corresponding liquid levels. The iron outflow first gradually increases to level out, while the slag outflow initially spikes, decrease to a minimum followed by an almost linear increase phase, reaching a final level of about twice the production rate. Nouchi et al. (2005) reported similar patterns from an industrial blast furnace, and also the experimental work and mathematical models by Nishioka el al. (2005) and Iida et al. (2009) show results in general agreement.

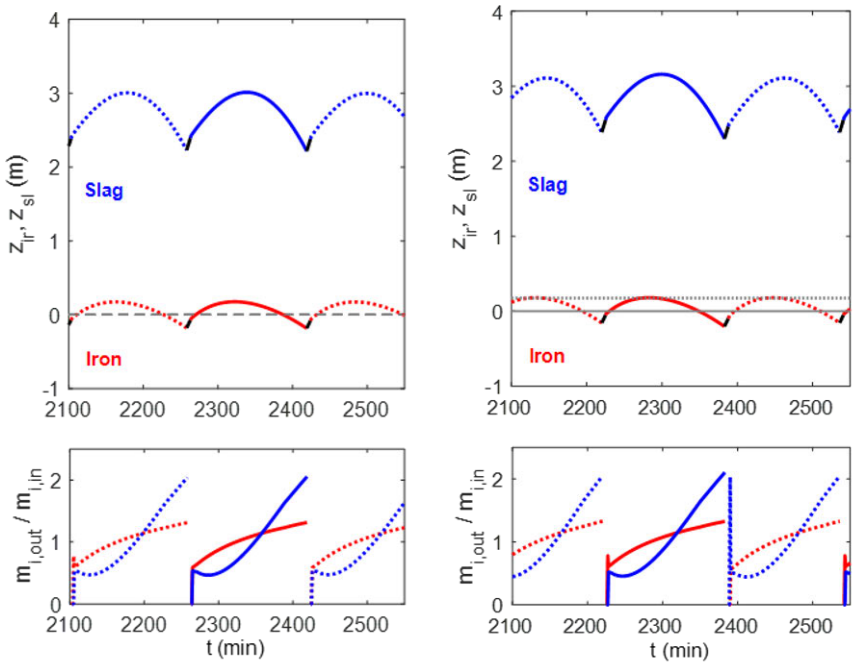

Figure 38. *Iron and slag levels (z_{ir}, z_{sl}) and normalized outflow rates ($m_{i,out}$/ $m_{i,in}$): for Case 1 (left) and tapholes of different length and diameter (cf. Table 2, Case 11).*

Table 2 summarizes the values for some characteristic indices identified in Papers I and II (tap duration, slag delay and slag share) for the 17 different cases of the sensitivity analysis in Paper III, where the base case represents Case 1. These cases study the effect of the production rate, slag ratio and viscosity, which may fluctuate in the process operation (cf. Table 2, Cases 2-5), the taphole conditions (Cases 6-11), and the dead-man permeability (Cases 12-17). The simulated outflow patterns were found to reproduce some of the recurrent patterns seen in the process data. Different conditions for the operating tapholes (Cases 10 and 11) and the dead-man regions in front of them (Cases 16 and 17) were also studied, yielding outflow patterns that reflect some of the disparities observed between the tapholes. The right panels of Figure 38 show an asymmetric case of tapholes of different lengths, but where the diameter of the shorter taphole has been adjusted in order to address the imbalance. This illustrates the importance of the operator's actions when imbalance occurs (cf. Table 1, Case 11) and how a balanced drainage could be restored.

Table 2. Perturbed terms and key drainage indices for different symmetric and asymmetric cases.

#	Perturbed term		Value		Unit	Tap duration (min)		Slag delay (min)		Slag ratio -	
1	Base case		-		-	156		0		0.2	
2	μ_{sl}		0.5		Pa·s	155		−1		0.2	
3	μ_{sl}		0.2		Pa·s	157		1		0.2	
4	$\dot{m}_{ir,in}$		12500		t/d	182		0		0.2	
5	γ_{in}		0.25		-	168		-1		0.25	
6	l_{th}		4		m	195		1		0.2	
7	l_{th}		2		m	105		0		0.2	
8	$d_{th,ini}$		0.058		m	199		0		0.2	
9	$d_{th,ini}$		0.070		m	122		1		0.2	
10	$l_{th,1}$ ($d_{th,1}$)	$l_{th,2}$ ($d_{th,2}$)	3 (0.064)	2 (0.064)	m	155	106	1	−1	0.19	0.22
11	$l_{th,1}$ ($d_{th,1}$)	$l_{th,2}$ ($d_{th,2}$)	3 (0.064)	2 (0.058)	m	158	148	1	−1	0.20	0.20
12	ε		0.39		-	159		0		0.2	
13	ε		0.31		-	150		1		0.2	
14	r_{min}		0.075		m	153		20		0.2	
15	r_{min}		0.15		m	159		−5		0.2	
16	ε_1	ε_2	0.3	0.4	-	122	176	−1	20	0.19	0.21
17	$r_{min,1}$	$r_{min,2}$	0.10	0.15	m	140	171	−8	1	0.25	0.16

Two other sources of asymmetry are presented here. In the first, the differences occur in the local dead-man voidage in front of the taphole (Case 16) while in the second they occur in the size of the entrance void region, which determines the extension of the dead man (Case 17). The role of a different voidage at the two operating tapholes, which may vary with time, was investigated by changing their values by ±0.05 from the *base case* while maintaining the overall voidage of the dead man, ε_h. The left panels of Figure 38 shows the arising draining imbalance. The lower coke-bed voidage gives rise to a tap of short duration due to the large Δp_{bed}. Conversely, a less compacted dead man (and smaller Δp_{bed}) delays the bending of the slag-gas interface. The different tap durations and different levels of the iron-slag

interface when the taphole is opened give rise to divergent outflow patterns that correspond to the system's response towards reaching a relatively balanced drainage as seen in the slag share.

The parameter $r_{\min}$ may be related to the rate at which coke is consumed in front of the taphole, where the mass transfer is fast due to high liquid velocities. Furthermore, the size of these regions may be different between the tapholes due to liquid distribution and the change in size of the taphole and mushroom. The right panels of Figure 31 show the simulated results for this case of asymmetry. The divergence of the drainage patterns is similar to the one seen for the asymmetric local dead-man voidage. However, the liquid distribution is notably imbalanced as seen in the slag share. Since the dead-man voidage is maintained at 0.35 the slag flows easier and at a higher rate than in the case of local voidage of 0.3 in TH1 (Case 15), and thus results in more negative slag delay and longer tap duration. The tilting of the iron-slag interface initially occurs upwards for TH1 and downwards for TH2 for both cases in Figure 39. Near the taphole, the (high) pressure drop in the slag phase and the low iron resistance (low viscosity) distorts the interface after TH1 is opened, lifting the iron phase. TH2 drainage shows that even though the liquid interface is just above the taphole the (low) pressure loss from the iron flow is sufficient to bend the interface down to let out slag.

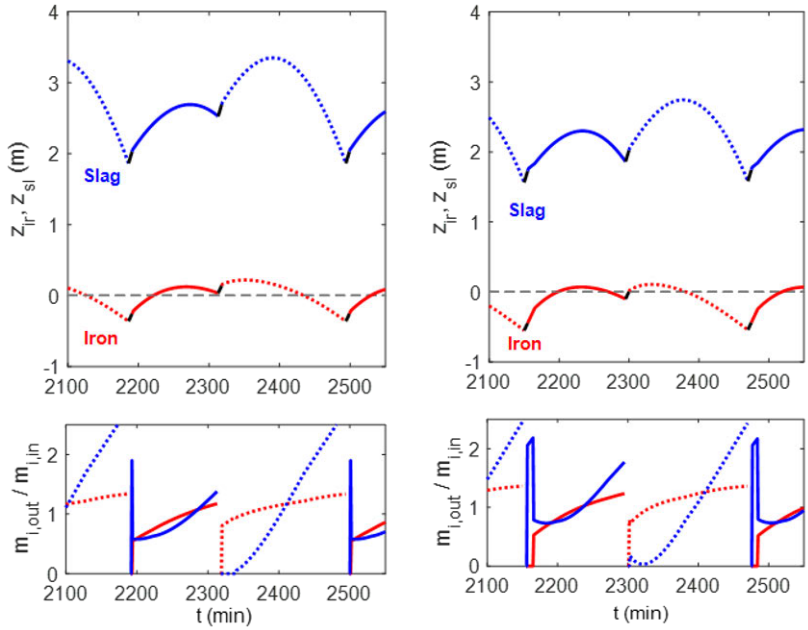

Figure 39. *Iron and slag levels (z_{ir}, z_{sl}) and normalized outflow rates ($m_{i,out}$/ $m_{i,in}$) for different coke-bed conditions at the tapholes: (a) different voidage ($\varepsilon_1 = 0.4, \varepsilon_2 = 0.3$, Case 16 in Table w) and (b) different size of taphole void regions ($r_{min,1} = 0.1\ m, r_{min,2} = 0.15\ m$, Case 17 in Table 2). i=ir (red), i=sl (blue).*

At a flow rate of about 1 mm/s (far from the taphole) and assuming the coke and liquid properties listed in Table 1, the Reynolds number falls in the range Re = 0.2…40, so the flow is laminar. Away from the taphole the gravitational and viscous forces define the pressure profile. However, near the taphole the pressure drop due to inertia cannot be neglected because of the high flow velocity that occurs during tapping. Figure 40 illustrates the contribution by the viscous (solid lines) and inertial (dashed lines) terms in Equation 19 for each phase as well as the pressure drop in the taphole (black line, right ordinate scale) for the Base case. Red and blue lines depict iron and slag, respectively. The pressure drop in the taphole is the clearly largest term (218-270 kPa), which increases slightly initially, but then decrease as the taphole erodes, lowering the velocities.

In the hearth, the inertial term is the clearly dominating one for iron, due to a low viscosity and high density. For slag, the viscous term is more important due to the higher viscosity, but the inertial term grows along with the slag outflow. Several models found in the literature have expressed the pressure drop in the bed with the Kozeny-Carman equation, which only applies to laminar flow. However, assuming a laminar flow through the bed and neglecting the inertial forces, in particular for the iron phase, seems to be an oversimplification of the system.

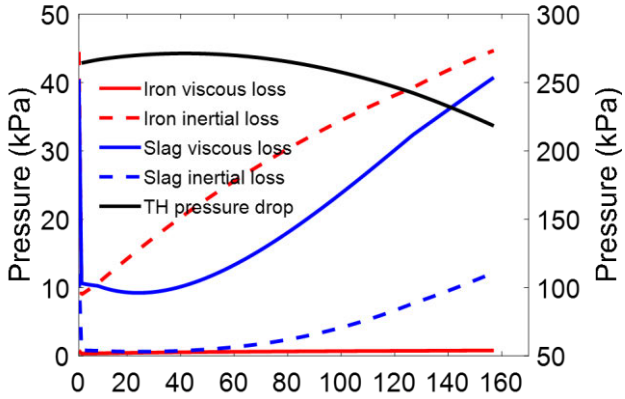

Figure 40. *Viscous and inertial pressure-drop terms in the dead man and in the taphole for the Base case.*

Model comparison with process data

The characteristics exhibited by the simulated outflows were found in some of the recurring patterns observed in the measurements of the outflows from the reference furnace. The measurements, however, hold an error associated with the delays and "buffering" that iron and slag experience in the trough and runners, so a direct comparison of the slag delay and slag share between the simulated and measured values is difficult. It is clear that the true system

shows more filtered changes as the levels in the trough and runners may vary with time, particularly at the beginning of the taps.

The top panels of Figure 41 show two consecutive taps from Data set 1, and in the panels below two consecutive simulated taps corresponding to the case of tapholes of different length (cf. Table 2, Case 10). Similarly, Figure 42 shows another pair of consecutive taps above a simulated pair with different entrance void regions. These two pairs of taps show striking similarities with the simulated ones despite noise in the measurements and the above-mentioned neglect of trough and runner dynamics in the model. However, according to the model results, several sets of conditions can produce similar outflow patterns, so it is not possible to uniquely determine the root cause. Nonetheless, these two cases represent potential causes of drainage imbalance observed in the furnace.

The taphole length is known to vary in the true operation and the extent of a high-permeability zone at the entrance of the taphole could vary in size because of differences in the liquid velocities and composition. As pointed out and modelled by Iida et al. (2009), the carbon appetite of the iron, which depends on its initial and equilibrium carbon concentration, may vary locally and in time, and certain oxides (e.g., FeO) in the slag may also contribute to the local void formation.

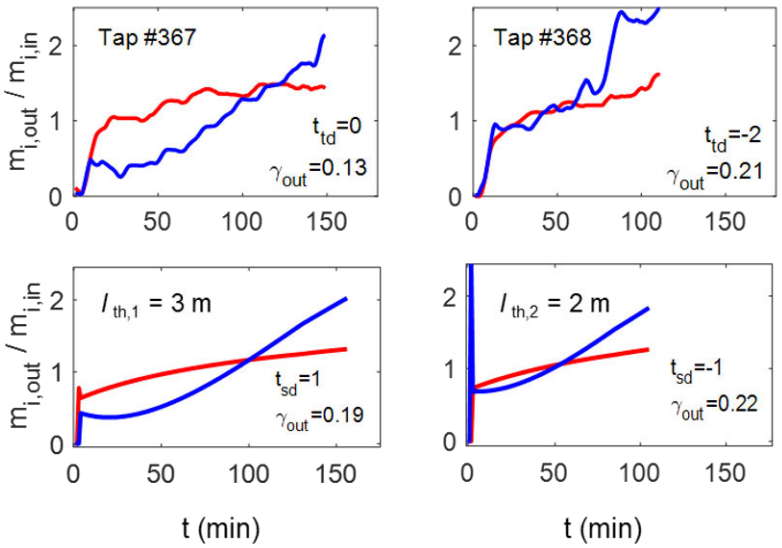

Figure 41. *Normalized outflows of iron (red) and slag (blue) of a pair of consecutive taps of the reference furnace from Data set 1 (top panels) and simulated pair for the case with different* l_{th} *from (bottom panels; cf. Table 2, case 10).*

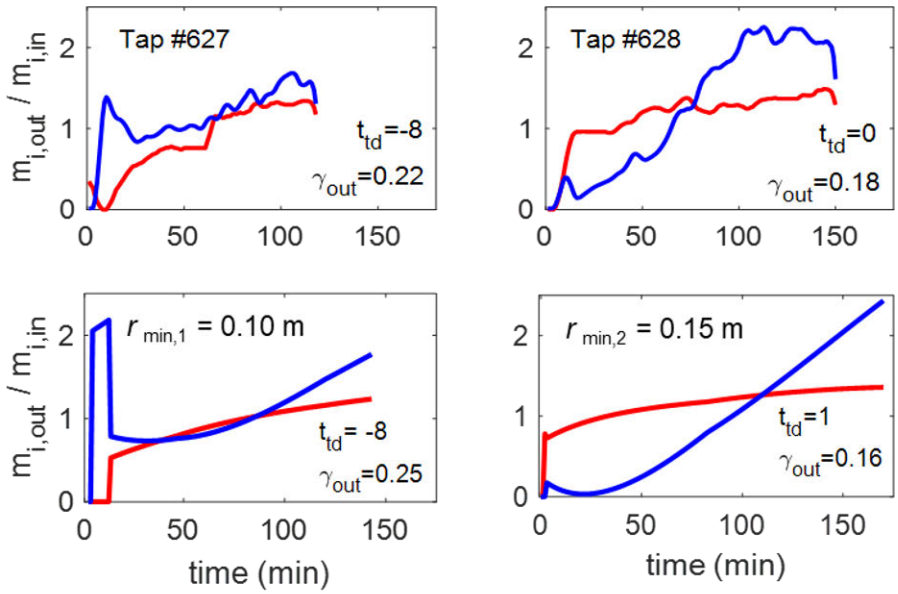

Figure 42. *Normalized outflows of iron (red) and slag (blue) of a pair of consecutive taps of the reference furnace from Data set 1 (top panels) and simulated pair for the case with different r_{min} (bottom panels; cf. Table 2, case 17).*

Estimates of the slag delay for the taps in Data set 1 were obtained by a detailed inspection of iron and slag outflow measurements. Figure 43 presents these estimates, where a larger number of negative slag delays in comparison with positive ones occur. It is important to keep in mind that very short positive slag delays may be due to delays in the through and runners, while clearly positive ones are often due to longer inter-cast periods. On the other hand, negative slag delays appear to be characteristic of the drainage. These are particularly frequent during the operation of the taphole pairs TH1-TH2 and TH1-TH3, where at certain periods one taphole shows a relatively long negative slag delay and the other a simultaneous flow from the beginning of the tap. Such imbalance was found to appear and disappear suddenly, in conjunction with taphole changes, or gradually with time, as also shown in Paper I.

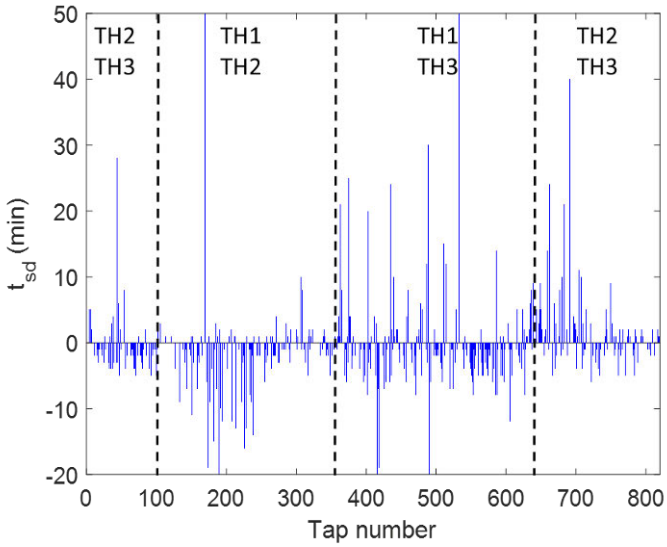

Figure 43. *Slag delay of taps in Data set 1 from the reference furnace. Dashed horizontal lines indicate the changes of taphole pair in operation. The operating tapholes are reported in the top of the figure.*

Figure 44 shows the measured taphole length corresponding to the first 600 taps in Data set 1. Most taphole lengths are distributed between 2.4 m and 2.9 m for all three tapholes and a good deal of variation is noted from tap to tap, which suggests a stochastic variation of this taphole condition regardless of the taphole. Naturally, the way in which the taphole was measured may also induce inaccuracies in these measurements.

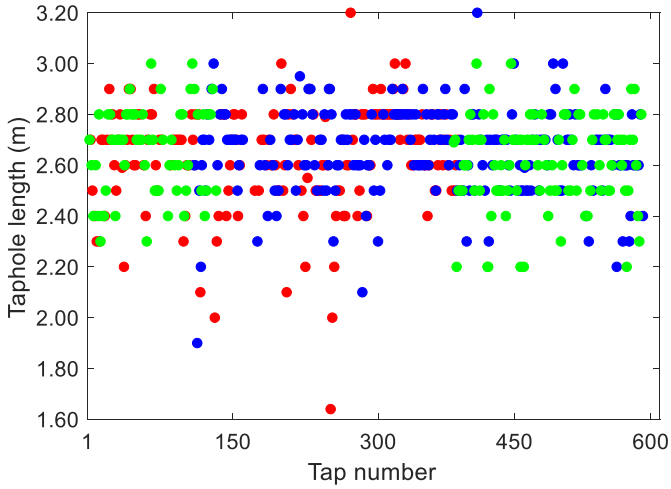

Figure 44. *Taphole length measurements for the first 600 taps of Data set 1 from the reference furnace.*

In order to evaluate such seemly random variation of the taphole length as well as assuming a random variation of the void region in front of the taphole, stochastics in l_{th} and r_{min} were considered in the model. l_{th} values were set to fall uniformly within the range of 2.60 ± 0.3 m and r_{min} within the range of 0.125 ± 0.025 m while keeping the rest of variables and parameters of the Base case. The dynamic response was simulated for a long enough time. Figure 45 depicts the normalized outflows of iron (red) and slag (blue) for seven consecutive taps equivalent to about 18 hours of (simulated) production. Table 3 presents the resulting tap duration, slag delay and slag share corresponding to these taps. The results show that even with a modest variation in l_{th} and r_{min} the model produced a variety of outflow patterns similar to those seen in the real process. In the real system, some of these key variables may fluctuate gradually, yielding distinctive patterns between the operating tapholes during some hours of operation as discussed in Paper III.

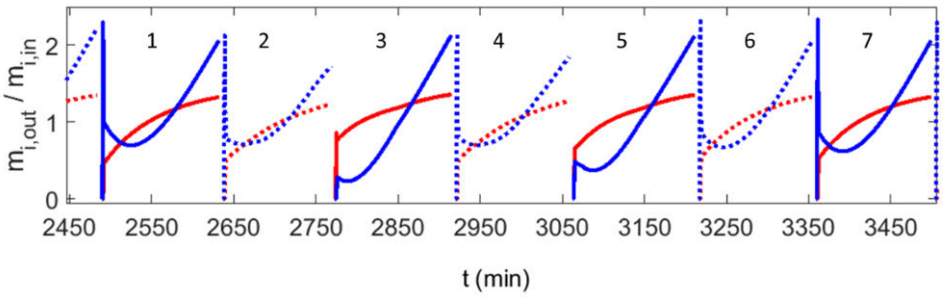

Figure 45. *Response to stochastic in l_{th} and r_{min} during 18 hours of simulated production using the model developed in Paper III.*

Table 3. Outflow indices for the taps shown in Figure 44.

Tap #	**1**	**2**	**3**	**4**	**5**	**6**	**7**
l_{th} (m)	2.62	2.7	2.48	2.77	2.64	2.49	2.54
r_{min} (m)	0.14	0.10	0.14	0.11	0.13	0.14	0.15
t_{tap} (min)	143	127	142	136	155	138	142
t_{sd} (min)	-2	-1	1	-1	0	-1	-2
γ_{out} (-)	0.21	0.22	0.17	0.22	0.18	0.22	0.20

Finally, the model was evaluated in terms of the dynamics seen in the process data after certain events, for instance, longer inter-cast periods and changes in the level of production. Figure 46 depicts seven consecutive taps from Data

set 1 with a short stoppage of about 3.5 hours after tap #408, and a longer inter-cast time between taps #409 and #410. The simulated response depicted in Figure 47 shows the liquid outflows and inflows as well as the liquid level in the hearth. The furnace pressure was decreased linearly within two hours (after $t = 1000$ min), kept at the ambient pressure during two hours, and ramped up to the normal furnace pressure in three hours. To consider the time lag of the liquids between the tuyere level and the hearth, the production rate was varied proportionally to the gauge pressure with a delay of 30 min. The taphole was kept closed until 1.5 h had elapsed after the pressure started to increase.

With respect to the simulated sequence, in tap #2 before the stoppage the liquids descend to low levels as a taphole stays open, but the levels increase considerably when the production is restated but the tapholes are kept closed (black lines). The high iron level gives rise to a slag delay of tap #3. Due to the long inter-cast period that follows between taps #3 and #4, the slag level raises further, yielding a long tap (#4) during which the iron level descends well below the taphole. Some discrepancies exist between the measured and simulated signals, e.g., the slag share distribution after the stoppage. During a stoppage, the conditions in front of the taphole and in the dead man may change significantly due to the stagnant liquids and this may have a lasting effect after the production is resumed. In the simulated case in Figure 47, and in the model in general, these particular conditions were not considered.

Overall, the model has been demonstrated to be able to reproduce the drainage patterns observed in the actual furnace. It makes it possible to study the system in quasi-stationary state and its dynamic response to changes under different sets of conditions. Despite the simplicity of the model, which makes it feasible to study numerous states and conditions, the mathematical description seems to have captured the main characteristics of the fluid mechanics.

One of the challenges of both off-line models (Paper II and Paper III) is that because of the large number of variables and parameters, different sets of values can result in similar outputs. Some parameters require a deeper evaluation based on solid theoretical or practical justification. However, the apparent process stochastics captured by both models and the lack of direct measurements limit the possibility to validate the models.

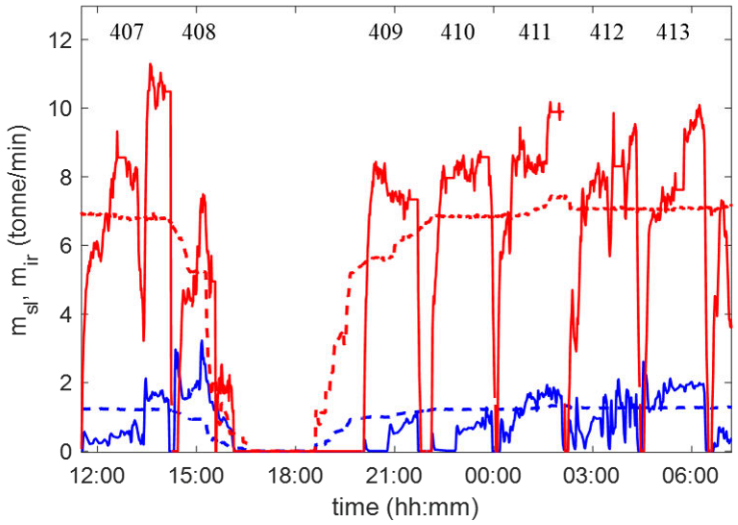

Figure 46. *Inflow and outflow rates (dashed and solid lines) of iron and slag for consecutive taps, including a 3.5-hour stoppage for the reference furnace.*

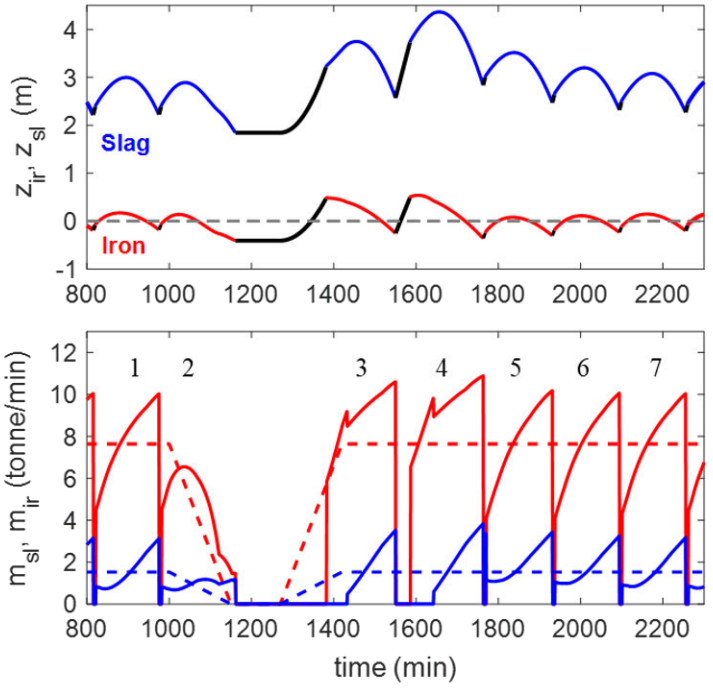

Figure 47. *Liquid levels (z_{ir} and z_{sl}) and inflow and outflow rates (dashed and solid lines) of iron and slag (m_{ir} and m_{sl}). The production is ramped down and up prior to and after a 3.5-hour stoppage, respectively. A longer inter-cast period occurs between taps #3 and #4. Base-case setting of all other variables.*

4.3 On-line estimation of liquid levels (Paper IV)

This section presents a model intended to provide an on-line view of the liquid levels in the hearth by processing continuous estimates of liquid outflows and inflows as well as the taphole length from the reference furnace. Other continuous techniques such as emf and strain gauges have been demonstrated to provide signals that reflect changes in the liquid levels in blast furnaces, but the noise and, above all, drift in the signal remain major challenges (Hattink et al. 2008). Substantial filtering and adjustments are required in order to obtain useful results (Cho et al., 2012), and for some furnaces the emf signals are useless. Furthermore, the signals are claimed to be affected by temperature and possibly by the composition of the liquids, and it is very challenging to obtain more than a qualitative indication of the liquid levels. Similarly, models based on short-term production and outflow signals count with associated errors that require a method for correcting the inputs or outputs to prevent the liquid-level estimates from drifting to unreasonable levels.

The mathematical model presented in this section is based on the same general assumption of Papers II and III (see Section 4.2) and applies similar equations as in Paper II. The method is motivated by the data analysis of Paper I and the key findings of Papers II and III with respect to the apparent liquid distribution in the hearth, also suggested by Iida et al. (2009) and Ito et al. (2014).

4.3.1 Model formulation

The two-pool scheme of Paper II is extended to an *m*-pool hearth based on the arrangement of the tapholes in the hearth in question. The left side of Figure 48 illustrates a four-pool hearth for the case of the reference furnace with discrete pool liquid levels and cross-pool communication between adjacent pools. The right side of Figure 48 depicts the scheme applied of four pools of same size and the location of the three tapholes.

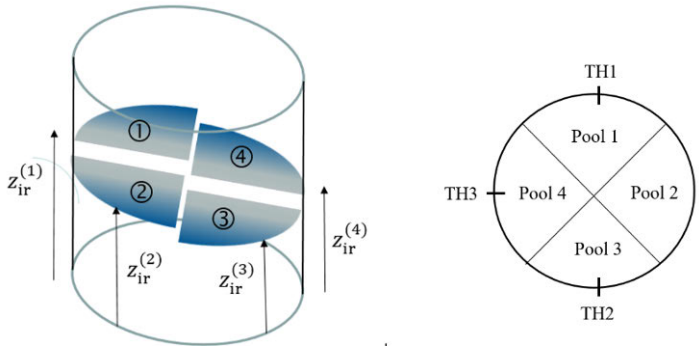

Figure 48. *Schematic illustration of the iron levels in a four-pool liquid level model (left) with the three tapholes in the reference furnace indicated (right).*

The liquid levels in the pools are expressed by the differential equations of Equation 12 and 13, where the communication factors, φ_{ir} and φ_{sl}, are used to parametrize the flow between pools as described in Paper II. The pool sizes are fixed in the on-line model and one-minute averages of the inflows and outflows are used in the discretized differential equations. As the mass of tapped iron is assumed to be more reliable in comparison with slag, it is used as a basis for a correction of the inflow rate of iron, which is taken to be proportional to the inflow rate of slag. The mass balance of slag, in turn, is then used to correct the slag outflow rate.

4.3.2 Tap cycle criteria

As there are no direct measurements of the liquid levels in the hearth, the corrections of the mass balances are introduced at moments when indirect information about the levels is available, i.e., at the tap start and tap end.

Considering the unknown and potentially changing conditions at the inner end of the taphole, an "uncertainty band" was introduced similar to that used in the model of Paper III. Figure 49 illustrates the principle, with a band Δz_{th} around the taphole, further extended downward by Δz_{lift} to account for the interface tilting towards the taphole during the two-phase outflow. The outer end of the taphole is defined as $z = 0$ m while the level of the inner end is calculated from measured taphole length and angle.

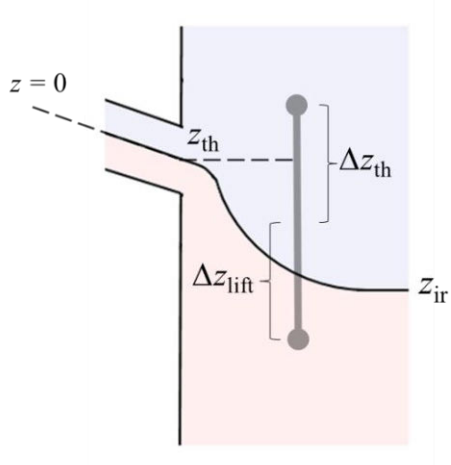

Figure 49. *Illustration of the band around the taphole that is used in the corrections of the mass balances.*

The band is used in the correction criteria for the estimated iron levels in the tapping pool by the following conditions, which depend on whether a taphole that is opened initially drains iron, slag or both phases:

i. If iron (slag) is the first phase to be tapped, the slag (iron) in the draining pool is assumed to be located above (below) the taphole band, so the iron

(slag) level should be at the upper (lower) limit of the band at the moment when slag (iron) enters the taphole. Otherwise, the iron level is corrected.

ii. If iron and slag start draining simultaneously, the iron level may fall anywhere within the taphole band at tap start. If the original level satisfies this condition, no correction is undertaken, and if the original level is above (below) the band a correction downwards (upwards) is made until the upper (lower) limit of the band is reached.

The condition for correcting the mass balance of slag is connected to the slag level in the tapping pool at the point when the tap ends, using the tap-end condition defined in Paper II. As the tap ends according to the casthouse records, the slag levels is required to fall within an uncertainty band

$$\left|(z_{\mathrm{sl}}^{(j^*)} - z_{\mathrm{th}}^{(j^*)}) - z_{\mathrm{sl,end}}\right| \leq \Delta z \tag{25}$$

around the target level

$$z_{\mathrm{sl,end}} = \omega^{(j^*)} \frac{\dot{m}_{\mathrm{sl,out}}^{(j^*)}}{\rho_{\mathrm{sl}} A^{(j^*)} \varepsilon} \tag{26}$$

This simple equation was used instead of the flow-out coefficient approach, since the slag viscosity, local dead-man voidage and coke diameter close to the taphole are largely unknown in practice. Additionally, those conditions may be different between tapholes. Figure 50 illustrates the principles for the level corrections, where it is seen that the mass balance of iron is corrected for the period between tap starts, while the mass balance of slag is corrected for periods between tap ends. In practice, the correction is implemented by introducing factors by which the iron inflow and slag outflow are corrected to satisfy the conditions mentioned above.

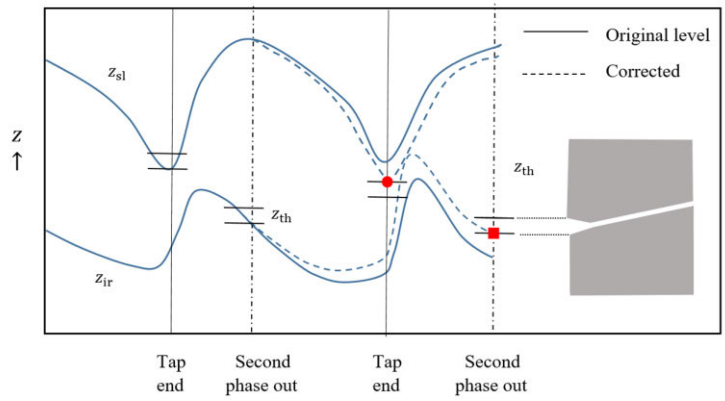

Figure 50. *Principles of corrections in the model. Vertical lines denote important times for the corrections during the tap cycles, while horizontal lines denote the bands around the taphole and the estimated slag-end level.*

It is interesting to note that the tap-end condition can be applied not only to correct the slag balance, but also to predict the end of the ongoing tap. To do so, the levels are predicted and the observed slag outflow rate, $\dot{m}_{\mathrm{sl,out}}^{(j^*)}(t)$, is used to calculate the quantity

$$\Delta z_{\mathrm{pred}}(t) = (z_{\mathrm{sl}}^{(j^*)}(t) - z_{\mathrm{th}}^{(j^*)}) - \omega^{(j^*)} \frac{\dot{m}_{\mathrm{sl,out}}^{(j^*)}(t)}{\rho_{\mathrm{sl}} A^{(j^*)} \varepsilon} \tag{27}$$

where the approach of $\Delta z_{\mathrm{pred}}(t)$ to zero is taken as an indication of the upcoming tap end.

4.3.3 Results and key findings

The on-line model was applied to the three-month process data of Data set 1 including the tap cycle records (cf. Figure 43) and taphole length record (cf. Figure 44). For the large furnace in question, four pools of equal size were considered, where a pair of pools is alternately tapped. Pool 2 has no taphole and is never directly drained. Figure 51 indicates the periods from Data set 1 described in this section (solid line). The periods studied in Paper IV also include the ones indicated by dashed boxes, but these are not treated here.

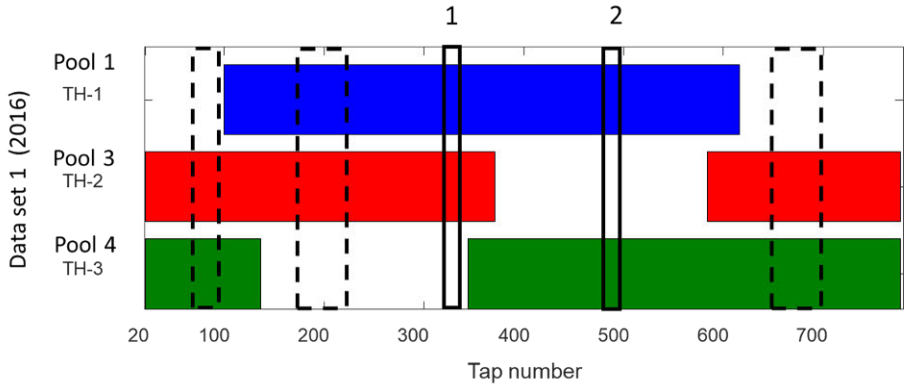

Figure 51. *Data set 1 and periods of interest included in Section 4.3 (full line) and included in Paper IV (dashed line).*

Figure 52 presents the results corresponding to two sets of consecutive taps, Period 1 and Period 2, with 14 and 13 taps, respectively. The top panels show the estimated pool liquid levels (after corrections) where the draining pool reaches the lowest level at the end of the taps, as seen for Pool 1 (blue solid line) and Pool 2 (red solid line) during Period 1, and for Pool 1 and Pool 3 (magenta dotted-dashed line) during Period 2. Since the tapping pools are located in opposite sides of the hearth during Period 1, the non-tapping pools display identical fluctuations of the liquid levels. Conversely, the asymmetric

arrangement of the tapping pools around the hearth during Period 2 yields a more complex liquid distribution.

The difference between the two periods is particularly clearly seen in the end levels of the slag, indicated by the red dots on the upper uncertainty bands in the middle panels of Figure 52. While the two operating pools in Period 1 show similar behavior, they show distinctively different levels in Period 2. This is seen as corrections of the slag levels that alternately fall on the upper and lower boundary of the uncertainty band. The taphole length varied little during the two periods, so the levels of the iron bands stayed practically constant. The imbalance observed in Period 2 may be caused by permeability differences as studied in Subsection 4.2.1 and/or the conditions in front of the taphole as explored in Subsection 4.2.2.

The stochastics noted when comparing the results of the off-line models to the process data are also reveled in the on-line application. This is noticed in the bottom panels of Figure 52 where the mass correction of the produced iron and tapped slag are presented for the two periods. In both periods, the amount of tapped slag was larger than expected at some taps and less at others, thus revealing the slag distribution expressed by C2 in the PCA analysis (cf. Section 4.1). Iron, on the other hand, required little correction in Period 1, while the outflows in Period 2 were lower than expected for most taps so the production rate was adjusted down. This may suggest a gradual accumulation of iron in the hearth. The seemingly coupled iron pools—notable in the levels and magnitude of the corrections—contrary to more imbalanced slag pools, supports the assumption of different permeability for iron and slag, parametrized as communication factors in the on-line model (and in the off-line model of Paper II, Subsection 4.2.1). The viscosity difference between iron and slag play an important role in the flow resistance and pressure drop in the dead man, and therefore, on the liquid distribution.

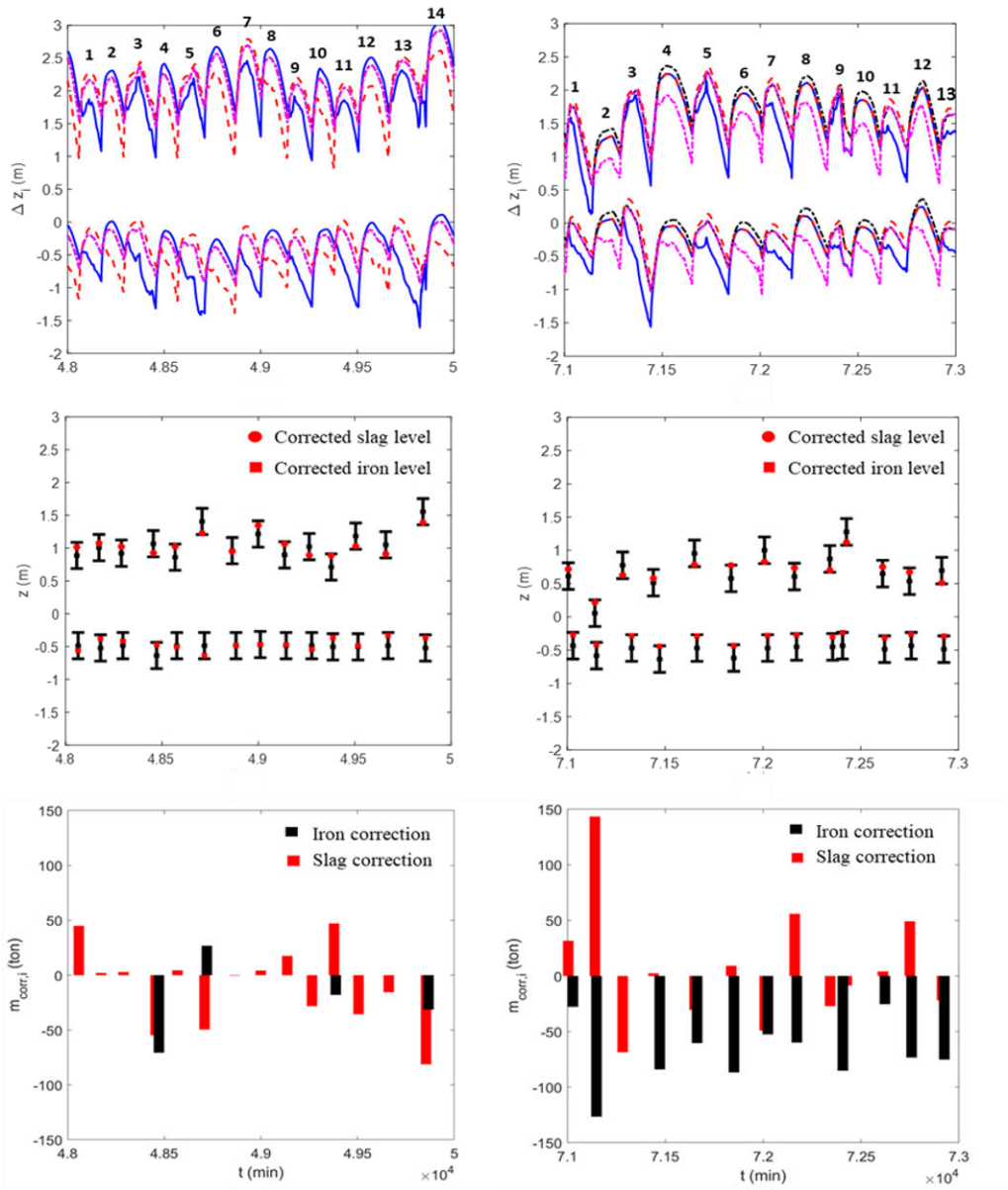

Figure 52. *Estimated liquid levels (top), location of bands around the (inner end of) the taphole and the nominal slag-end level (middle) and correction of the mass of produced iron and tapped slag (bottom) for a Period 1 and Period 2 (cf. Figure 51) Pool 1: blue solid line, Pool 2: black dash-dotted line, Pool 3: red dashed line, and Pool 4: magenta dash-dotted line.*

The results presented in Figure 52 correspond to periods were the pair of tapholes have been in operation for quite some time (cf. Figure 51). The

model, however, showed even more imbalance in periods when one of the tapholes had been operated a few taps only. This imbalance was already illustrated by the behavior of the principal components C1 and C2. Paper IV demonstrates that applying different tap-end parameters (ω) for the two operating tapholes could substantially reduce the extent of the required corrections of the mass balances, suggesting that different conditions in front of the operating tapholes are a likely reason for the observed imbalance in slag draining, as studied in more detail in Paper III (cf. Subsection 4.2.2).

Finally, an example of the on-line tap-end prediction is presented in Figure 53 for the same nominal parameters and the same periods as depicted in Figure 52, where the time when the tap is predicted to end corresponds to $\Delta z_{\mathrm{pred}}(t) = 0$ m. The model was relatively successful for most TH2 taps during Period 1, but clearly underestimated the tapping duration for TH1. During Period 2, the overall performance was worse, underestimating tap duration for TH1 and overestimating those for TH3. Better results were obtained by applying different values of ω, suggesting that this parameter may vary with time. It is important to keep in mind that ω parametrizes the local dead-man conditions that govern the end slag level, so a constant value is unrealistic considering the dynamic nature of the system.

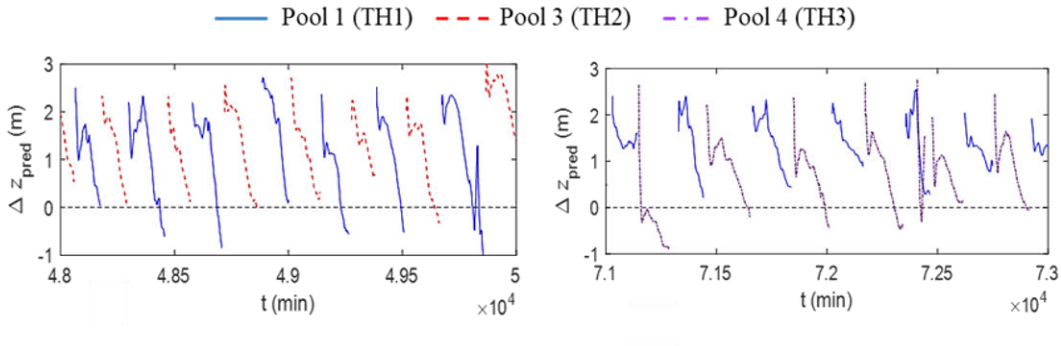

Figure 53. *Predicted vertical distance between the estimated slag level in the draining pool and the slag-end level, Δz_{pred}. Results for the periods studied in Figures 52 using nominal parameter values, Period 1 (left) Period 2 (right).*

Overall, the estimation method developed proved adequate to correct the otherwise drifting signals. However, the model faced clear challenges when it comes to the tap-end prediction. The apparent stochastic behavior of the system parameters adds to the process complexity, and therefore, makes its modeling challenging. The model can be expanded to consider pools of different sizes or with dynamic growth, as applied in the model in Paper II. Analysis of independent indirect liquid level information such as emf signals may help to improve or validate the model.

5. Conclusions

The main goal of this thesis was to study the iron and slag drainage of a large multi-taphole blast furnace and to gain a better understanding of the complex system by model-based analysis. The models that were developed were aimed to describe the hearth system and drainage process by considering fluid dynamics and assumptions based on the process data from an operating furnace (Papers II-IV) or by a purely data-driven approach (Paper I).

Section 4.1 (Paper I) presents a study of two sets of iron and slag outflow data from a reference blast furnace. After an appropriate pre-processing of the raw data, principal component analysis (PCA) was conducted by which a set of indicators that reflect the features of the outflow patterns such as, slag delay, slag share and outflow rate progression, were identified. The results revealed distinctive outflow patterns between the operating tapholes in the principal component space. These patterns appeared to drift apart from each other at particular instants as well as converge at others. The tapping patterns farthest from the *mean pattern* occurred right after an idle period of a taphole, suggesting that the local conditions at the inner end of the taphole are different but gradually change over time when the taphole is operated. Therefore, by the end of the operation period of a taphole pair, the outflow patterns were found to be more stable and closer to the *mean pattern*. Generally, two key factors seemed to play a role: iron and slag distribution, and local conditions that govern the outflow.

In Section 4.2, the role of the two presumed factors were studied by developing two off-line models. Section 4.2.1 presents a liquid level model that focuses on the dead-man permeability differences to evaluate the iron and slag distribution in the hearth. The model considers a hearth divided into two pools with a parametrized expression for cross-pool liquids communication. With given inflows and parametrized outflows according to the *mean pattern* in Section 4.1, the liquid levels were constructed. A sensitivity analysis was conducted, where a case of asymmetric pools and stochastics in the tap-end condition yielded tap sequences similar to some observed in the process data from the reference blast furnace. Section 4.2.2 presents a one-pool hearth model that focuses on the taphole state and different dead-man permeability in front of the tapholes. By a sensitivity analysis of the model it was demonstrated to be able to yield outflows resembling a variety of patterns observed in the real blast furnace. Asymmetry in the conditions, in particular taphole length and dead-man permeability in front of the taphole, was found to reproduce certain frequently recurring outflow patterns showing imbalance in the hearth drainage. The model was also able to reproduce the dynamic response of the system fairly accurately under certain events and to illustrate that

stochastics may play a role in the variation detected by the PCA analysis in Section 4.1. The off-line models would still require independent information in order to validate or reject some of the assumptions made since different sets of model parameters can produce similar outcomes.

The hearth drainage is a dynamic process and the lack of direct measurements makes it extremely challenging reconstruct the internal conditions of the hearth in real time. Nonetheless, the quantities of iron weighed in torpedoes represent the most reliable source of information regarding the drainage. Section 4.3 presents an on-line model implemented to reconstruct the liquid levels in the hearth and predict the end of the tap based on continuous corrections of the observed quantities. The basis of the model were borrowed from the model in Section 4.2.1, but expanded to a four-pool hearth considering the three-taphole arrangement in the reference blast furnace. The results showed an uneven distribution of iron and slag, also noted in Paper I and studied in Paper II. The tap-end prediction was found challenging due to a high degree of stochastics and the gradual changes observed in the conditions of the dead man in front of the tapholes, as studied in more detail in the off-line model of Paper III.

The different approaches covered in the present thesis shed some light on drainage process and the unknowns of the hearth system despite its complexity. The data analysis of Paper I was key to identify the complex dynamics and to provide the basis for the off-line models of Papers II and III. The knowledge of the system gained in the development of these models was utilized in the work on the on-line model presented in Paper IV.

6. Future work

The models of the thesis have brought about deeper understanding of hearth drainage in large blast furnaces, but have also revealed knowledge gaps that have to be filled in future work.

The PCA method developed for Paper I provides a way to compress and visualize the otherwise staggering amount of information that the drainage data holds. Even though two quite large data sets were used in the analysis, the method should be applied to more extensive data sets to be make it possible to draw more definitive conclusions about the system dynamics. In particular, the state where an idle taphole is taken into operation should be studied. Additionally, the results of the PCA-based approach should be correlated with other blast furnace variables.

An interesting extension of the off-line models (Papers II and III) and on-line model (Paper IV) is to consider the possibility of a floating dead man. The motion of the dead man strongly affects the liquid levels and this extension would make it possible to study a broader range of cases and to apply the models to other blast furnaces with different conditions than the one studied in this thesis. To do so, some conditions or simplification could be revised. For instance, the formulation of the pressure-loss equations, and particularly those concerning the entrance loss, could be improved. The gradual changes studied in Paper I as well as some measurements (production estimates, taphole length and diameter, etc.) could be incorporated in the model to construct a virtual on-line representation of the hearth system. The model could also be extended to consider the different casting strategies including overlapping taps.

A way to validate the liquid levels reconstructed by the models could be by correlating the results with emf or strain-gauge measurements. However, a deeper study and evaluation of these techniques is necessary. A possible synergy between the balance-based models and such data-driven models may be a key to improving the accuracy of the liquid level estimates.

It could also be interesting to develop an on-line application of the model of Paper III to reconstruct and potentially predict the liquid levels in the hearth using fluid mechanics rather than the purely data-driven approach taken in Paper IV. To do so, many aspects should be taken into account, such as production estimates, taphole length and diameter measurements, a more realistic hearth geometry, etc. Moreover, the delays and attenuation that occur in the iron and slag runners could be considered in order to compare the estimated outflows of the models with the outflow measurements. If the model of Paper III could be adaptively updated to reflect the prevailing conditions of the hearth, it could be applied to evaluate and anticipate the system's response, e.g., at stoppages, changes in the production rate or in the tapping strategy.

References

Agrawal, A., Kor, S.C., Nandy, U., Choudhary, A.R. & Tripathi, V.R. 2016, "Real-time blast furnace hearth liquid level monitoring system", *Ironmaking & Steelmaking,* vol. 43, no. 7, pp. 550-558.

Agrawal, A., Kothari, A.K., Ramakrishna Rao, K., Padmapal & Singh, M.K. 2019, "Effect of Hearth Liquid Level on the Productivity of Blast Furnace", *Transactions of the Indian Institute of Metals,* vol. 72, no. 4, pp. 867-876.

Babich, A. & Senk, D. 2019, *13 - Coke in the iron and steel industry*, Woodhead Publishing.

Bambauer, F., Wirtz, S., Scherer, V. & Bartusch, H. 2018, "Transient DEM-CFD simulation of solid and fluid flow in a three dimensional blast furnace model", *Powder Technology,* vol. 334, pp. 53-64.

Bartholomew, D.J. 2010, *Principal Components Analysis*, Elsevier, Oxford.

Bean, I. 2008, *Blast Furnace Hearth Drainage Improvement of the Residual-Flowout Correction*, University of New South Wales, Sydney, Australia.

Biswas, A.K. 1981, *Principles of blast furnace ironmaking: theory and practice,* Cootha, Brisbane, Australia.

Brännbacka, J., Torrkulla, J. & Saxén, H. 2005, "Simple simulation model of blast furnace hearth", *Ironmaking & Steelmaking,* vol. 32, no. 6, pp. 479-486.

Brännbacka, J. & Saxén, H. 2003, "Model Analysis of the Operation of the Blast Furnace Hearth with a Sitting and Floating Dead Man", *ISIJ International,* vol. 43, no. 10, pp. 1519-1527.

Brännbacka, J. & Saxén, H. 2001, "Modeling the Liquid Levels in the Blast Furnace Hearth", *ISIJ International,* vol. 41, no. 10, pp. 1131-1138.

Cameron, I., Sukhram, M., Lefebvre, K. & Davenport, W. 2020a, *Chapter 1 - The Iron Blast Furnace Process*, Elsevier.

Cameron, I., Sukhram, M., Lefebvre, K. & Davenport, W. 2020b, *Chapter 57 - Casting the Blast Furnace*, Elsevier.

Cameron, I., Sukhram, M., Lefebvre, K. & Davenport, W. 2020c, *Chapter 58 - Blast Furnace Slag*, Elsevier.

Chibwe, D.K., Evans, G.M., Doroodchi, E., Monaghan, B.J., Pinson, D.J. & Chew, S.J. 2020, *Charge material distribution behaviour in blast furnace charging system*.

Colebrook, C.F., White, C.M. & Taylor, G.I. 1937, "Experiments with fluid friction in roughened pipes", *Proceedings of the Royal Society of London.Series A - Mathematical and Physical Sciences,* vol. 161, no. 906, pp. 367-381.

Danloy, G., Stolz, C., Crahay, J. & Dubois, P. 1999, "Measurement of of Iron and Slag Levels in Blast Furnace ", , pp. 89.

Dash, S.K., Ajmani, S.K., Kumar, A. & Sandhu, H.S. 2001, "Optimum taphole length and flow induced stresses", *Ironmaking & Steelmaking,* vol. 28, no. 2, pp. 110-116.

de Castro, J.A., da Silva, A.J., Sasaki, Y. & Yagi, J. 2011, "A Six-phases 3-D Model to Study Simultaneous Injection of High Rates of Pulverized Coal and

Charcoal into the Blast Furnace with Oxygen Enrichment", *ISIJ International,* vol. 51, no. 5, pp. 748-758.

Desai, D. 1993, "Analysis of the Hearth Furnace Drainage Based on the Measurement of Liquid Pressure Inside of the Hearth ", *Transactions of the Iron & Steel Society of AIME,* vol. 14, pp. 45-50.

Dong, X.F. & Zulli, P. 2019, *Prediction of blast furnace hearth condition: part I– a steady state simulation of hearth condition during normal operation*.

Dorofeev, V.N. & Novokhatskii, A.M. 1984, "Origin of Difference in Electric Potentials on Blast Furnace Shell", *Steel in the USSR,* vol. 14, no. 1, pp. 10-12.

Ergun, S. 1952, "Fluid flow through packed columns", *Chem.Eng.Prog.,* vol. 48, pp. 89-94.

Fu, D., Chen, Y. & Zhou, C.Q. 2015, *Mathematical modeling of blast furnace burden distribution with non-uniform descending speed*.

Fukutake, T. & Okabe, K. 1976a, "Experimental Studies of Slag Flow in the Blast Furnace Hearth during Tapping Operation", *Transactions of the Iron and Steel Institute of Japan,* vol. 16, no. 6, pp. 309-316.

Fukutake, T. & Okabe, K. 1976b, "Influences of Slag Tapping Conditions on the Amount of Residual Slag in the Blast Furnace Hearth", *Transactions of the Iron and Steel Institute of Japan,* vol. 16, no. 6, pp. 317-323.

Geerdes, M., Chaigneau, R. & Kurunov, I. 2015, *Modern Blast Furnace Ironmaking: An Introduction (Third Edition, 2015),* IOS Press.

Guo, B., Maldonado, D., Zulli, P. & Yu, A. 2008, "CFD Modelling of Liquid Metal Flow and Heat Transfer in Blast Furnace Hearth", *ISIJ International,* vol. 48, no. 12, pp. 1676-1685.

Hattink, M., vd Stel, J., Lecacheux, B., Zaïmi, S.A., Mielenz, O., Rüther, H., Bläsner, M., Köchner, H., Ojeda, C., da Costa, E., Abreu, E., Sheng, D.Y., Sundqvist, L. & Wikström, J.O. 2008, *RFCS, Report EUR 24976*, The European Commission.

He, Q., Zulli, P., Tanzil, F., Lee, B., Dunning, J. & Evans, G. 2002, "Flow Characteristics of a Blast Furnace Taphole Stream and Its Effects on Trough Refractory Wear", *ISIJ International,* vol. 42, no. 3, pp. 235-242.

Helle, M. & Saxén, H. 2003, *Tool for What-If-Analysis of the Conditions in the Tuyere and Raceway Region of the Blast Furnace*.

Huang, C., Du, S. & Cheng, W. 2008, "Numerical Investigation on Hot Metal Flow in Blast Furnace Hearth through CFD", *ISIJ International,* vol. 48, no. 9, pp. 1182-1187.

Iida, M., Ogura, K. & Hakone, T. 2009, "Numerical Study on Metal/Slag Drainage Rate Deviation during Blast Furnace Tapping", *ISIJ International,* vol. 49, no. 8, pp. 1123-1132.

Iida, M., Ogura, K. & Hakone, T. 2008, "Analysis of Drainage Rate Variation of Molten Iron and Slag from Blast Furnace during Tapping", *ISIJ International,* vol. 48, no. 4, pp. 412-419.

Ito, T., Yotsuji, J. & Nagamune, A. 2014, "Development of Pig Iron and Molten Slag Level Measurement Technique for Blast Furnace", *ISIJ International,* vol. 54, no. 11, pp. 2618-2622.

Kourti, T. 2009, *4.02 - Multivariate Statistical Process Control and Process Control, Using Latent Variables*, Elsevier, Oxford.

Kurpisz, K. 1988, "A Method for Determining Steady State Temperature Distribution within Blast Furnace Hearth Lining by Measuring Temperature at Selected Points", *Transactions of the Iron and Steel Institute of Japan,* vol. 28, no. 11, pp. 926-929.

Liu, L., Jiang, Z., Zhang, X., Lu, Y., He, J., Wang, J. & Zhang, X. 2018, "Effects of top gas recycling on in-furnace status, productivity, and energy consumption of oxygen blast furnace", *Energy,* vol. 163, pp. 144-150.

Liu, W., Shao, L., Saxén, H. 2020, "Experimental Model Study of Liquid–Liquid and Liquid–Gas Interfaces during Blast Furnace Hearth Drainage." *Metals,* vol. 10, no. 4, p. 496.

Matsui, Y., Tadai, R., Ito, K., Matsuo, T., Nagai, N. & Imai, T. 2006, "Stabilization of Tapping Hole Length by Controlling Blast Furnace Raceway Depth", *Tetsu-to-Hagane,* vol. 92, no. 12, pp. 926-931.

Mitra, T. & Saxén, H. 2015a, "Evolution of Charging Programs for Achieving Required Gas Temperature Profile in a Blast Furnace", *Materials and Manufacturing Processes,* vol. 30, no. 4, pp. 474-487.

Mitra, T. & Saxén, H. 2015b, "Simulation of Burden Distribution and Charging in an Ironmaking Blast Furnace", *IFAC-Papers On Line,* vol. 48, no. 17, pp. 183-188.

Naito, M., Takeda, K. & Matsui, Y. 2015, "Ironmaking Technology for the Last 100 Years: Deployment to Advanced Technologies from Introduction of Technological Know-how, and Evolution to Next-generation Process", *ISIJ International,* vol. 55, no. 1, pp. 7-35.

Nightingale, R.J. 2000, *The development and application of hearth voidage estimation and Deadman Cleanliness Index for the control of blast furnace hearth operation* (doctoral thesis), University of Wollongong (Ausitralia).

Nightingale, R.J., Tanzil, F. W. B. U., Beck, A.J.G. & Price, K. 2001, "Blast Furnace Hearth Condition Monitoring and Taphole Management Techniques", *Rev.Met.Paris,* vol. 98, no. 6, pp. 533-540.

Nishioka, K., Maeda, T. & Shimizu, M. 2005a, "Effect of Various In-furnace Conditions on Blast Furnace Hearth Drainage", *ISIJ International,* vol. 45, no. 10, pp. 1496-1505.

Nishioka, K., Maeda, T. & Shimizu, M. 2005b, "A Three-dimensional Mathematical Modelling of Drainage Behavior in Blast Furnace Hearth", *ISIJ International,* vol. 45, no. 5, pp. 669-676.

Nouchi, T., Sato, M., Takeda, K. & Ariyama, T. 2005, "Effects of Operation Condition and Casting Strategy on Drainage Efficiency of the Blast Furnace Hearth", *ISIJ International,* vol. 45, no. 10, pp. 1515-1520.

Nouchi, T., Yasui, M. & Takeda, K. 2003, "Effects of Particle Free Space on Hearth Drainage Efficiency", *ISIJ International,* vol. 43, no. 2, pp. 175-180.

Omori, Y. 1987, *Blast furnace phenomena and modelling,* ISIJ, Elsevier, London.

Park, J., Jung, H., Jo, M., Oh, H. & Han, J. 2011, "Mathematical modeling of the burden distribution in the blast furnace shaft", *Metals and Materials*

International, vol. 17, no. 3, pp. 485-496.

Pettersson, F., Saxén, H. & Hinnelä, J. 2005, "A Genetic Algorithm Evolving Charging Programs in the Ironmaking Blast Furnace", *Materials and Manufacturing Processes,* vol. 20, no. 3, pp. 351-361.

Post, James, 2019*, Simulation of the Inhomogeneous Deadman of an Ironmaking Blast Furnace* (doctoral thesis), TU Delft (the Netherlands).

Roche, M. 2020*, Quasi-time Evolution of Outflow Patterns from PCA Results.* Available: https://youtu.be/MTUWxIh7N44.

Sawa, Y., Takeda, K., Taguchi, S., Matsumoto, T., Watanabe, Y. & Kamano, H. 1992, "Influence of Low Permeability Zone in Blast Furnace Hearth on Temperature Distribution in Furnace Bottom and on Iron and Slag Tapping Indices", *Tetsu-to-Hagane,* vol. 78, no. 7, pp. 1171-1178.

Saxén, H., Lassus, L., Seppänen, M. & Karjalahti, T. 2000, "Pattern recognition and classification of blast furnace wall temperatures", *Ironmaking & Steelmaking,* vol. 27, no. 3, pp. 207-211.

Saxén, H. 2015, "Model of Draining of the Blast Furnace Hearth with an Impermeable Zone", *Metallurgical and Materials Transactions B,* vol. 46, no. 1, pp. 421-431.

Saxén, H. & Brännbacka, J. 2005, "Dynamic model of liquid levels in the blast furnace hearth", *Scandinavian Journal of Metallurgy,* vol. 34, no. 2, pp. 116-121.

Shao, L. 2013, *Model-Based Estimation of Liquid Flows in the Blast Furnace Hearth and Taphole (doctoral thesis)*, Åbo Akademi University, Turku, Finland.

Shao, L. & Saxén, H. 2011, "A Simulation Study of Blast Furnace Hearth Drainage Using a Two-phase Flow Model of the Taphole", *ISIJ International,* vol. 51, no. 2, pp. 228-235.

Shen, Y., Guo, B., Chew, S., Austin, P. & Yu, A. 2016, "Modeling of Internal State and Performance of an Ironmaking Blast Furnace: Slot vs Sector Geometries", *Metallurgical and Materials Transactions B: Process Metallurgy and Materials Processing Science,* vol. 47, no. 2, pp. 1052-1062.

Shi, L., Li, Z., Yu, T. & Li, J. 2011, "Model of Hot Metal Silicon Content in Blast Furnace Based on Principal Component Analysis Application and Partial Least Square", *Journal of Iron and Steel Research International*, vol. 18, no. 10, pp-13-16.

Shibata, K., Kimura, Y., Shimizu, M. & Inaba, S. 1990, "Dynamics of Dead-man Coke and Hot Metal Flow in a Blast Furnace Hearth", *ISIJ International,* vol. 30, no. 3, pp. 208-215.

Sun, H. 2005, "Analysis of Reaction Rate between Solid Carbon and Molten Iron by Mathematical Models", *ISIJ International,* vol. 45, no. 10, pp. 1482-1488.

Sunahara, K., Inada, T. & Iwanaga, Y. 1993, "Size Degradation of Deadman Coke by Reaction with Molten FeO in Blast Furnace", *ISIJ International,* vol. 33, no. 2, pp. 275-283.

Sunahara, K., Inada, T. & Iwanaga, Y. 1992, "Size Degradation of Dead-man Coke by Reaction with Molten FeO in Blast Furnace", *Tetsu-to-Hagane,* vol. 78, no. 7, pp. 1156-1163.

Swartling, M., Sundelin, B., Tilliander, A. & Jönsson, P.G. 2010, "Heat Transfer Modelling of a Blast Furnace Hearth", *steel research international,* vol. 81, no. 3, pp. 186-196.

Swartling, M., Tilliander, A., Saxén, H. & Jönsson, P.G. 2012, "Interpretation of Tap Induced Cyclic Temperatures in the Blast Furnace Lining", *steel research international,* vol. 83, no. 7, pp. 695-704.

Tanzil, W.B.U. & Pinczewski, W.V. 1987, "Blast furnace hearth drainage: Physical mechanisms". *Chemical Engineering Science,* vol. 42, no. 11, pp.2557-2568.

Tanzil, W.B.U., Zulli, P., Burgess, J.M. & Pinczewski, W.V. 1984, "Experimental Model Study of the Physical Mechanisms Governing Blast Furnace Hearth Drainage*". Trans Iron Steel Inst Jpn.,* vol. 24, no. 3, pp.197-205.

Torrkulla, J., Brännbacka, J., Saxén, H. & Waller, M. 2002, "Indicators of the Internal State of the Blast Furnace Hearth", *ISIJ International,* vol. 42, no. 5, pp. 504-511.

Torrkulla, J. & Saxén, H. 2000, "Model of the State of the Blast Furnace Hearth", *ISIJ International,* vol. 40, no. 5, pp. 438-447.

Tsuchiya, N., Fukutake, T., Yamauchi, Y. & Matsumoto, T. 1998, "In-furnace Conditions as Prerequisites for Proper Use and Design of Mud to Control Blast Furnace Taphole Length", *ISIJ International,* vol. 38, no. 2, pp. 116-125.

Ueda, S., Natsui, S., Nogami, H., Yagi, J. & Ariyama, T. 2010, "Recent Progress and Future Perspective on Mathematical Modeling of Blast Furnace", *ISIJ International,* vol. 50, no. 7, pp. 914-923.

Upadhyay, H. & Kundu, T. 2013, "Drain Rate and Liquid Level Simulation in Blast Furnace Hearth Using Plant Data", *ISRN Metallurgy,* vol. 2013.

Vångö, M., Feilmayr, C., Pirker, S. & Lichtenegger, T. 2019, "Data-assisted CFD modeling of transient blast furnace tapping with a dynamic deadman", *Applied Mathematical Modelling,* vol. 73, pp. 210-207.

Vogelpoth, H.B., Still, G. & Peters, M. 1985, "Estimations Converning the Flow Behavior of Hot in Blast Furnace ", *Stahl und Eisen,* vol. 105, pp. 451-457.

Watakabe, S., Takeda, K., Sawa, Y. & Kawai, T.I. 2000, "Estimation of Metal Flow in the Hearth and the Hearth Brick Protection Mechanism in Chiba No. 6 Blast Furnace", *Tetsu-to-Hagane,* vol. 86, pp. 301-308.

World Steel Association*, Steel Statistical Yearbooks 2010 to 2019*. Available: https://www.worldsteel.org/steel-by-topic/statistics/steel-statistical-yearbook.html. Visited: 02/04/2020.

Yang, Y., Raipala, K. & Holappa, L. 2014, "Ironmaking" in *Treatise on Process Metallurgy* Elsevier Ltd, , pp. 2-88.

Zhou, Z., Zhu, H., Yu, A. & Zulli, P. 2010, "Numerical Investigation of the Transient Multiphase Flow in an Ironmaking Blast Furnace", *ISIJ International,* vol. 50, no. 4, pp. 515-523.

Zulli, Paul, 1991*, Blast furnace hearth drainage with and without a coke free layer* (doctoral thesis), University of South Wales (Australia).

ISBN 978-952-12-3983-0